A Harmonic Mitigation Scheme by Micro-APF for Residential Distributed
Systems

by

Xiang Li

A thesis submitted to the Faculty of Graduate Studies and Research in partial
fulfillment of the requirements for the degree of

Master of Science

In

Energy Systems

Department of Electrical & Computer Engineering
University of Alberta

Abstract

The proliferation of power-electronic-based modern residential loads can produce excessive voltage and current waveform distortions in residential power distribution systems. With their unique advantages such as flexible control and dynamic compensation over traditional passive power filters (PPFs), active power filters (APFs) have become one of the most effective means to suppress harmonics and eliminate distortion in modern distribution systems. The existing application of distributed APFs has been limited to the installations in the primary feeder and all the design issues were not considered.

In this thesis, a Micro-APF scheme is proposed to address the harmonic mitigation for residential systems. Unlike the traditional MV APFs, this novel LV distributed APF can be installed at the secondary side of service transformers or even at one of the customers' houses. This thesis mainly discusses some design issues for the proposed Micro-APF.

Acknowledgement

First of all, I would like to show my deepest appreciation to my supervisors, Professor Yunwei (Ryan) Li and Professor Wilsun Xu. I would have never conducted this work without Dr. Li's endless patience and tireless will to guide and supervise me. Also, I would like to thank Dr. Xu for his continuous support and guidance.

As well, I should highly appreciate other professors from my M.Sc examining committee, Professor Ali Khajehoddin and Professor Ami Kumar, for their great support and valuable suggestions for my thesis revision.

I would like to thank all my colleagues for their friendship, and it was a great opportunity to work with them. I should express my special appreciation to Mr. Tianyu Ding, for his selfless help during these three years.

Last but not least, I would like to express my gratitude to my parents for encouraging and supporting me throughout my life.

Contents

List of Figures

List of Tables

List of Abbreviations

PPF   Passive Power Filter

APF   Active Power Filter

DC   Direct Current

AC   Alternating Current

LV   Low Voltage

MV   Medium Voltage

UHC   Universal Harmonic Compensation

SHC   Selective Harmonic Compensation

PWM   Pulse Width Modulation

THD   Total Harmonic Distortion

PCC   Point of Common Coupling

PR   Proportional and Resonant

Chapter 1

Introduction

The development of new techniques in the area of electronics has provided numerous benefits to humanity. The use of electrical and electronic equipment in residential, commercial and industrial electrical installations has been growing dramatically in recent years. The proliferation of this type of equipment has caused great concern, since they absorb non sinusoidal currents from the mains, causing harmonic distortion. For this reason the problem of power quality from harmonic distortion has been the subject of much interest and discussion in recent years [1].

Harmonic mitigation is the major methodology to improve the power quality problem in power system and ensure the safety and reliability of electrical equipment. To achieve the purpose of harmonic mitigation, two approaches can be involved, i.e., harmonic mitigation aimed at the harmonic source and harmonic mitigation at the transmission path. As for the former, high power factor rectifiers based on multi-phase rectifier technique and pulse width modulation rectifier technique can be used since the rectifiers account for a large proportion of the power electronic devices, and this can reduce the harmonic generation from the source side. For the latter, specific harmonic filtering approaches can be carried out to realize the local compensation for harmonics generated by the numerous nonlinear electronic equipment.

This introductory chapter presents an overview of the harmonics in the modern distribution systems. Then, the traditional harmonic mitigation methods are

reviewed. Next, a Micro-APF mitigation scheme for residential systems is proposed. Finally, this chapter presents the scope and outline of this thesis.

1.1 Harmonic Situation in Today's Distribution Systems

The proliferation of power-electronic-based modern residential loads has resulted in significant harmonic distortions in the voltages and currents of residential power distribution systems. These new harmonic sources have comparable sizes and are distributed all over the networks. Especially for the home appliances such as compact fluorescent lights (CFLs), LCD TVs and personal computers (PCs), which are normally nonlinear, they can generate a large amount of harmonic currents and the harmonics can be injected into supply systems. Although home appliances produce insignificant amount of harmonic currents individually, the massive growth in the usage of such energy-efficient consumer electronic devices and the collective effect of a large number of such loads can be so substantial [2]-[4] that the excessive waveform distortions in urban distribution systems are becoming increasingly dominated by the harmonics of residential loads [5]-[8].

The serious harmonic distortion problem in modern distribution systems can result in so many troublesome and unwanted effects. The harmonics injected into the distribution systems may cause voltage and current stress on power cables and lead to dielectric failure [9]. The high level of harmonic distortion in power systems can increase the dielectric loss and thermal stress when they flow through capacitor banks due to the fact that power factor correction capacitors provide low shunt impedance at high-order harmonics, and the capacitors may be damaged if they are overloaded especially when the stress is excessive [10]. With the capacitors added to the power system, the series and parallel resonances can occur and amplify the harmonic levels, and then the amplified harmonic currents will flow into the resonant circuit [11]. In addition, the severe harmonic distortion in distribution systems can also lead to problems such as transformer overheating

[12], premature ageing [13], losses and pulsating torque on electrical machines [14], metering errors [15], etc. As for the residential systems, one of the most common problems resulting from high levels of harmonic distortion is telephone interference, and this has been recently experienced by the utility companies in Alberta, Canada [16].

As the usage of nonlinear electronic devices is inevitable in modern life, and the trend is even increasingly rising, the harmonic problem in distribution power systems is surely much worse in the near future. With so many severe potential unwelcome effects, harmonic distortion has raised widespread concerns. Also, so many harmonic mitigation methods have been tried to address this issue.

1.2 Harmonic Distortion Mitigation Approaches

Harmonic mitigation approaches can be mainly sorted into two categories: one is aimed at the harmonic source and the other is the mitigation at harmonic transmission path [17]. As for the former, improvement should be made for the design of electronic devices in order to attain the goal of making them produce fewer harmonics. As the harmonics generated by these power electronic devices account for a considerable proportion, multi-phase rectifier technique and pulse width modulation rectifier technique have been widely used for modern power electronic equipment. However, this approach is restricted for the existing devices in distribution systems and helpless to other types of harmonic source. So the installation of harmonic compensation devices at transmission path seems to be necessary to address this restriction. Overall, there are two major types of harmonic compensation devices based on the harmonic mitigation mechanisms, i.e., the traditional passive power filters (PPFs) and active power filters (APFs).

1.2.1 Harmonic Mitigation by Passive Power Filters

Based on the L-C resonance characteristics, the shunt branch of passive power filters can exhibit low impedance around resonant frequency, for example, when

$2\pi h f_1 L = 1/2\pi h f_1 C$ (f_1 is resonant frequency), the impedance of LC branch is 0. Thereby, the passive power filters tuned at a certain frequency can absorb the corresponding harmonics nearby the resonant frequency by behaving as small impedance. L-C passive filters are widely used to achieve the harmonic suppression and improvement of loads' power factor. According to the structure, there are mainly two categories of passive power filters, i.e., tuned filters and high-pass filters.

Although PPFs have many advantages such as simplicity in terms of design, low cost and high efficiency, no requirements for control links, and easy maintenance, etc., there are still many drawbacks in practical design and applications [18]-[22]:

- PPFs can only mitigate the specific harmonics as they are usually tuned at certain frequencies. So additional devices are needed to address different harmonics.
- The harmonic suppression performance strongly depends on parameters of the passive components and grid impedances. Also, if there is a frequency variation in the system harmonics, the effectiveness of existing devices on harmonic suppression will be reduced.
- Series or parallel resonance may occur due to the existence of PPFs and grid impedances. This will result in worse impacts on distribution systems.
- PPFs may be overloaded or even damaged when there is a significant increase in harmonic currents.

In addition to the above shortcomings, PPFs tend to be in large dimension and high weight, and this will certainly restrict their widespread application in modern distribution systems. Compared with PPFs, APFs are more flexible as far as the impact of system harmonics and impedances are concerned. Also the unique advantages over traditional PPFs such as no risks of resonance and realization of dynamic compensation have made APFs become one of the most effective means to suppress harmonics and eliminate distortion in voltage and current waveforms.

1.2.2 Harmonic Mitigation by Active Power Filters

Unlike their passive counterparts, APFs contain energy storage elements at the DC link of inverters, and the elements are usually DC inductor or DC capacitor, accordingly, the filters can be sorted into current source inverter based APFs (Figure 1.1 (a)) or voltage source inverter based APFs (Figure 1.1 (b)). In terms of the applied environment, there are single-phase APFs and three-phase APFs. Based on the voltage level, APFs can be typically classified into MV filters and LV filters as well. According to the topology, APFs can be also divided into two major categories, i.e., series active power filters and shunt active power filters [23].
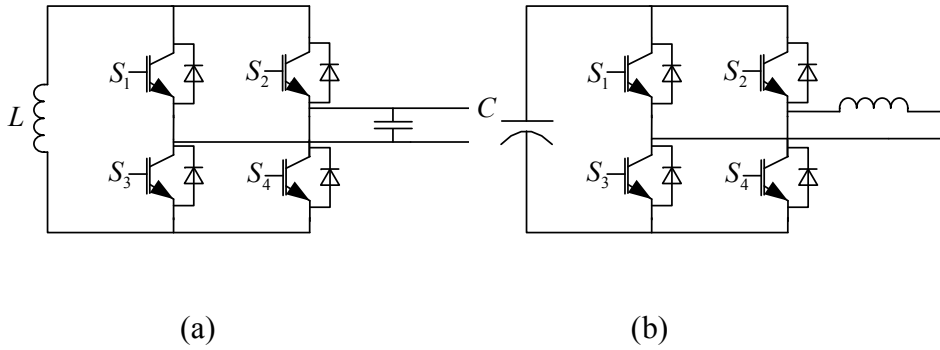
Figure 1.1 (a) Current source based APF. (b) Voltage source based APF.

As shown in Figure 1.2 (a), the series APF is connected in series with the grid through a matching transformer. A compensation voltage V_{APF} can be generated across the primary side of the transformer based on the extracted harmonic current I_{Sh} from the detected grid current I_S. The compensation voltage V_{APF} is equal to $-GI_{Sh}$, where G is the feedback gain of grid current. Figure 1.2 (b) shows the typical topology of a shunt APF. The harmonic component I_{Lh} is extracted from the detected load current I_L and then the shunt APF can be controlled to generate a current component I_F which is equal to $-I_{Lh}$ in order to achieve the purpose of harmonic compensation. Compared with series APFs, shunts APFs have been

more widely used in different situations. Owing to the advantage in flexible control realization, APFs can be applied to compensate harmonics only, reactive power, three-phase unbalanced currents or all of the above cases.
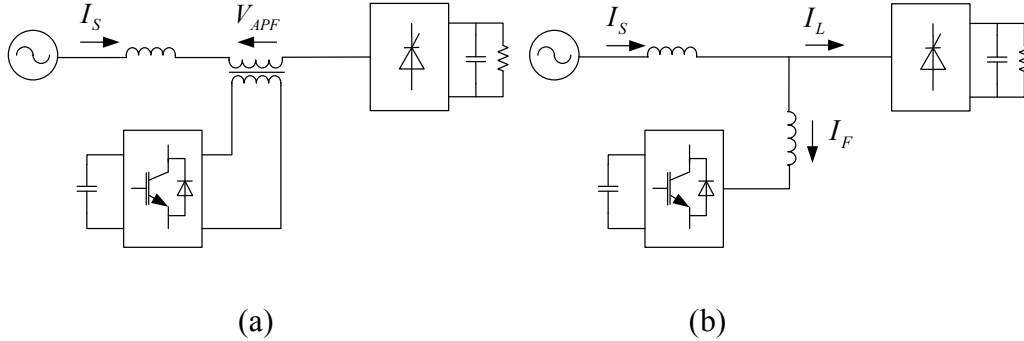
Figure 1.2 (a) Series active power filter. (b) Shunt active power filter.

As is discussed in previous section, harmonic mitigation by APFs can overcome the shortcomings of PPFs, however, due to the voltage/current ratings of power electronic switches, very high capacity is hard to achieve. Accordingly, the cost will rise notably with the capacity. So together with traditional PPFs, pure APFs can be extended to hybrid active power filters, which can inherit the advantages of both PPFs and APFs, and at the same time the drawbacks will be avoided as possible as they can [24]. In addition to hybrid filters, another new trend for the study on APFs focuses on the novel topologies of inverters [25].

1.3 Proposed Micro-APF Scheme for Residential Systems

Single-phase commercial and residential loads are the main sources of harmonic distortion in low-voltage distribution systems. In spite of their small sizes, domestic appliances such as TV sets, computers and fluorescent lamps can still generate significant harmonic currents. The cumulative effect of the harmonics produced by a larger number of households is not negligible. Figure 1.3 shows a general residential distribution feeder in North America. The harmonics generated by home appliances can flow into the grid via service transformers, and the

massive harmonics in transmission lines can result in unwanted effects as is discussed in Section 1.1, so harmonic mitigation for residential systems turns out to be necessary.
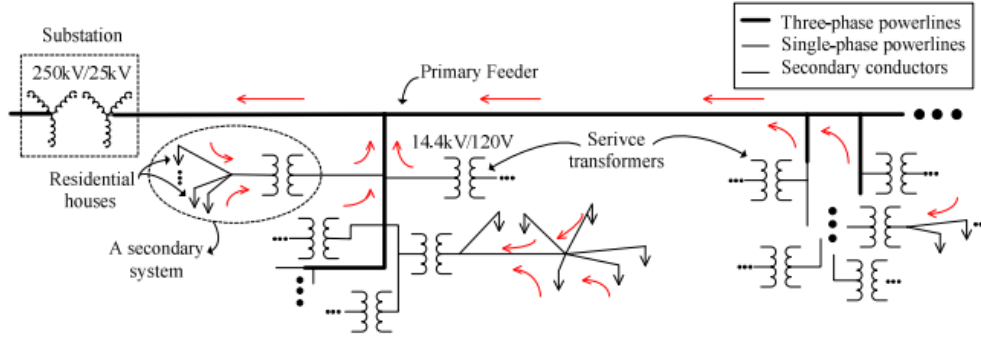
Figure 1.3 A general residential distribution feeder in North America

1.3.1 Topology and Specifications of Micro-APF

The existing application of distributed APFs has been limited to the installations in the primary feeder [26]-[31]. PPFs have been also tried to realize the mitigation of some dominant harmonics (3rd, 5th and 7th) for low voltage customers, but the results were unsatisfactory, and all the design issues were not considered [32]. In this thesis, a Micro-APF scheme is proposed for residential systems. Unlike traditional MV APFs, the distributed APFs in this proposed mitigation scheme can be installed at the secondary side of service transformers or even at one of the houses. In [33], sensitivity study has been carried out to demonstrate the truth that distributed APFs installed at service transformers and one of the nearest houses can result in better performance than in other locations. Figure 1.4 illustrates different harmonic approaches for a general North American residential distribution feeder. As the distributed APFs are installed at low voltage circumstance, and if designed properly, they can be mounted on the surface of electric meters due to their unique feature of low capacity, the distributed filters in this application are called "Micro-APFs" in this thesis. Supposed to be connected between the two hot wires of secondary side of service transformers, this novel single-phase APF can absorb the massive harmonics generated by single phase

7

residential nonlinear loads and prevent them flowing into the grid via service transformers.

As a matter of fact, LV distributed filters can also be realized by passive approaches. The reason why APFs are chosen is based on their unique advantages over PPFs, as is discussed in Section 1.2. Also, it is noticeable that the system impedance at secondary side of service transformers is very low, so in order to achieve desired compensation results, the filters need to exhibit small impedance at harmonic frequencies. However, this seems to be unrealistic for PPFs, as the series resistance of their capacitor and inductor already exists and is fixed. But for APFs, this can be more flexibly achieved by a power electronics circuit and its control system. As for the economic concerns, the cost for Micro-APF will be significantly cut down and comparable with their passive counterparts due to the fact that they are used in low voltage circumstance.
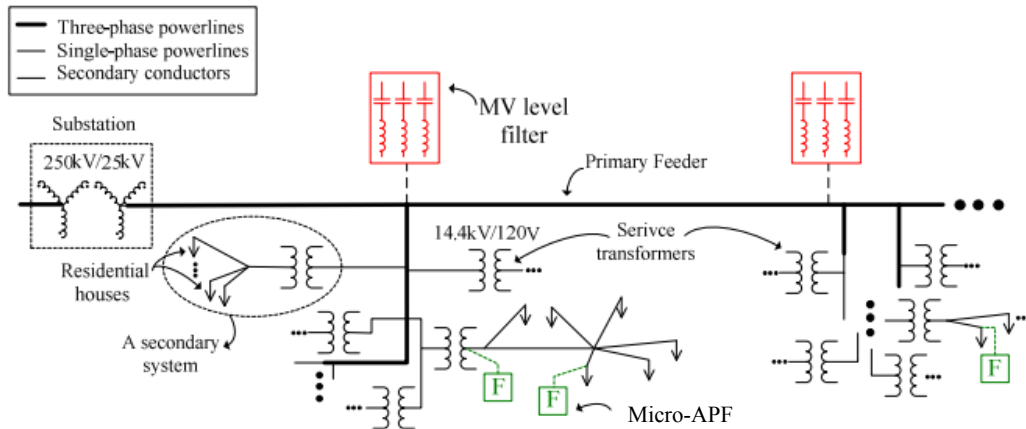
Figure 1.4 Different harmonic approaches for a general North American residential distribution feeder

Figure 1.5 shows the topology of a Micro-APF. The output LCL-filter is used to suppress the impact of high frequency ripples. Field measurement is carried out to study the spectrum of harmonic currents at service transformers in [34], and the results show that the majority of the harmonics produced by residential loads are certain low-order dominant harmonics such 3rd, 5th, 7th,

etc. Therefore, this Micro-APF can be designed to compensate harmonics up to 15th order. Table 1.1 shows the designed parameters and basic performance specifications.
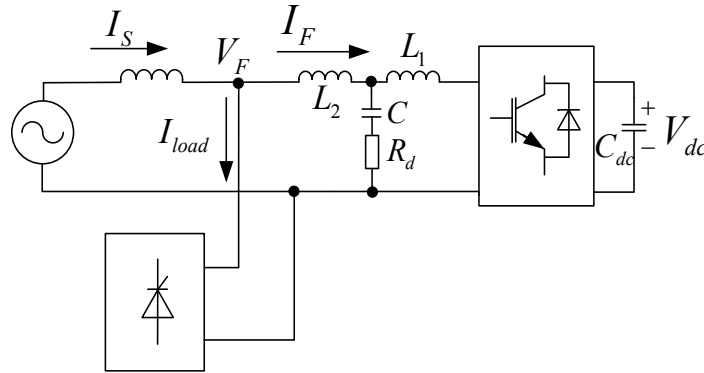
Figure 1.5 Topology of Micro-APF

Table 1.1 Designed parameters and performance specifications

Basic Designed Parameters	
LCL Filter	$L_1 = L_2 = 1\text{mH}$ $C = 15\mu\text{F}$
Damping Resistor	$R_d = 0.75\Omega$
DC Link Capacitor	$C_{dc} = 10\text{mF}$
DC Link Voltage	$V_{dc} = 450\text{V}$
Switching Frequency	$f_s = 10\text{kHz}$
Basic Specifications	
Compensation Outcome	Up to 15th order harmonic
Maximum Compensation Current	50A RMS
Power Ratings	12kVA

1.3.2 Comparison of Control Approaches

Based on the detected signals, there are two typical control approaches for APFs used to compensate harmonics only, i.e., current-detection and voltage-detection. Accordingly, APFs can also be classified into two types, i.e., current-detection based APFs and voltage-detection (virtual impedance) based APFs. As is shown

9

in Figure 1.6 (a), current-detection based APFs connected to the grid can appear as a controlled current source to inject a compensation harmonic current into the grid to cancel the harmonics flowing from the downstream side. Unlike their counterparts, voltage-detection (virtual impedance) based APFs can sink a current proportional to the extracted harmonic component from PCC voltage instead of injecting compensation current as they can be controlled as a small resistor at harmonic frequencies, as is discussed before. So the harmonics from both upstream and downstream sides of the grid can be absorbed by APFs (Figure 1.6 (b)).
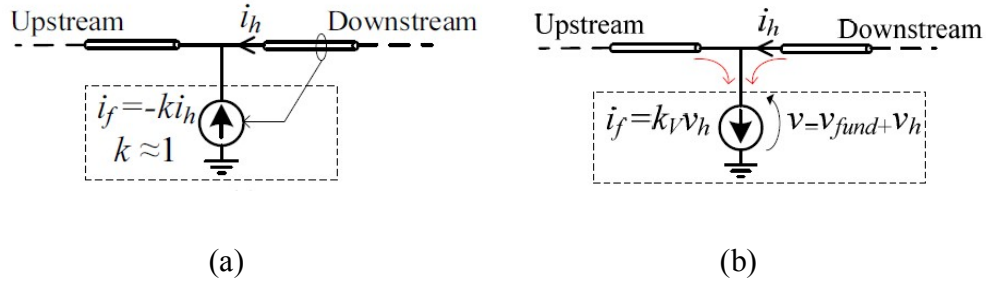
Figure 1.6 (a) Current-detection based APF. (b) Voltage-detection (virtual impedance) based APF.

The current-detection based approach can also be divided into load current feedback control and source current feedback control [35-38]. As is shown in Figure 1.7 (a), a harmonic component I_{Lh} is extracted from the detected load current I_L to generate the compensation current reference $I_F^* = -I_{Lh}$. Similarly, a harmonic component I_{Sh} is extracted from the detected source current I_S in Figure 1.7 (b), and after being multiplied by a coefficient k, the compensation current reference is formed, i.e., $I_F^* = -kI_{Sh}$. The detected compensation current I_F in Figure 1.7 (a) and (b) is controlled to track the reference I_F^* and produce PWM driving signals for switches.
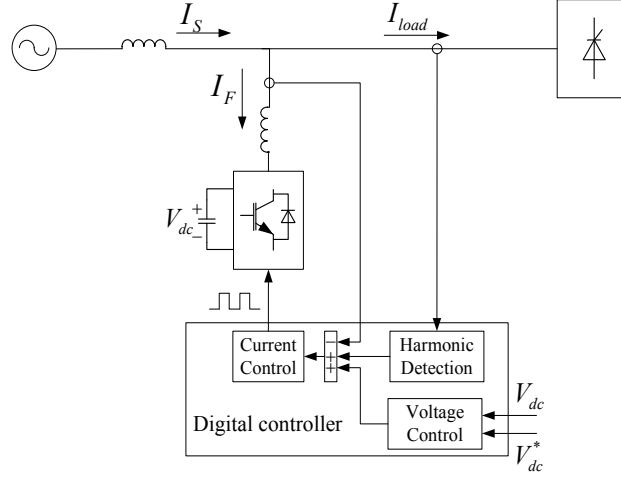
(a)
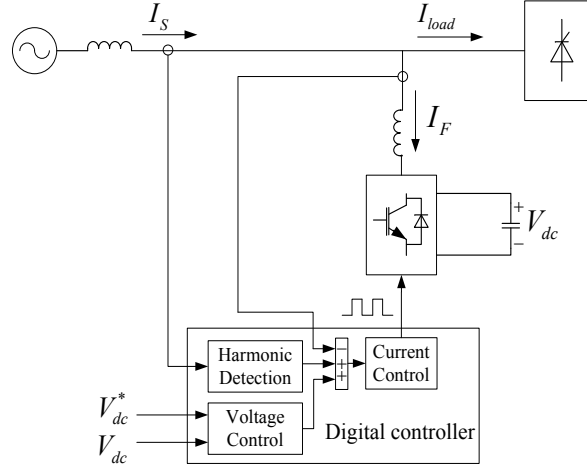
(b)

Figure 1.7 (a) Load current is detected. (b) Source current is detected.

As for voltage detection based approach, the PCC voltage V_F (shown in Figure 1.8) is detected instead of the currents [39]-[41]. Also, the harmonic reference current generation block is a bit different from the one in current-detection based control, as the goal is to make the Micro-APF exhibit a small resistor under harmonics and ideally infinite resistor under fundamental frequency, i.e.:

$$R_V(f) = \begin{cases} V_F(f)/I_F(f), f \neq f_{fund} \\ \infty, f = f_{fund} \end{cases} \tag{1.1}$$

So the compensation current reference I_F^* in voltage-detection based control can be expressed as:

$$I_F^* = G_V V_{Fh} = V_{Fh} / R_V \qquad (1.2)$$

where G_V and R_V are control gain and virtual impedance, respectively. V_{Fh} is the extracted harmonic component from PCC voltage V_F.

As the APFs can be controlled to be a small resistor at harmonic frequencies, the voltage-detection based control is also regarded as "virtual impedance based control" in this thesis.
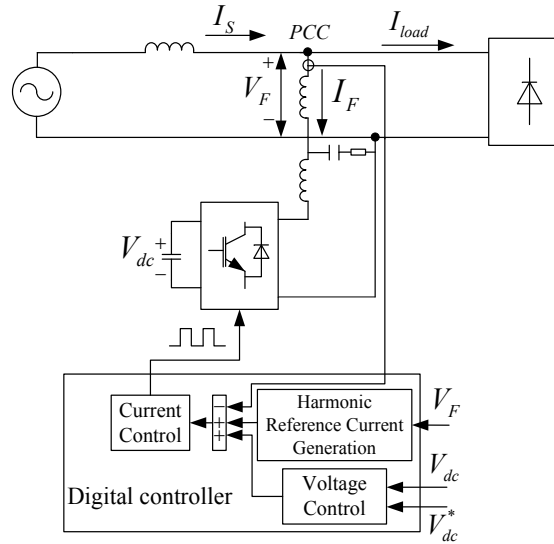
Figure 1.8 Voltage-detection (virtual impedance) based control

Based on the above discussion, it is obvious that voltage-detection (virtual impedance) based control approach has its unique advantages over the current-detection counterpart for residential distribution systems. Unlike the current-detection based APFs, voltage-detection (virtual impedance) based APFs can be installed at one of the houses to absorb the harmonics produced by other customers' houses supplied by the same service transformer. Also, no extra current sensor is needed for voltage-detection (virtual impedance) based APFs compared with their counterparts, as either the load current or source current

12

needs to be detected. So voltage-detection (virtual impedance) based control is more suitable for distributed APFs.

With above concerns, the proposed Micro-APF scheme in this thesis adopts voltage-detection (virtual impedance) based control approach, and the design of virtual impedance turns out to be the key point for Micro-APF. The virtual impedance should be smaller than the system impedance to achieve good performance of harmonic mitigation. However, virtual impedance cannot attain as small as possible as it is restricted by stability problem. Therefore, the design of virtual impedance inevitably becomes one of the major tasks that need further discussion in this thesis.

1.4 Thesis Scope and Outline

Most of the existing research in the field of harmonic mitigation focused only on the lumped, large and known industrial loads. However, the harmonic distortions in the modern distribution systems are dominated by the large number of randomly dispersed sources associated with residential loads[42]. Therefore, harmonic mitigation for residential distribution system is necessary with this background. The scope of this thesis is to develop a novel Micro-APF scheme for residential systems. As is discussed above, this new type of distributed APFs are installed at LV circumstance, i.e., secondary side of service transformers. With its unique advantage, voltage-detection (virtual impedance) based control is adopted for the proposed Micro-APF.

In the rest of the thesis, Chapter 2 introduces the control realization of Micro-APFs. The two control schemes (voltage-detection based control), i.e., universal harmonic compensation (UHC) and selective harmonic compensation (SHC), are presented. Stability analysis and case study are carried out to obtain the attainable range of virtual impedances for these two schemes, respectively.

Harmonic impedance of Micro-APF and its impact on system performance are discussed in Chapter 3. For the practical scenario where interharmonics are

regarded as useful carrier signals and cannot be filtered out together with the dominant harmonics, SHC scheme is selected to implement the harmonic mitigation for residential distribution systems. Sensitivity studies are carried out to study the factors that can influence harmonic impedance. The schemes under stationary frame and multiple d-q frames are compared in this chapter as well.

In Chapter 4, the situation of multiple Micro-APF is studied. To investigate the stability of multiple Micro-APF system, simplified equivalent circuitry analysis is involved for a typical distribution feeder. The estimation on the attainable range of virtual impedance is conducted for multiple Micro-APF system. In addition, the interference on harmonic compensation is discussed as well. The time-domain simulation and theoretical analysis are carried out to illustrate the influence of service transformers in this interference between Micro-APFs installed at different sites.

The main conclusions from this thesis and suggestions for future studies and improvements are presented in Chapter 5.

Chapter 2

Control Realization of Micro-APF

In Chapter 1, two major compensation approaches for APFs are discussed, i.e., the current-detection and voltage-detection based compensation. With the unique advantages, voltage-detection (virtual impedance) compensation is assumed to be a better option than its counterpart for distributed filters. So this chapter presents the control realization of Micro-APF based on the voltage-detection (virtual impedance) compensation approach. For voltage-detection strategies, the selection of virtual impedances is a crucial factor for the control realization of Micro-APF. Apparently, smaller virtual impedance can achieve better steady state performance. However, if the value is small enough, the stability cannot be maintained. Therefore, it is necessary to figure out the attainable range of virtual impedances. In this chapter, stability analysis is carried out to obtain the minimum value of virtual impedances.

2.1   Control Schemes

This section discusses the voltage-detection based control strategy of Micro-APF for residential systems. The Micro-APF can be controlled to behave as a small resistor under harmonics and ideally open-circuit (infinite resistor) under fundamental frequency. According to the structure of harmonic reference current generation block, there are two approaches to achieve harmonic compensation, i.e., universal harmonic compensation (UHC) and selective harmonic compensation (SHC). The principles of these two strategies are presented in Section 2.1.2 and Section 2.1.3, respectively.

2.1.1 Voltage-detection (Virtual impedance) based control

Figure 2.1 shows the Micro-APF connected to the grid. The PCC voltage V_F is detected and used to form the feedback path via harmonic extraction block to generate harmonic reference current. The current control loops are shown in Figure 2.2. V_{grid} and I_L are disturbance signals. The feedforward path of V_F is added to the output of PR controllers to enhance the dynamics. G_i represents the transfer function of harmonic extraction block. According to Figure 2.2, it is obvious that equation (2.1) holds, and equation (2.2) can be derived from (2.1).
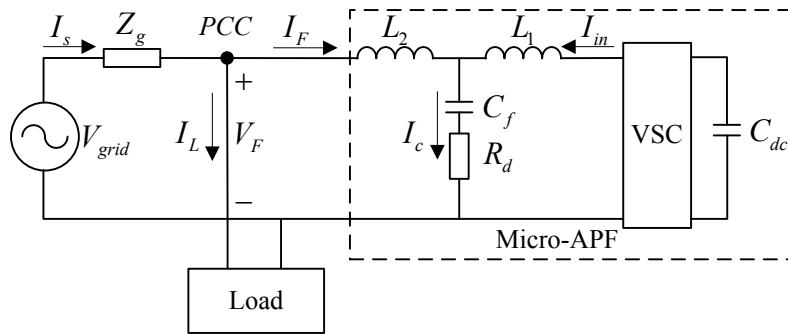
Figure 2.1 Micro-APF connected to the grid
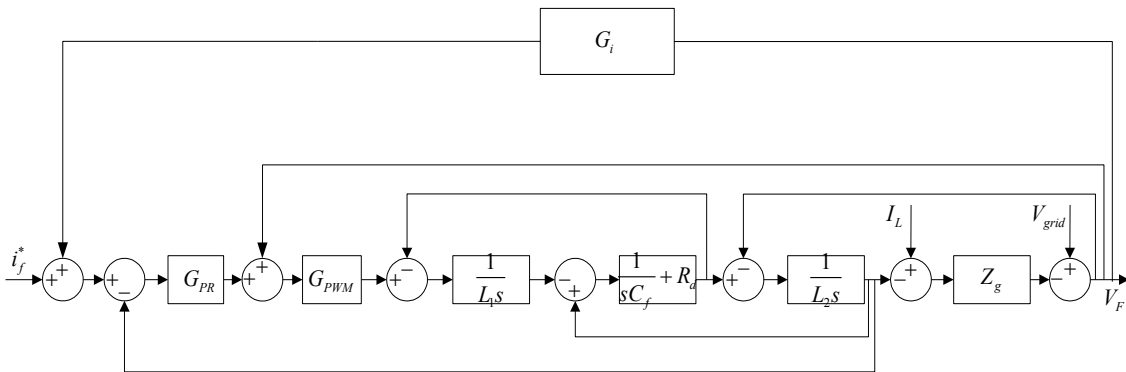
Figure 2.2 Current control loops

16

$$\begin{cases} I_F + \dfrac{1}{L_1 s}\left\{\left[\left(I_f^* + V_F G_i - I_F\right)G_{PR} + V_F\right]G_{PWM} - V_C\right\} = I_C \\[2mm] I_C\left(\dfrac{1}{sC_f} + R_d\right) = V_C \\[2mm] (V_F - V_C)\dfrac{1}{L_2 s} = I_F \\[2mm] V_{grid} - (I_L + I_F)Z_g = V_F \end{cases} \tag{2.1}$$

$$I_F = Y_1(s)I_f^* + G(s)V_{grid} + Y_2(s)I_L \tag{2.2}$$

where

$$Y_1(s) = \frac{(1 + sC_f R_d)G_{PR}G_{PWM}}{(1 + sC_f R_d)K(s) - s^2 L_1 C_f(L_2 s + Z_g)}$$

$$G(s) = \frac{(1 + sC_f R_d)(G_{PR}G_{PWM}G_i + G_{PWM} - 1) - s^2 L_1 C_f}{(1 + sC_f R_d)K(s) - s^2 L_1 C_f(L_2 s + Z_g)}$$

$$Y_2(s) = \frac{Z_g(1 + sC_f R_d)(1 - G_{PR}G_{PWM}G_i - G_{PWM}) + s^2 Z_g L_1 C_f}{(1 + sC_f R_d)K(s) - s^2 L_1 C_f(L_2 s + Z_g)}$$

$$K(s) = G_{PR}G_{PWM} + Z_g G_{PR}G_{PWM}G_i + Z_g G_{PWM} - L_1 s - L_2 s - Z_g$$

Figure 2.3 illustrates the DC voltage control loop. A low-pass filter is added to the feedback path of DC-Link voltage to resist the high frequency noise. PI controller is used to control the DC-Link voltage to stabilize around the given reference value. The fundamental component of the reference compensation current I_F^* is generated by the product of PI controller outcome and a unit sinusoidal signal which is in phase with V_F. The dynamics of voltage loop are much slower than the current loops, so it is not considered in the following analysis.

As far as the harmonic reference current extraction is concerned, the two major approaches, i.e., universal extraction and selective extraction, are shown in Figure 2.4. Accordingly, the compensation schemes are named as universal harmonic compensation (UHC) and selective harmonic compensation (SHC). For the UHC

17

scheme, only a control gain G is involved, so the Micro-APF is controlled to behave as the same virtual resistor R_V throughout the harmonic frequency spectrum. In this case, a high-pass filter is enough to achieve the harmonic extraction. As for the SHC scheme, multiple control gains $G_i(i=3,5,7,....,15)$ are involved, and the harmonics can be controlled to exhibit as unequal virtual resistors $R_i(i=3,5,7,....,15)$. So in order to achieve the goal of harmonic extraction, a series of band-pass filters tuned at the dominant harmonic frequencies are needed.
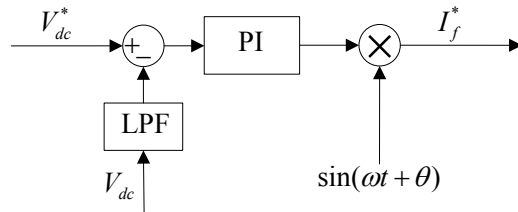
Figure 2.3 DC-Link voltage control

(a)   (b)
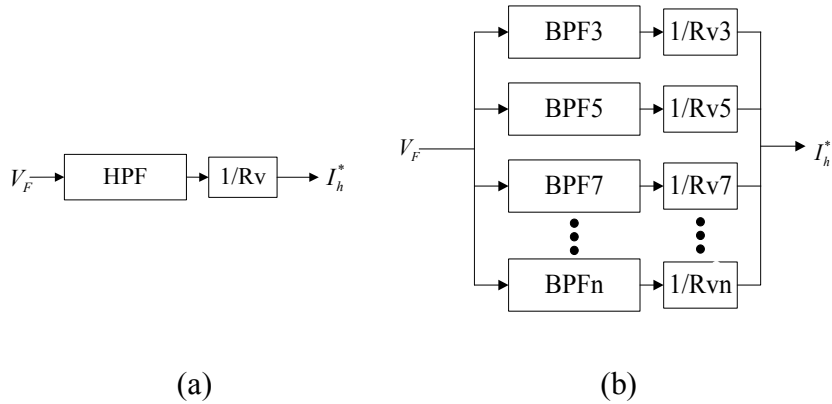
Figure 2.4 Harmonic reference current extraction. (a) UHC scheme. (b) SHC scheme.

Apparently, UHC scheme and SHC scheme have their unique advantages and disadvantages respectively. In UHC scheme, only a high-pass filter is involved and the harmonics throughout the spectrum can be extracted altogether. However, the harsh requirement for control bandwidth is difficult to be satisfied in UHC scheme. Also, in some other special cases, where the specific dominant harmonics

or interharmonics (this issue is discussed in Chapter 3) are extremely concerned about, the advantage of SHC scheme stands out. It should be noted that in practical residential systems, the situation of high order harmonics is not so serious, so only limited low order dominant harmonics need to be chosen as compensation objectives.

Unlike UHC scheme, the dominant harmonics are treated as compensation objectives in SHC scheme, which means that the harmonics in widespread spectrum are approximated by limited harmonic components. As a matter of fact, the selected dominant harmonics account for the majority proportions of the total harmonic content in residential load current. Accordingly the specific dominant harmonics or interharmonics can be well suppressed or unaffected. However, trade-off still exists in terms of THD since only the selected harmonics can be compensated. The following sections will discuss these two approaches in detail respectively.

2.1.2 Universal Harmonic Compensation (UHC)

It is obvious that equation (2.3) holds according to Figure 2.4.

$$G_i = G_{HP} / R_V \tag{2.3}$$

where G_{HP} is the transfer function of high-pass filter.

So

$$I_F = Y_1'(s)I_f^* + G'(s)V_{grid} + Y_2'(s)I_L \tag{2.4}$$

where

$$Y_1'(s) = \frac{R_V(1+sC_fR_d)G_{PR}G_{PWM}}{(1+sC_fR_d)K'(s)-s^2R_VL_1C_f(L_2s+Z_g)}$$

$$G'(s) = \frac{(1+sC_fR_d)(G_{PR}G_{PWM}G_{HP}+R_VG_{PWM}-R_V)-s^2R_VL_1C_f}{(1+sC_fR_d)K'(s)-s^2R_VL_1C_f(L_2s+Z_g)}$$

$$Y_2^{'}(s) = \frac{Z_g(1+sC_fR_d)(R_V - G_{PR}G_{PWM}G_{HP} - R_VG_{PWM}) + s^2 Z_g R_V L_1 C_f}{(1+sC_fR_d)K^{'}(s) - s^2 R_V L_1 C_f(L_2 s + Z_g)}$$

$$K^{'}(s) = R_V(G_{PR}G_{PWM} + Z_g G_{PWM} - L_1 s - L_2 s - Z_g) + Z_g G_{PR}G_{PWM}G_{HP}$$

The inverter link transfers function $G_{PWM} = 1/(T_1 S + 1)$, where $T_1 = 0.5T = 1/2f_s$, and the current controller G_{PR} represents PR controllers for selected dominant harmonics here, with identical parameters $k_p = 1$, $k_i = 240$, $\omega_i = 0.5 \text{rad/s}$.

In voltage-detection compensation schemes, one crucial task is to determine the selected control gains (virtual impedances). It is obvious that the virtual impedance should be chosen as small as possible in order to achieve better steady state performance. However, the virtual impedances cannot be chosen too small as well. On the one hand, it takes the system longer time to achieve steady state under smaller virtual impedances. On the other hand, too small virtual impedances (larger control gains) may usually lead to stability-related problems. So with the above consideration, stability analysis is needed to determine the attainable range of virtual impedances.

According to equation (2.4), the root locus of transfer function can decide the minimum R_V. Figure 2.5 shows the pole positions of $Y_1^{'}(s)$ when R_V is seen as variable (the arrows in Figure 2.5 represent the rising trend of R_V), and it is obvious that the selection of R_V should meet the following requirement for UHC scheme:

$$R_V > 0.00046\Omega$$

Although the value of virtual impedance can be as small as 0.00046Ω, to ensure better dynamics, the recommendation range is $0.01 \sim 0.02\,\Omega$. Figure 2.6 illustrates the steady state performance (harmonic content and THD of grid current) under several typical R_V values by time-domain simulation.
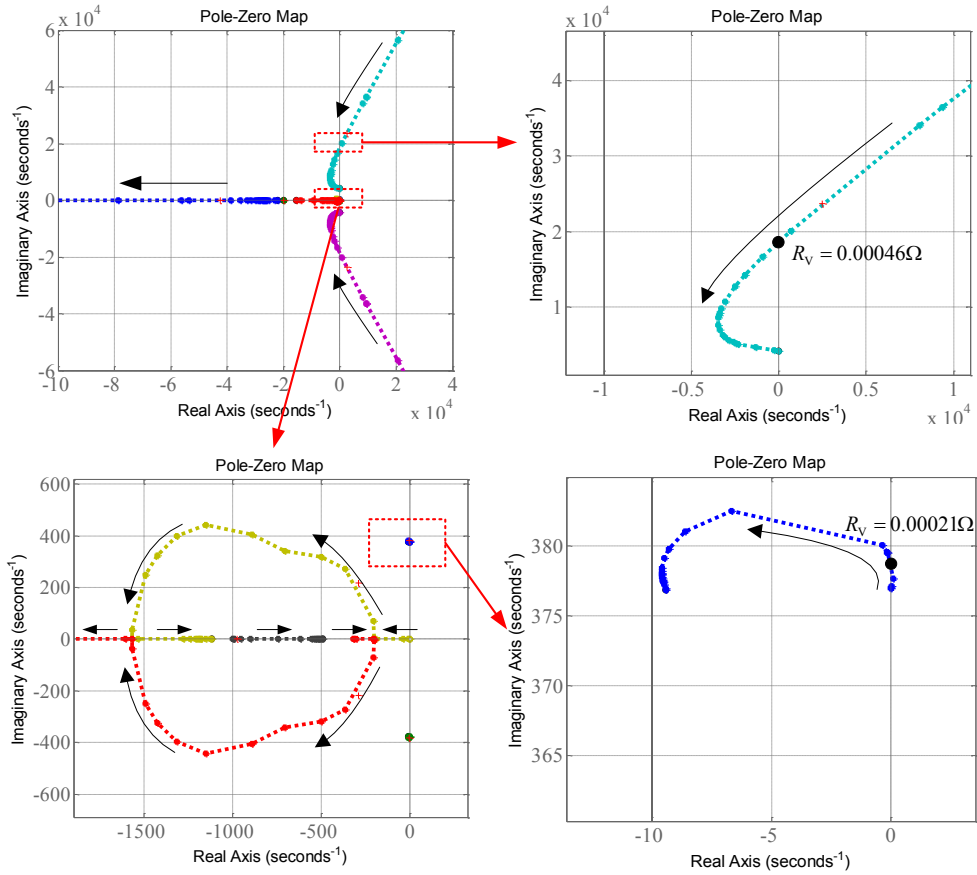
Figure 2.5 Pole positions of $Y_1^{'}(s)$ when R_V is seen as variable
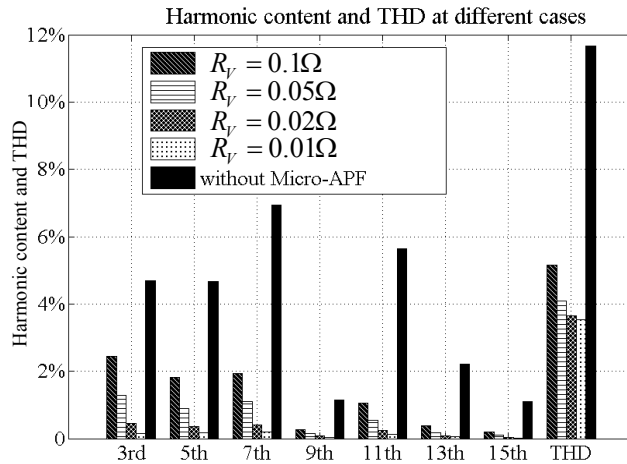
Figure 2.6 Steady-state performance (harmonic content and THD of grid current) by UHC scheme under different R_V values

It is clear that the contents of selected dominant harmonics and THD can be reduced with the decrease of R_V. For $R_V = 0.1\Omega$ and $R_V = 0.05\Omega$, the THD is

deceased from 11.6% to 5.2% and 4.1% respectively by UHC scheme, i.e., when $R_V \leq 0.1\Omega$, THD can be dropped by more than 50% after compensation.

2.1.3 Selective Harmonic Compensation (SHC)

As is shown in Figure 2.4(b), the harmonic extraction block in SHC scheme consists of several band-pass filters tuned at the desired harmonic frequencies. This approach is more flexible since the band-pass filter (BPF) arrays can extract the selected harmonic components separately and the harmonic reference current can be controlled by either identical or unequal gains to force the Micro-APF to behave as identical or unequal virtual impedances at the various selected harmonic frequencies. This flexibility is a unique advantage over UHC scheme.

Similar to the UHC scheme, stability analysis is also needed in order to determine the attainable range of virtual impedance $R_i (i = 3, 5, 7...15)$ for each harmonic. However, it is more complicated than the UHC case where only one virtual resistance value R_v needs working out. This problem can be solved by control variate method.

If virtual impedance for the jth harmonic is R_j, then equation (2.5) holds.

$$G_i = G_{BPFj} / R_j + \sum_{k \neq j} G_{BPFk} / R_k = G_{BPFj} / R_j + G_{\Sigma j} \qquad (2.5)$$

Therefore, similar to equations (2.2) and (2.4), equation (2.6) can be derived.

$$I_F = Y_1^{"}(s)I_f^* + G^{"}(s)V_{grid} + Y_2^{"}(s)I_L \qquad (2.6)$$

where

$$Y_1^{"}(s) = \frac{R_j(1 + sC_f R_d)G_{PR}G_{PWM}}{(1 + sC_f R_d)K^{"}(s) - s^2 R_j L_1 C_f (L_2 s + Z_g)}$$

22

$$G^{''}(s) = \frac{(1+sC_fR_d)(G_{PR}G_{PWM}G_{BPFj} + G_{PR}G_{PWM}R_jG_{\Sigma j} + R_jG_{PWM} - R_j) - s^2R_jL_1C_f}{(1+sC_fR_d)K^{''}(s) - s^2\,R_jL_1C_f(L_2s + Z_g)}$$

$$Y_2^{''}(s) = \frac{Z_g(1+sC_fR_d)(R_j - G_{PR}G_{PWM}G_{BPFj} - R_jG_{PR}G_{PWM}G_{\Sigma j} - R_jG_{PWM}) + s^2\,Z_g\,R_jL_1C_f}{(1+sC_fR_d)K^{''}(s) - s^2\,R_jL_1C_f(L_2s + Z_g)}$$

$$K^{''}(s) = R_j(G_{PR}G_{PWM} + Z_g\,G_{PR}G_{PWM}G_{\Sigma j} + Z_g\,G_{PWM} - L_1s - L_2s - Z_g) + Z_g\,G_{PR}G_{PWM}G_{BPFj}$$

G_{BPFi} is used to represent the notch filters tuned at dominant harmonics (3$^{\text{rd}}$, 5$^{\text{th}}$, 7$^{\text{th}}$ ...). So according to equation (2.6), stability analysis can be carried out to determine the attainable range of $R_i(i=3,5,7...15)$ and this is discussed in the next section.

2.2 Case Study for Attainable Virtual Impedances

This section illustrates the decision on the attainable range of virtual impedances in the SHC scheme. The designed parameters of Micro-APF are assumed to be maintained as constants, so the only factor that may influence the attainable range of virtual impedances is the grid impedance. A series of sensitivity study based on stability analysis and time-domain simulation is carried out to study this impact.

2.2.1 Base Case Study

The system impedance $Z_g = Z_{g\_base}$ (R=0.04Ω, L=0.126mH) is regarded as the base case. As far as the stability analysis is concerned, the brought-in notch filter arrays enhance the complexity in the SHC scheme. However, control variate method can be used to study the impact of each notch filter on stability firstly. Assume that the harmonic extraction block is simplified as a single notch filter tuned at one of the dominant frequencies divided by the corresponding virtual impedance, i.e., $G_i = G_{BPF_i}/R_i(i=3,5,7,...,15)$. So based on equation (2.6), Figure 2.7 shows the pole positions of $Y_1^{''}(s)$ for $G_i = G_{BPF_3}/R_3$ when R_3 is seen as

variable (the arrows in Figure 2.7 represent the rising trend of R_V). It is clear that R_3 should meet the following requirement in the SHC scheme:

$$R_3 > 0.00033\Omega$$

Also, this method can be used to determine the attainable range of the virtual impedances for other dominant harmonics. Table 2.1 shows the minimum R_i for each single dominant harmonic based on stability analysis. It is obvious that a larger virtual impedance value is needed for higher order harmonics to maintain the stability.
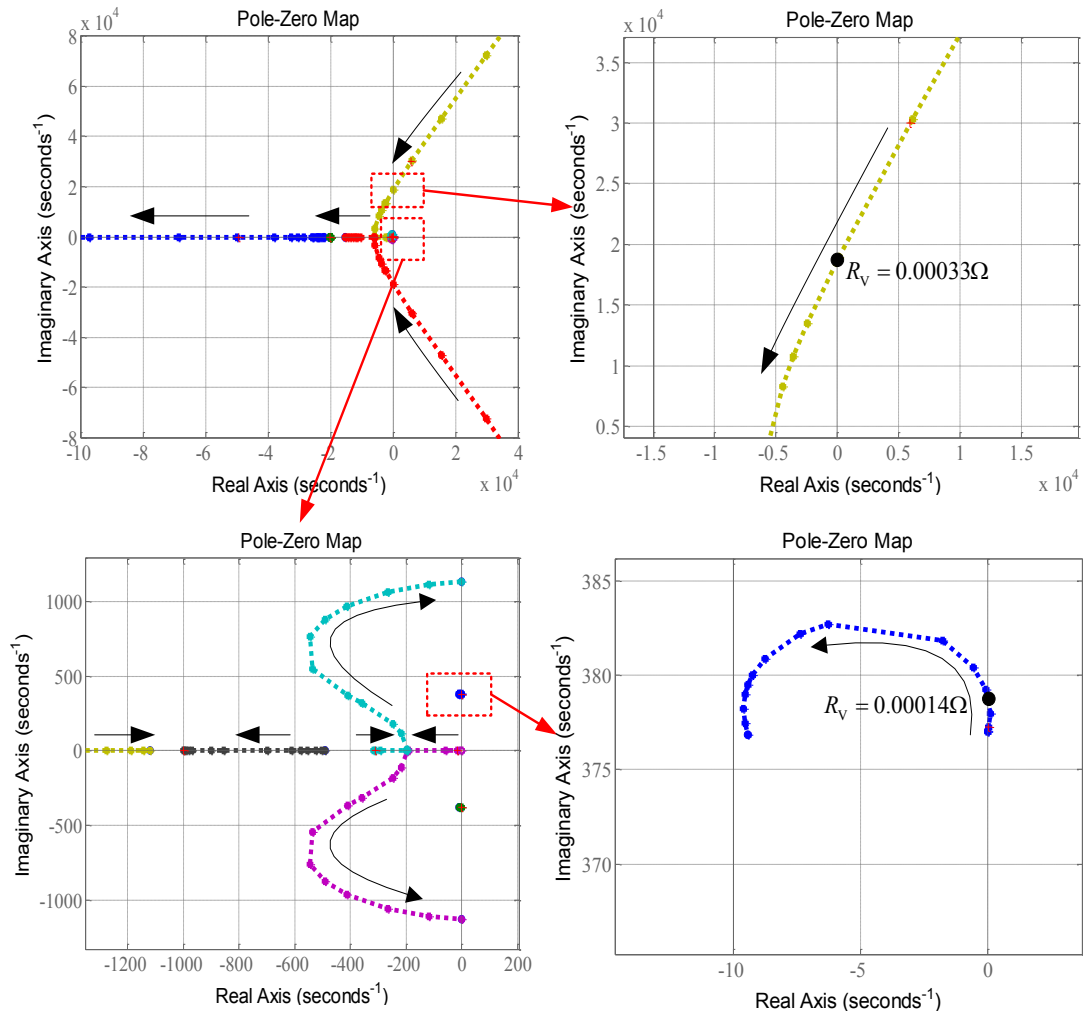
Figure 2.7 Pole positions of $Y_1''(s)$ for $G_i = G_{BPF_3} / R_3$ when R_3 is seen as variable

Table 2.1 Minimum values of R_i for each single dominant harmonic (mΩ)

	3rd	5th	7th	9th	11th	13th	15th
R_i	0.33	0.35	0.37	0.40	0.45	0.53	0.68

Control variate method is implemented to determine the minimum R_i for each single harmonic to maintain stability, and within the attainable range, R_i should be as small as possible. However, this is just an ideal case since the dynamics cannot be ignored in practical occasions. So trade-off has to be made if both steady state performance and dynamic response are taken into consideration. Similar to the UHC scheme, the recommendation range of virtual impedances is $0.01 \sim 0.02\,\Omega$. But due to the existence of notch filter arrays, more work is needed to check whether stability can be ensured or not under this recommendation range.

Assume that R_i for each of the dominant harmonics is seen as variable while the rest are maintained at the same constant, control variate method can be used for multiple-harmonic cases to determine more rigorous range of the attainable virtual impedances.

Figure 2.8 shows the pole positions when R_3 is seen as variable while the rest of virtual impedances, i.e., $R_i (i = 5,7,...,15)$ are maintained at several typical values (0.01Ω, 0.02Ω, 0.05Ω and 0.1Ω). It is clear that R_3 can be as small as 0.46mΩ (when $R_{i(i=5,7,...,15)} = 0.01\Omega$). Also, the similar analysis can be done to determine minimum $R_i (i = 5,7,...,15)$ respectively when the virtual impedances $R_j (j \neq i)$ are maintained at these typical values. Figure 2.9 presents the minimum virtual impedances for each harmonic when the rest are identical, at several typical values. It is obvious that the stability margin is reduced as the harmonic frequency goes up. A smaller stability margin is seen for each dominant harmonic when smaller virtual impedances are chosen for the rest of dominant harmonics. For

25

example, the minimum virtual impedance can be as small as $0.89\text{m}\Omega$ when $R_i = 0.01\Omega$ (for the 15th harmonic).
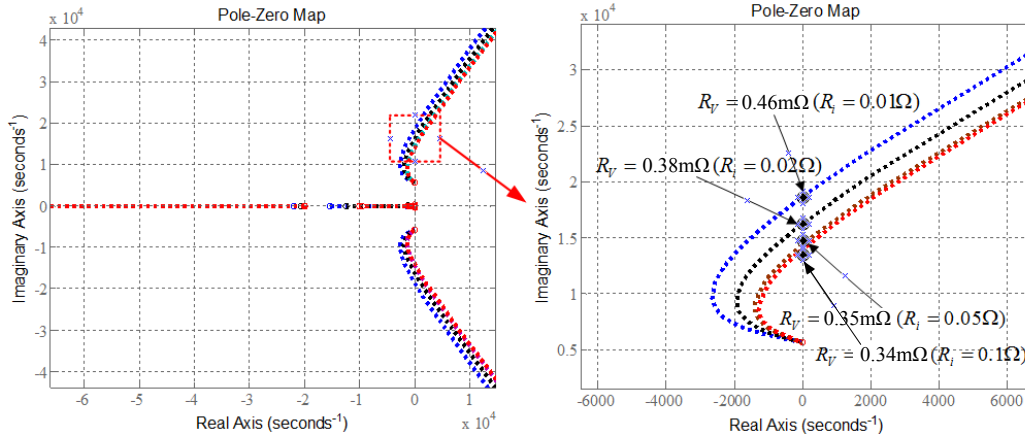
Figure 2.8 Pole positions of $Y_1^{\prime\prime}(s)$ when R_3 is seen as variable while $R_i(i = 5,7,...,15)$ are maintained at several typical values
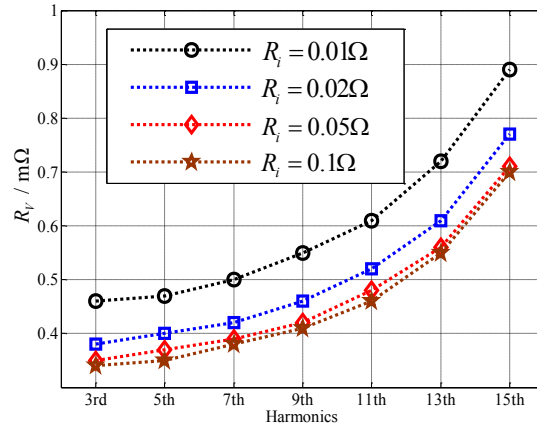
Figure 2.9 Minimum virtual impedances for each harmonic when the rest are identical, at several typical values

According to Figure 2.9, it is obvious that the range of $0.01\sim0.02\Omega$ is attainable for the virtual impedances corresponding to different dominant harmonics. Time-domain simulation is carried out when identical virtual impedances are selected for the dominant harmonics. Figure 2.10 shows the compensation performance when 0.01Ω is chosen for all of the selected dominant harmonics.

26
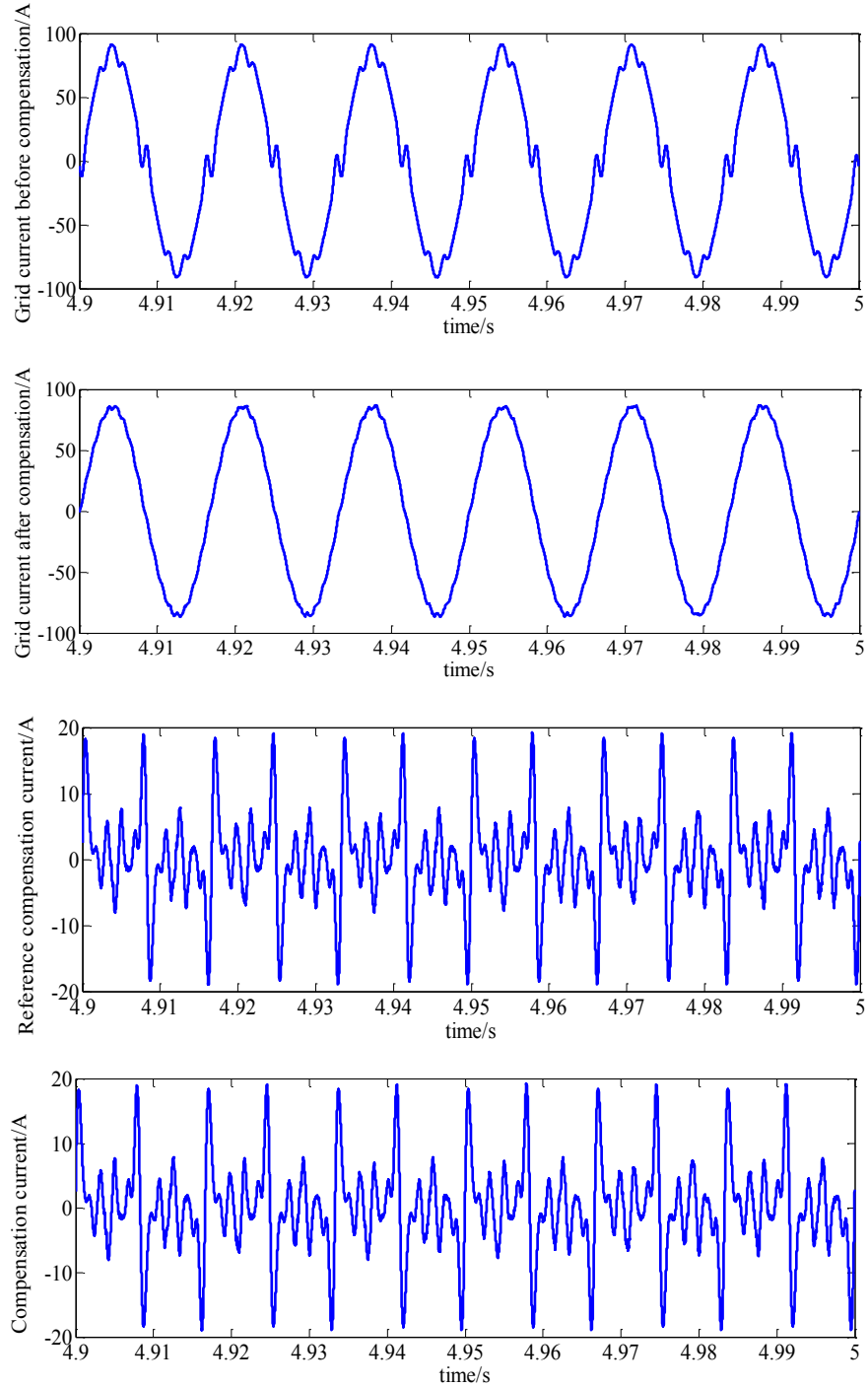
Figure 2.10 Compensation performance when $R_i = 0.01\Omega(i = 3, 5, ..., 15)$.

Figure 2.11 compares the steady state performances (harmonic content and THD of grid current) by SHC scheme and the virtual impedances for all of the dominant harmonics are chosen as several identical values, i.e., 0.01Ω, 0.02Ω,

0.05Ω and 0.1Ω, respectively. Compared with the UHC scheme (Figure 2.6), SHC scheme can achieve almost the same harmonic decrease. Although the existence of notch filter arrays in SHC scheme enhances the complexity of decision on the attainable range of virtual impedances, the unique control flexibility on the selected frequencies makes it stand out.
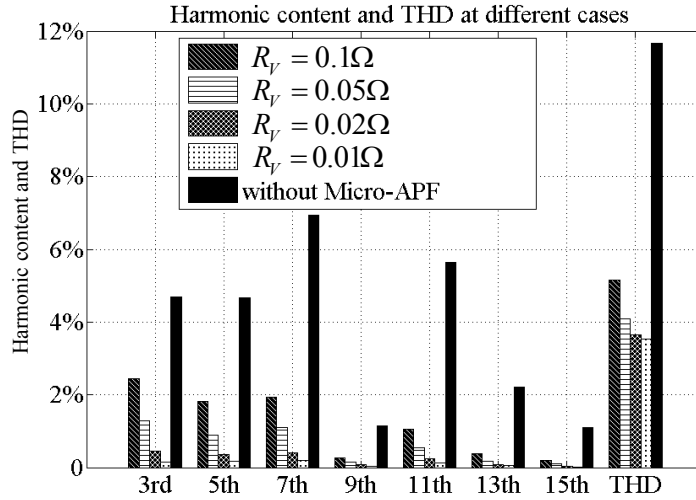
Figure 2.11 Steady state performance (harmonic content and THD of grid current) under several typical values of identical virtual impedances

2.2.2 Impact of grid impedance

Grid impedance may influence the attainable range of virtual impedances, and the analysis for base case, i.e., $Z_g = Z_{g\_base}$ (R=0.04Ω, L=0.126mH) is presented in Section 2.2.1. Similar to the base case study, sensitivity study can be carried out to study how grid impedance makes a difference as far as stability is concerned.

Firstly, the harmonic extraction block is simplified as a single notch filter tuned at one of the dominant frequencies divided by the corresponding virtual impedance, i.e., $G_i = G_{BPF_i} / R_i (i = 3, 5, 7, ..., 15)$. Stability analysis can be implemented to study the impact of grid impedance on the virtual impedances $R_i (i = 3, 5, 7, ..., 15)$ under single-harmonic cases respectively. Figure 2.12 shows the pole positions of $Y_1^{''}(s)$

for $G_i = G_{BPF_3} / R_3$ when R_3 is seen as variable. It is clear that the minimum value of R_3 that can ensure stability goes up as the grid impedance is increased, which means that the stability margin is reduced with the increase in the grid impedance when the 3rd harmonic is considered only. For example, when Z_g increased from Z_{g_base} to $10Z_{g\_base}$, the corresponding minimum R_3 to maintain stability is increased from 0.33mΩ to 0.46mΩ.
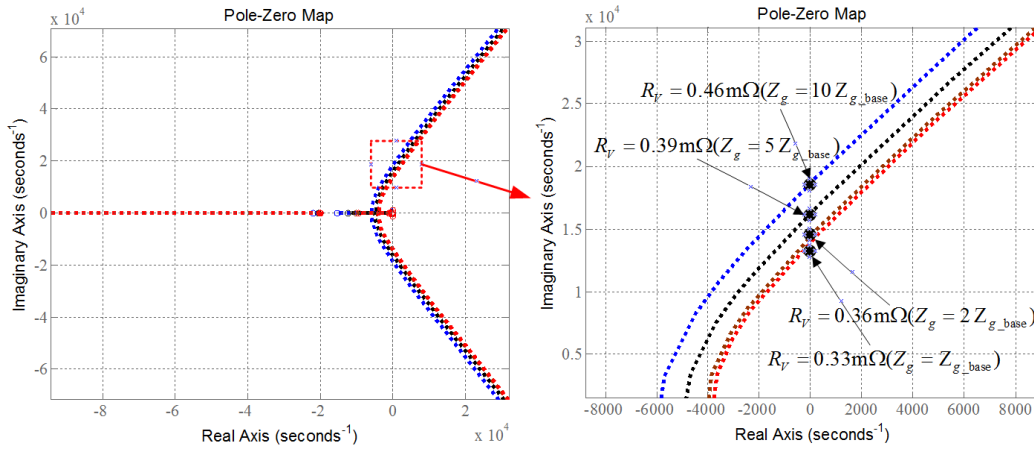
Figure 2.12 Pole positions of $Y_1''(s)$ for $G_i = G_{BPF_3} / R_3$ when R_3 is seen as variable

Accordingly, similar analysis can be done for other dominant harmonics, and Figure 2.13 shows the minimum virtual impedances for each single dominant harmonic under different settings of grid impedance. The overall trend is consistent with previous results. The stability margin for higher order harmonics is smaller compared with the lower ones. Also, the increases in grid impedance and minimum virtual impedances show a significant positive-correlation trend.
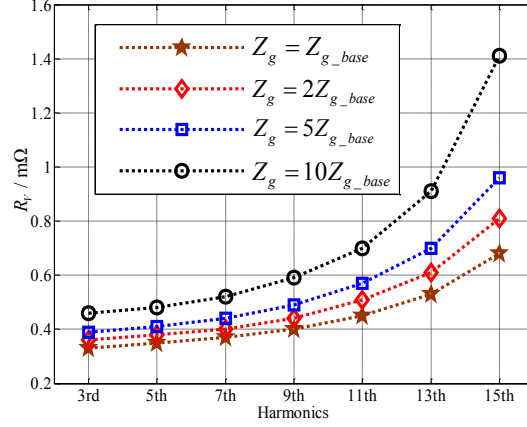
Figure 2.13 Minimum virtual impedances for each single dominant harmonic
under different settings of grid impedance

Further, control variate method is used for multiple-harmonic cases to study the
impact of grid impedance. Assume that R_i for each of the dominant harmonics is
seen as variable while the rest are maintained at the same constant, stability
analysis is carried out to determine more rigorous range of the attainable virtual
impedances.

Figure 2.14 shows the pole positions when R_3 is seen as variable while the rest of
virtual impedances are all maintained at 0.01Ω. It is clear that R_3 can be as small
as 0.84mΩ (when $R_{i(i=5,7,...,15)} = 0.01\Omega$).

Also, the similar sensitivity study can be done to determine minimum
$R_i(i = 5,7,...,15)$ under different grid impedance settings when the virtual
impedances $R_j(j \neq i)$ are maintained at identical values. Figure 2.15 presents the
minimum virtual impedances for each harmonic while the rest are at 0.01Ω,
0.02Ω, 0.05Ω and 0.1Ω, respectively. The results show that for minimum virtual
impedance can be as small as 2.22mΩ when $R_i = 0.01\Omega$ and $Z_g = 10Z_{g\_base}$ (for the
15th harmonic).

Time-domain simulation is carried out under different grid impedances when
identical virtual impedances are selected for the dominant harmonics. Figure 2.16

(a) ~ (d) shows the steady state performance (the ratio of harmonic content and THD of grid current after/ before compensation) under different grid impedances when identical virtual impedances are at 0.01Ω, 0.02Ω, 0.05Ω and 0.1Ω, respectively.
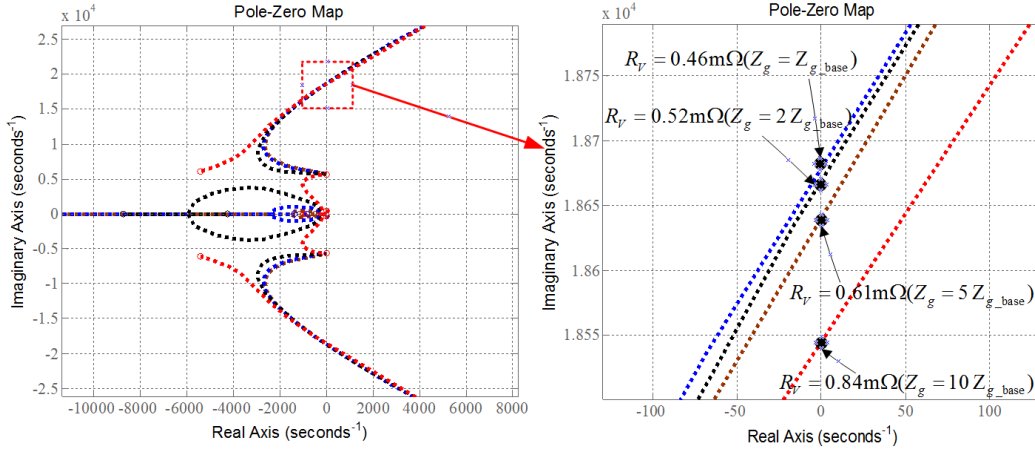
Figure 2.14 Pole positions when R_3 is seen as variable while the rest of virtual impedances are all maintained at 0.01Ω for different grid impedances

(c)   (d)
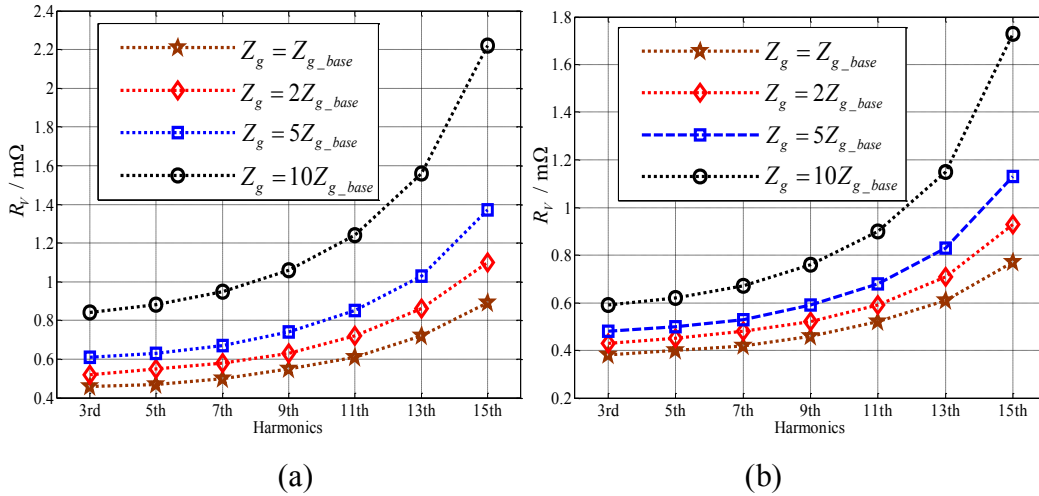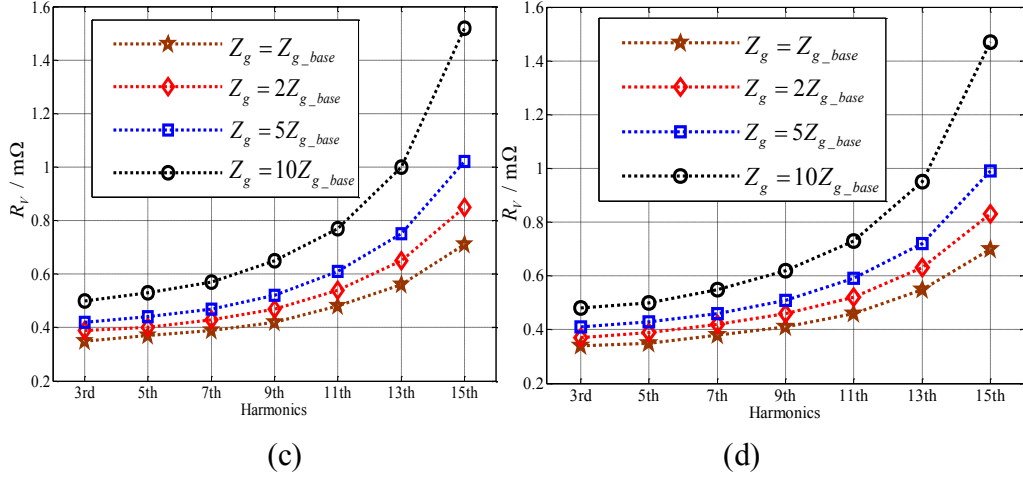
Figure 2.15 Minimum virtual impedances for each harmonic while the rest are maintained at (a) 0.01Ω. (b) 0.02Ω. (c) 0.05Ω. (d) 0.1Ω.

(a)   (b)

(c)   (d)
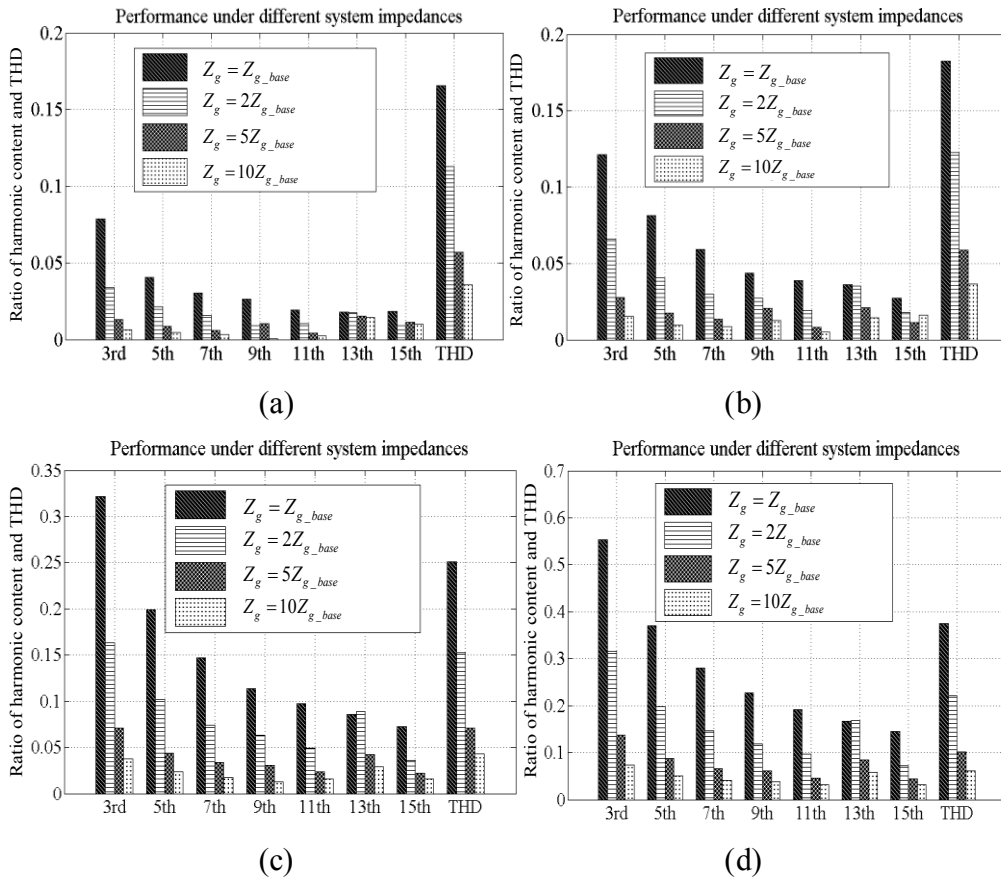
Figure 2.16 Steady state performances (ratio of harmonic content and THD of grid current) under different grid impedances when identical virtual impedances are at (a) 0.01Ω. (b) 0.02Ω. (c) 0.05Ω. (d) 0.1Ω.

It is clear that harmonic mitigation performance by Micro-APF with SHC scheme is more significant for higher order harmonics. Better steady state performance can be obtained under larger grid impedance. Also, the impact of virtual impedances (control gains) becomes less significant as the grid impedance is increased, and the impact of grid impedance on lower order harmonics is more obvious.

Overall, the recommendation range of virtual impedances (0.01~0.02Ω) is attainable when Z_g is increased up to ten times of base case value. Also, both dynamics and steady state performance can be guaranteed within this range.

2.3 Summary

This chapter discusses the control realization of Micro-APF based on voltage-detection compensation (virtual impedance) approach. Both universal harmonic compensation (UHC) scheme and selective harmonic compensation (SHC) scheme are presented. If both dynamics and steady state performance are taken into consideration, a recommendation range of virtual impedances is necessary. So stability analysis is carried out to determine the attainable range of virtual impedances for UHC and SHC schemes, respectively. Sensitivity study is implemented to study the impact of grid impedance on the minimum values of virtual impedances in SHC scheme. Time-domain simulation is carried out to verify the compensation performances by these two schemes. The stability analysis and time-domain simulation results illustrate that the recommendation range of virtual impedances (0.01~0.02Ω) is attainable.

Chapter 3

Harmonic Impedance and Impact on System Performance

In Chapter 2, the control realization of Micro-APF based on UHC scheme and SHC scheme are discussed. In spite of the fact that UHC scheme is simpler than SHC scheme, i.e., only a high-pass filter is involved in the harmonic extraction block, and the harmonics throughout the spectrum can be extracted altogether, more challenging issue in UHC scheme exists considering the requirement for control bandwidth. Another concern is that UHC scheme is proved to be helpless in some cases, especially where specific dominant harmonics or even interharmonics are mainly concerned about.

This chapter mainly focuses on the harmonic impedance of Micro-APF and its impact on system performance. Based on its unique advantage in selective compensation, SHC scheme is adopted throughout the discussion. In Section 3.1, a practical scenario is introduced, where interharmonics are seen as the 'useful' harmonics and should not be filtered out together with the dominant harmonics. Some sensitivity studies are also done to study the impact of control realization on interharmonics based on SHC scheme. Control under rotational d-q frame is also involved in this chapter to compare with compensation under stationary frame.

3.1 Problem Definition

3.1.1 A Practical Scenario

In real powerline transmission, some specific interharmonics are often not regarded as unwanted noise but useful signals. For example, powerline carrier based AMR (Automatic meter reading) system uses 555Hz and 585Hz for command signals from substation to meters. Figure 3.1 shows the powerline

carrier meter reading system operates at 555Hz and 585Hz, two interharmonics highlighted in red.

Considering about this case, if UHC scheme is adopted, these interharmonics will also be filtered out since high-pass filter cannot selectively compensate specific harmonic while 555Hz and 585Hz are close to 9th harmonic (540Hz). SHC scheme can select to compensate the desired dominant harmonics, at the same time mitigate the impact on other frequencies. However, this does not mean that SHC scheme has no influence in interharmonics between two dominant harmonics in spectrum. Therefore, the frequency domain response of Micro-APF needs to be studied.
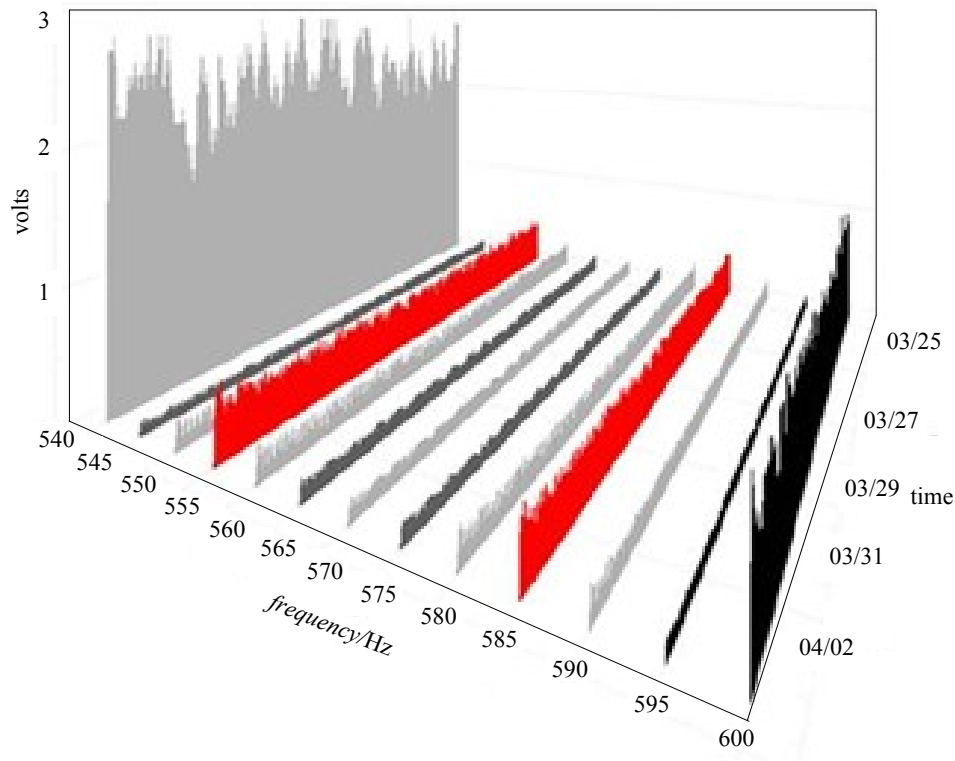
Figure 3.1 Powerline carrier meter reading system operates at 555Hz and 585Hz
(two interharmonics highlighted in red)

3.1.2 Qualitative Description for Equivalent Impedance of Micro-APF

The diagram in Figure 3.2 illustrates the current control loops of voltage-detection compensation approach. Equation (3.1) and (3.2) hold for SHC scheme.
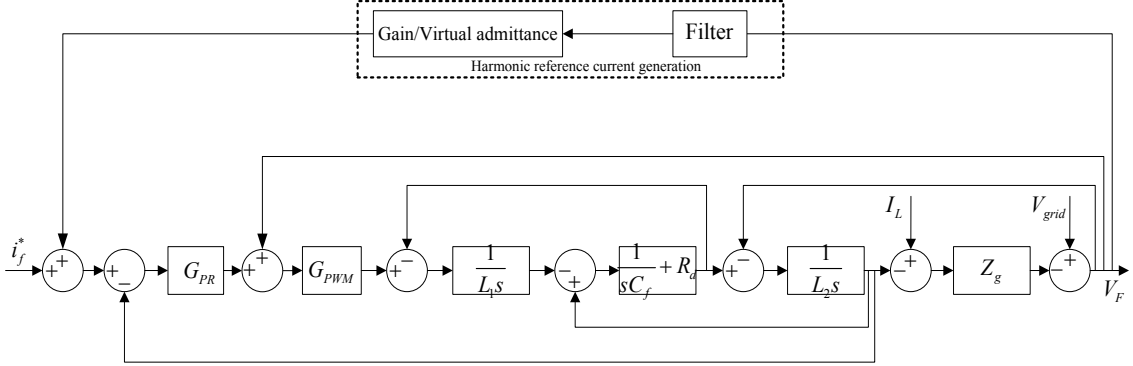
Figure 3.2 Current control loops of voltage-detection compensation approach

$$\begin{cases} I_F + \dfrac{1}{L_1 s}\left\{\left[\left(I_f^* + V_F G_i - I_F\right)G_{PR} + V_F\right]G_{PWM} - V_C\right\} = I_C \\[3mm] I_C\left(\dfrac{1}{sC_f} + R_d\right) = V_C \\[3mm] (V_F - V_C)\dfrac{1}{L_2 s} = I_F \\[3mm] V_{grid} - (I_L + I_F)Z_g = V_F \\[3mm] G_i = \displaystyle\sum_{j=3,5,7...} G_{BPFj} / R_j \end{cases} \qquad (3.1)$$

$$V_F = Z_F(s)\cdot I_F - Z_f(s)\cdot I_f^* \qquad (3.2)$$

where

$$Z_F(s) = \frac{s^3 L_1 L_2 C_f + (1 + sC_f R_d)(L_1 s + L_2 s - G_{PR}G_{PWM})}{s^2 L_1 C_f + (1 + sC_f R_d)(1 - G_{PWM} - G_i G_{PR}G_{PWM})}$$

$$Z_f(s) = \frac{(1 + sC_f R_d)G_p G_{PWM}}{s^2 L_1 C_f + (1 + sC_f R_d)(1 - G_{PWM} - G_i G_{PR}G_{PWM})}$$

The transfer function from I_F to V_F can be used to qualitatively describe the equivalent impedance of Micro-APF. According to equation (3.2), it is obvious that the grid impedance Z_g is not included in the expression of $Z_F(s)$. So if other designed parameters of Micro-APF are decided, the control gains (virtual impedances) and notch filter are the two major factors that may contribute to the variation of harmonic impedance. Figure 3.3 shows the Bode diagram of $Z_F(s)$ when $R_{i(i=3,5,\ldots,15)} = 0.01\Omega$. It is clear that at fundamental frequency, the magnitude of $Z_F(s)$ is much higher than other frequencies which means that under fundamental frequency the equivalent impedance of Micro-APF behaves as a large value compared with the selected dominant harmonics in SHC scheme. At the selected dominant harmonics, the magnitude is around -40dB, i.e., the equivalent impedance under these frequencies is around 0.01Ω, which is expected since $R_V = 0.01\Omega$ is selected for all the selected dominant harmonics. Also, the phase diagram shows that the phase at these frequencies is close to 0, which means that the impedance is resistive.
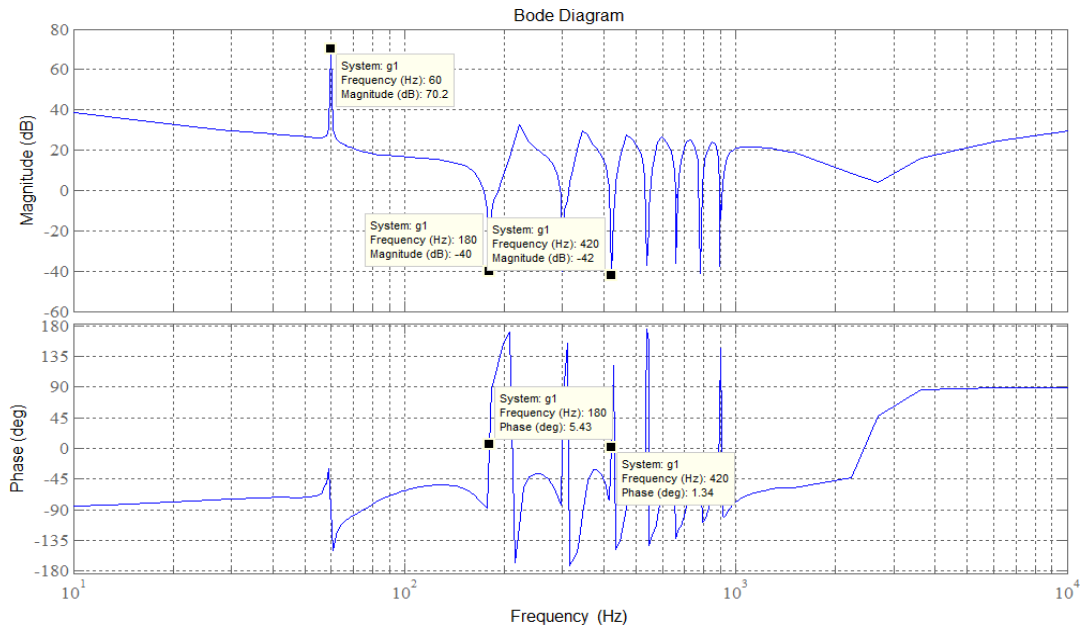
Figure 3.3 Bode diagram of $Z_F(s)$ when $R_{i(i=3,5,\ldots,15)} = 0.01\Omega$

Figure 3.4 shows the zoomed-in Bode diagram of $Z_F(s)$ from 525Hz to 675Hz under different control gains (virtual impedances). Overall, at the dominant frequencies, the magnitudes are almost as large as the set virtual impedances. Due to the existence of notch filters tuned at 540Hz (9th harmonic) and 660Hz (11th harmonic), before reaching its maximum value the magnitude curve goes up and then goes down until arrives at next dominant frequency. The control gains (virtual impedances) can significantly influence the impedance curves, i.e., larger gains are corresponding to larger virtual impedances, so the curves are higher in the magnitude diagram.
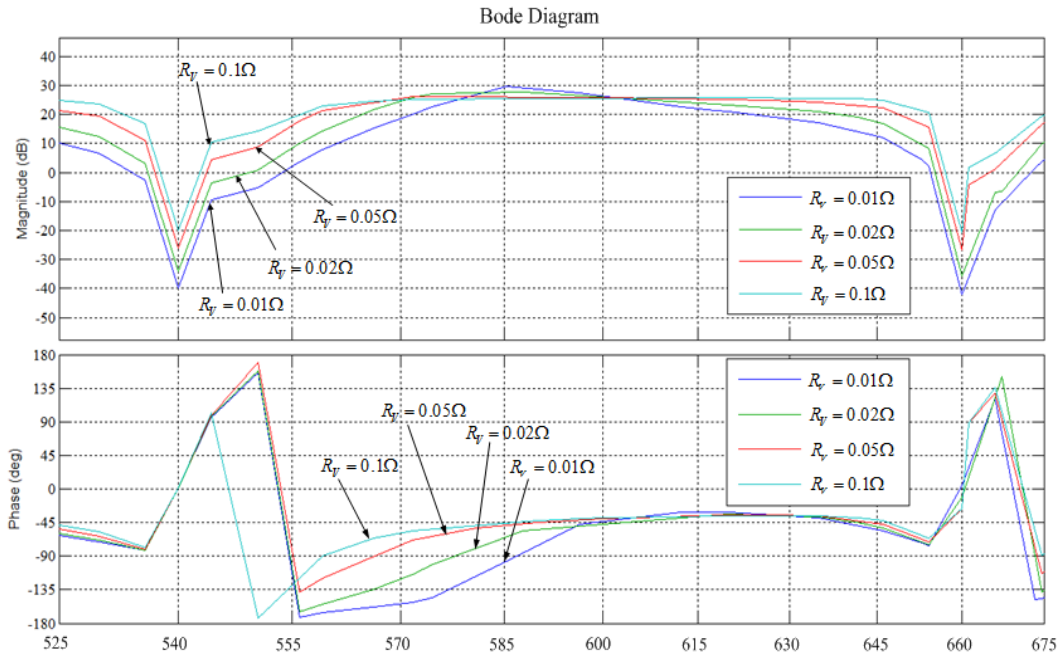
Figure 3.4 Bode diagram of $Z_F(s)$ at different gains (525Hz~675Hz)

As AMR carrier signals are mainly interharmonics of 555Hz and 585Hz, so in the following sensitivity studies, harmonic voltage source of 555Hz and 585Hz is added to the grid side based on the previous time-domain simulation model. Therefore, the current source of dominant harmonics at load side together with the voltage source of interharmonics at source side will contribute to the distortion of V_F and I_S altogether.

3.2 Theoretical Analysis

The qualitative description for equivalent impedance of Micro-APF is discussed in the previous section, and it is obvious that the harmonic impedance is variable under frequency-domain. This section focuses on the impact of harmonic impedance on system performance based on theoretical analysis.

Figure 3.5 shows the equivalent circuit under AMR harmonic signals (555Hz and 585Hz). Equation (3.5) can be obtained from (3.3) and (3.4), and (3.8) can be derived from (3.6) and (3.7).
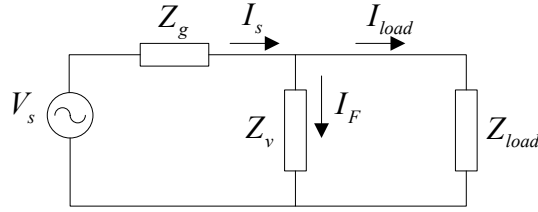
Figure 3.5 Equivalent circuit under AMR harmonic signals

$$I_{load}^{with\,APF} = \frac{V_s}{\dfrac{Z_{load}Z_v}{Z_{load}+Z_v}+Z_g}\cdot\frac{Z_v}{Z_{load}+Z_v} = \frac{V_s}{Z_{load}+Z_g(1+\dfrac{Z_{load}}{Z_v})} \tag{3.3}$$

$$I_{load}^{without\,APF} = \frac{V_s}{Z_{load}+Z_g} \tag{3.4}$$

$$\frac{I_{load}^{with\,APF}}{I_{load}^{without\,APF}} = \frac{Z_{load}+Z_g}{Z_{load}+Z_g(1+\dfrac{Z_{load}}{Z_v})} = \frac{Z_{load}Z_v+Z_gZ_v}{Z_{load}Z_v+Z_gZ_v+Z_{load}Z_g} = \frac{1}{1+\dfrac{1}{Z_v(\dfrac{1}{Z_{load}}+\dfrac{1}{Z_g})}} \tag{3.5}$$

$$V_{load}^{with\,APF} = \frac{V_s}{\dfrac{Z_vZ_{load}}{Z_v+Z_{load}}+Z_g}\cdot\frac{Z_vZ_{load}}{Z_v+Z_{load}} = \frac{Z_vZ_{load}}{Z_vZ_{load}+Z_g(Z_v+Z_{load})}\cdot V_s = \frac{Z_v}{Z_v+Z_g(1+\dfrac{Z_v}{Z_{load}})}\cdot V_s \tag{3.6}$$

39

$$V_{load}^{without\,APF} = \frac{Z_{load}}{Z_{load} + Z_g} \cdot V_s \tag{3.7}$$

$$\frac{V_{load}^{with\,APF}}{V_{load}^{without\,APF}} = \frac{\dfrac{Z_v}{Z_v + Z_g(1 + \dfrac{Z_v}{Z_{load}})} \cdot V_s}{\dfrac{Z_{load}}{Z_{load} + Z_g} \cdot V_s} = \frac{Z_v Z_{load} + Z_v Z_g}{Z_v Z_{load} + Z_g Z_{load} + Z_v Z_g} = \frac{1}{1 + \dfrac{1}{Z_v(\dfrac{1}{Z_{load}} + \dfrac{1}{Z_g})}} \tag{3.8}$$

If the variation of harmonic content (voltage/current) is used to evaluate the impact of Micro-APF on the existing AMR signals, then two terms can be defined as equation (3.9) and (3.10).

$$Attenuation_V = \frac{V_{load}^{with\,APF}}{V_{load}^{without\,APF}} \tag{3.9}$$

$$Attenuation_I = \frac{I_{load}^{with\,APF}}{I_{load}^{without\,APF}} \tag{3.10}$$

It is obvious that the expressions of *Attenuation_I* and *Attenuation_V* in equation (3.5) and (3.8) share the same forms and are both affected by the harmonic impedance Z_V of Micro-APF, grid impedance Z_g and the load impedance Z_{load}.

As is shown in previous study, the grid impedance Z_g is not included in the expression of equivalent impedance (equation (3.2)), which means harmonic impedance of Micro-APF is not affected by the variation of grid impedance. However, the grid impedance does influence the system performance, which can be concluded according to equation (3.5) and (3.8). A larger value of Z_g can directly bring down $Attenuation_{I(V)}$. Also, the control gains (virtual impedances) and designed parameters of notch filters will affect harmonic impedance Z_V, so the factors that can increase Z_V will also raise the value of $Attenuation_{I(V)}$. In addition, the impact of load impedance cannot be ignored as far as

40

Attenuation$_{I(V)}$ is concerned. It is obvious that greater load impedance will reduce *Attenuation*$_{I(V)}$. However, both the load impedance and grid impedance can be seen as constant for a specific system, so only the harmonic impedance Z_V will contribute to the system performance, i.e. the designed parameters of notch filters and control gains (virtual impedances) are the two major factors that impact on system performance. In practical situations, $Z_{load} \gg$ usually holds, so equation (3.11) can be obtained. According to equation (3.11), all factors that may influence system performance can be attributed to the comparison between system impedance and harmonic impedance. For AMR signals, *Attenuation*$_{I(V)} \approx 1$ if $Z_V \gg$, which means the impact of Micro-APF on AMR signals can be ignored, and the larger the difference between Z_V and Z_g is, the more approximately to 1 *Attenuation*$_{I(V)}$ will be.

$$Attenuation_{I(V)} = \frac{1}{1 + \dfrac{Z_g Z_{load}}{Z_v Z_{load} + Z_v Z_g}} = \frac{1}{1 + \dfrac{Z_g}{Z_v(1 + \dfrac{Z_g}{Z_{load}})}} \approx \frac{1}{1 + \dfrac{Z_g}{Z_v}} \qquad (3.11)$$

The above analysis is for AMR signals (interharmonics), however, the dominant harmonics (540Hz) are not the case. Figure 3.6 shows the equivalent circuit under dominant harmonic frequencies (540Hz). Equation (3.14) can be obtained from (3.12) and (3.13).
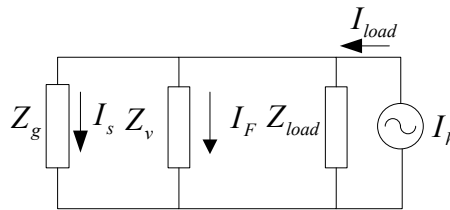
Figure 3.6 Equivalent circuit under dominant harmonic signals (540Hz)

$$I_S^{with\,APF} = \frac{I_{load}}{\dfrac{\dfrac{1}{Z_g} + \dfrac{1}{Z_V} + \dfrac{1}{Z_{load}}}{Z_g}} = \frac{Z_g^2 Z_V Z_{load}}{Z_V Z_{load} + Z_g Z_{load} + Z_g Z_V} I_{load} \qquad (3.12)$$

$$I_S^{without\,APF} = \frac{Z_{load}}{Z_g + Z_{load}} I_{load} \qquad (3.13)$$

$$\frac{I_S^{with\,APF}}{I_S^{without\,APF}} = \frac{\dfrac{Z_g^2 Z_V Z_{load}}{Z_V Z_{load} + Z_g Z_{load} + Z_g Z_V} I_{load}}{\dfrac{Z_{load}}{Z_g + Z_{load}} I_{load}} = \frac{Z_g^2 Z_V (Z_g + Z_{load})}{Z_V (Z_{load} + Z_g) + Z_g Z_{load}} = \frac{Z_g^2 (Z_g + Z_{load})}{Z_{load} + Z_g + \dfrac{Z_g Z_{load}}{Z_V}} \quad (3.14)$$

It is obvious that the value of $I_S^{with\,APF} / I_S^{without\,APF}$ should be minimized as possible as it can be in terms of the dominant harmonics (540Hz) when it comes to the mitigation performance. According to equation (3.14), Z_V should be also minimized as possible. However, according to the previous analysis for AMR signals' equivalent circuit, Z_V should be maximized as possible for interharmonics (555Hz and 585Hz). Overall, the trends of Z_V for the dominant harmonics and interharmonics are the same when we try to optimize the parameters of Micro-APF. So trade-offs have to be made when considering about these two cases at the same time.

3.3 Factors that Influence Harmonic Impedance

Section 3.2 has discussed how harmonic impedance can influence the system performance from the theoretical aspect, and it is pointed out that the difference between grid impedance and harmonic impedance of Micro-APF is the ultimate factor that can contribute to system performance. So in this section, sensitivity studies are carried out to study how these factors, i.e., grid impedance, control gains (virtual impedances) and notch filters, can influence the harmonic

impedance of Micro-APF and how harmonic impedance of Micro-APF can impact the system performance in return.

3.3.1 Impact of Grid Impedance

Similar to the case study in Section 2.2, time-domain simulation is carried out under different settings of Z_g to study the impact of grid impedance. Based on the simulation results of V_F and I_F, Figure 3.7~3.9 show the calculated harmonic impedance at 540Hz, 555Hz and 585Hz under different grid impedance and control gains (virtual impedances).

From Figure 3.7~3.9, it is obvious that grid impedance almost has no impact on harmonic impedance, which agrees with the expression of V_F / I_F in equation (3.2). However, control gains (virtual impedances) will significantly contribute to the harmonic impedance, i.e., larger control gains (smaller virtual impedances) can conduct smaller harmonic impedance and vice versa. Due to the existence of notch filter tuned at 540Hz, the AMR signal at 555Hz will be more significantly influenced compared with the counterpart of 585Hz. Therefore, $Attenuation_{I(V)}$ at 555Hz can be used to judge the impact of Micro-APF on AMR signals. So in the following discussion, 555Hz is considered for $Attenuation_{I(V)}$.
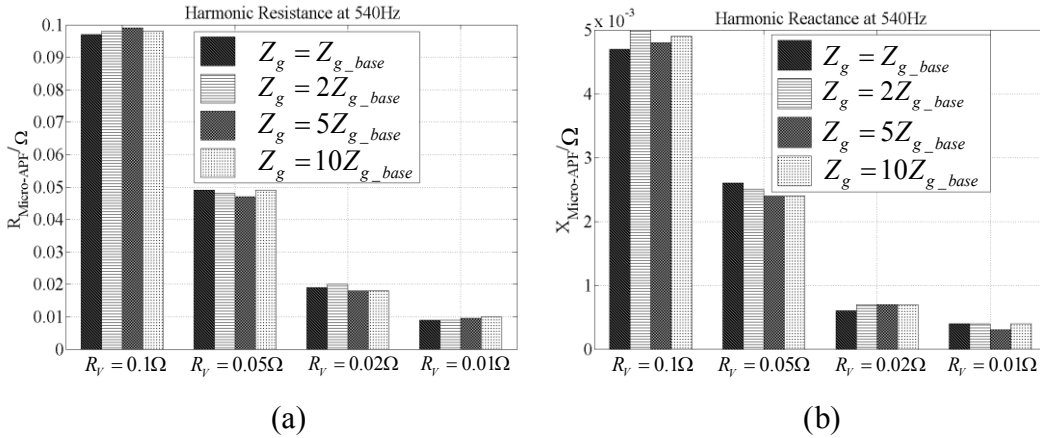
Figure 3.7 Harmonic impedance under 540Hz. (a) Harmonic resistance. (b) Harmonic reactance.

43

(a)   (b)
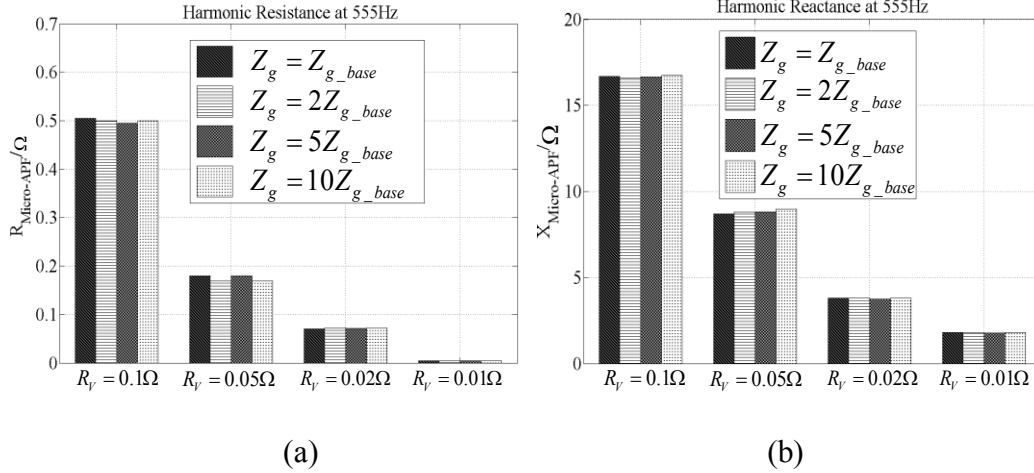
Figure 3.8 Harmonic impedance under 555Hz. (a) Harmonic resistance. (b) Harmonic reactance

(a)   (b)

Figure 3.9 Harmonic impedance under 585Hz. (a) Harmonic resistance. (b) Harmonic reactance

Figure 3.10 shows the performance of Micro-APF under different grid impedances and control gains (virtual impedances). It is obvious that control gains (virtual impedances) can significantly influence the impact of Micro-APF on the carrier signals (*Attenuation$_{I(V)}$* at 555Hz). Larger gains (smaller virtual impedances) lead to greater reduction of AMR interharmonic signals contained in the load current or voltage. By comparing Figure 3.10 (a) and (b), it is obvious that the impact of gains (virtual impedances) or grid impedance on load current and

voltage are almost the same, which is consistent with the definition of *Attenuation$_I$* and *Attenuation$_V$* expressed in equation (3.5) and (3.8). As for the grid impedance Z_g, more significant impact can be seen when it goes up. Moreover, for the dominant harmonic (540Hz), larger grid impedance will lead to better mitigation performance for a certain control gain (virtual impedance) value while the impact of grid impedance will become less significant as the virtual impedances are decreased.

(a)

(b)

(c)
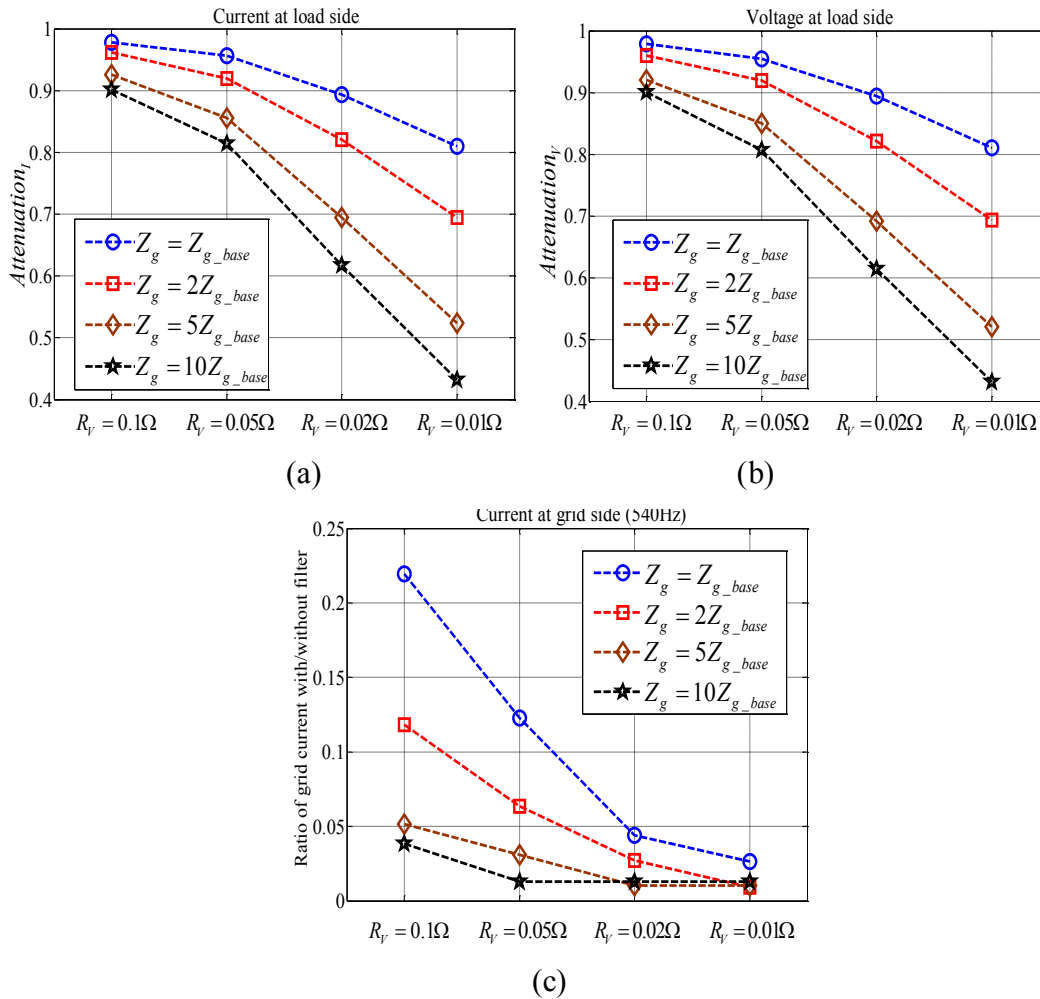
Figure 3.10 Impact of grid impedance on system performance under different control gains (virtual impedances). (a) *Attenuation$_I$* (555Hz) at different virtual impedances and Z_g. (b) *Attenuation$_V$* (555Hz) at different virtual impedances and Z_g. (c) Impact on 540Hz (comparison of with/without Micro-APF)

3.3.2 Impact of Notch Filter

In Section 3.3.1, sensitive study is carried out in terms of grid impedance at different control gains (virtual impedances). Apart from the control gains (virtual impedances), notch filters are another factor that can contribute to the influence in system performance.

Figure 3.11 shows the SHC scheme under stationary frame. Overall, the notch filter tuned at 540Hz is the key factor in terms of the AMR carrier signals (555Hz and 585Hz) since these two interharmonics are so close to the central frequency. The transfer function of the ith notch filter is shown as equation (3.15).

$$G_{BPFi} = \frac{2K_C\omega_C s}{s^2 + 2\omega_C s + (i\omega_e)^2} \tag{3.15}$$
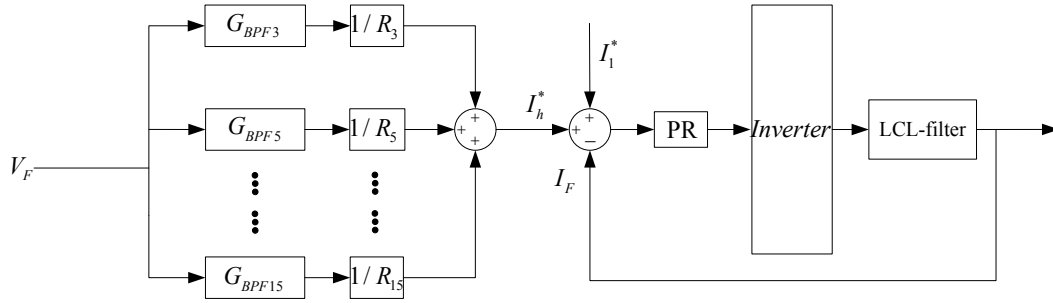
Figure 3.11 filtering under stationary frame

For a notch filter tuned at a specific dominant frequency, the bandwidth ω_C and integral K_C are the only two parameters that may affect the performance of notch filters. Apparently, the integer K_C should be maintained as 1 in order to realize no attenuation for non-dominant harmonics. Figure 3.12 shows the frequency-domain response of the 9th order notch filter under different values of ω_C ($K_C = 1$). It is clear that ω_C can significantly influence the magnitude of bands around the central frequency. When $K_C = 1$, the magnitude of G_{BPFi} is almost equal to 1 and

narrower bandwidth, i.e., smaller ω_C, will lead to more significant impact on the magnitude of G_{BPFi} under interharmonics. Also, when $\omega_C = 0.5\,\text{rad/s}$ and $K_C = 1$, it is obvious that the magnitude of G_{BPFi} at 585Hz is almost 1/3 of that at 555Hz, which means that the impact of notch filter is more significant at 555Hz, compared with 585Hz.

The ideal case for the 9th order notch filter should satisfy two conditions: (1) it can allow the 9th harmonic (540Hz) to pass without being damped; (2) other frequencies should be stopped altogether. The case study and theoretical analysis demonstrate that trade-offs have to be made as for the selection of ω_C values.
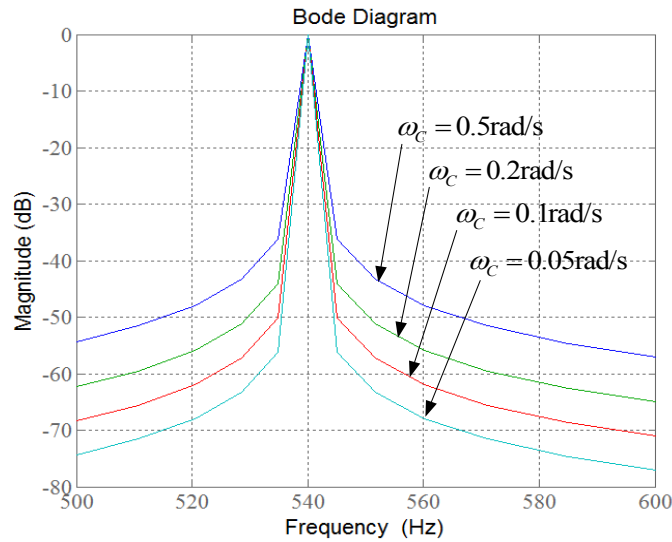
Figure 3.12 Frequency-domain response of the 9th order notch filter under different ω_C ($K_C = 1$)

Figure 3.13~3.15 show the calculation results of harmonic impedance at 540Hz, 555Hz and 585Hz under different ω_C and virtual impedances based on time-domain simulation.

According to the calculation results, it is obvious that smaller bandwidth leads to larger harmonic impedance. As the interharmonic 555Hz is closer to the dominant frequency 540Hz, the impact of Micro-APF is much more significant on it

compared with the 585Hz. Overall, harmonic impedance of Micro-APF at 585Hz is much greater than that of 555Hz. The impedance at the dominant frequency 540Hz is much smaller than the interharmonics due to the existence of the 9th notch filter. However, only in the case of $\omega_C = 0.5\text{rad/s}$, the harmonic impedance at 540Hz can be almost equal to the desired virtual impedance value, for example, the resistance is 0.095Ω, 0.046Ω, 0.019Ω and 0.0085Ω when $R_V = 0.1\Omega$, $R_V = 0.05\Omega$, $R_V = 0.02\Omega$ and $R_V = 0.01\Omega$, respectively. Also, the reactance X is almost zero when $\omega_C = 0.5\text{rad/s}$, which means that the harmonic impedance of Micro-APF at 540Hz is resistive as desired. In addition, the selection of ω_C will almost have no impact on harmonic impedance when the virtual impedance is chosen as $0.01 \sim 0.02\Omega$.

(a)   (b)
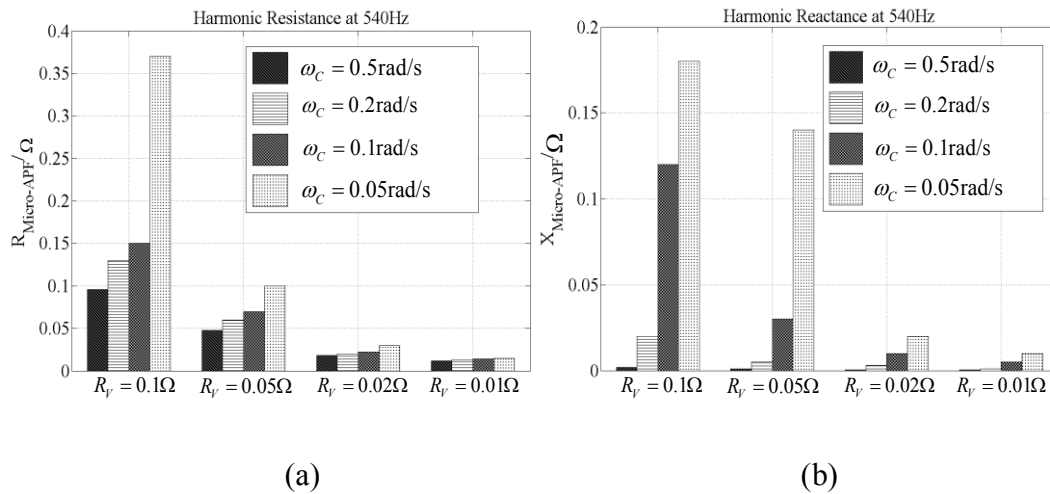
Figure 3.13 Harmonic impedance under 540Hz. (a) Harmonic resistance. (b) Harmonic reactance.

(a)   (b)
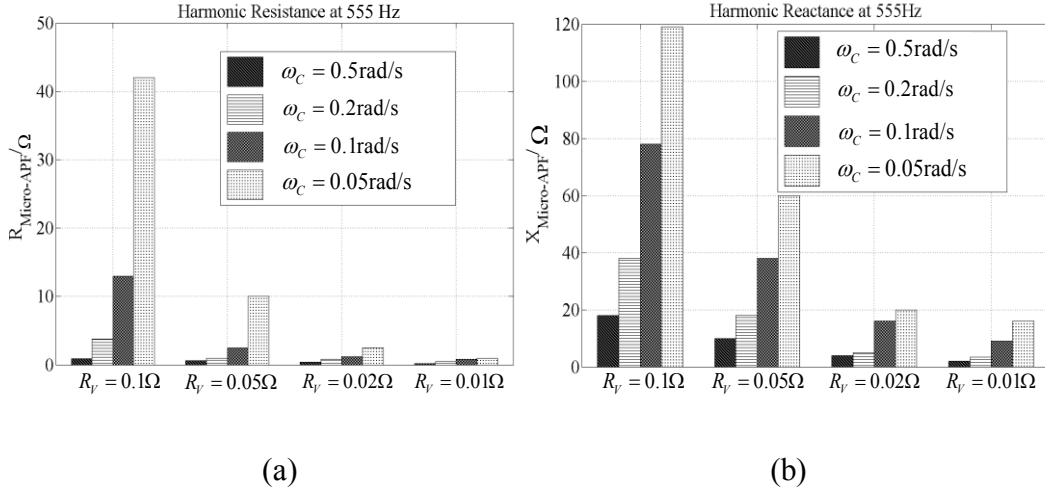
Figure 3.14 Harmonic impedance under 555Hz. (a) Harmonic resistance. (b)
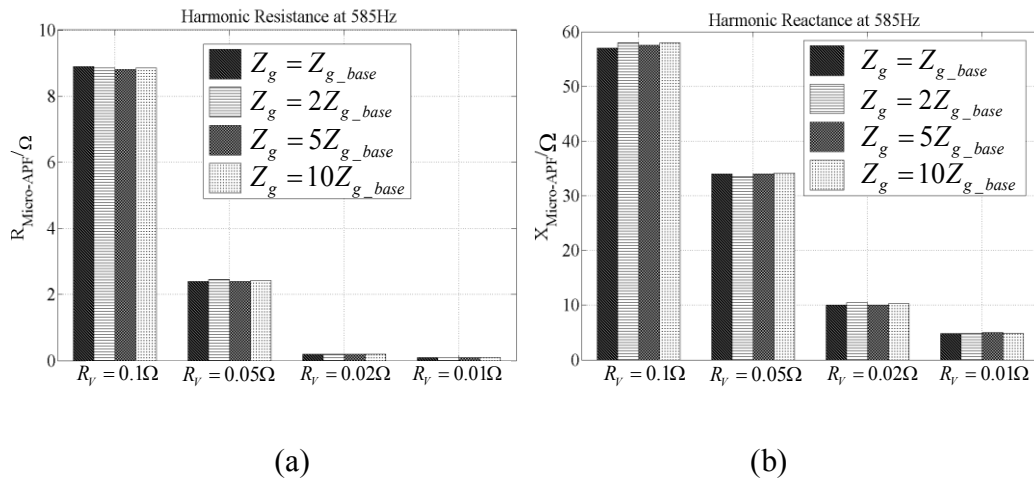
Harmonic reactance

(a)   (b)
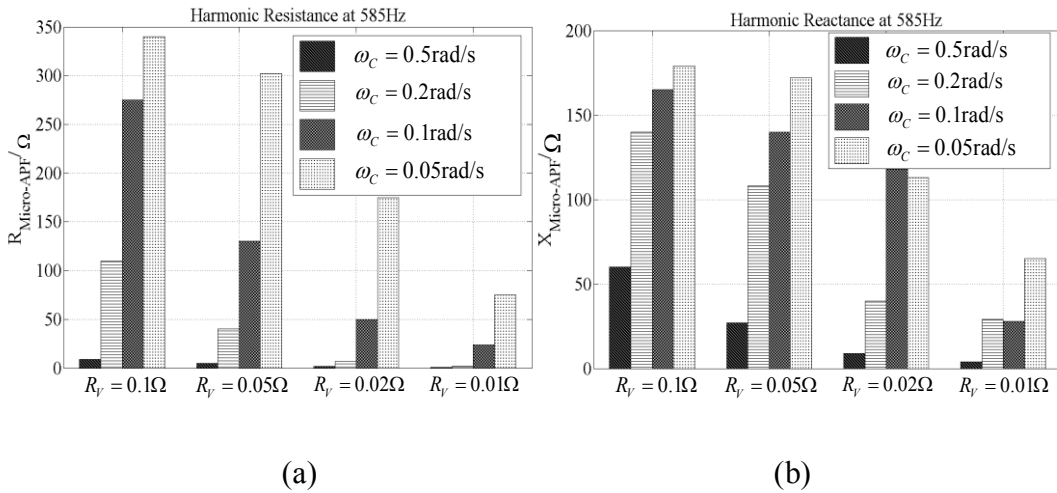
Figure 3.15 Harmonic impedance under 585Hz. (a) Harmonic resistance. (b)

Harmonic reactance.

Figure 3.16 shows the impact of ω_C on system performance under different control gains (virtual impedances). As far as the control gains (virtual impedances) are concerned, the results in Figure 3.16 are similar to those in Figure 3.10, i.e., control gains (virtual impedances) can significantly influence the impact of Micro-APF on the carrier signals ($Attenuation_{I(V)}$ at 555Hz) and larger gains (smaller virtual impedances) tend to result in more significant reduction of AMR

interharmonic signals contained in the load current or voltage. Also, the impact of control gains (virtual impedances) or ω_C on the load current and voltage (*Attenuation_I* and *Attenuation_V*) are almost the same. Overall, smaller bandwidth conducts less reduction of AMR signals contained in load current or voltage, in other words, smaller bandwidth can lessen the impact of Micro-APF on interhamonics.

It is obvious that considering interharmonics, bandwidth of notch filters should be as small as possible. However, this is not the case for the dominant harmonics apparently. According to the results shown in Figure 3.16(c), if the bandwidth is narrowed, the impedance of the dominant harmonic (540Hz) is also increased, which leads to less significant mitigation performance in terms of the harmonic current content (540Hz) at the grid side. However, ω_C = 0.1~0.5rad/s is acceptable for 540Hz when $R_V \leq 0.05\Omega$. As for 555Hz, ω_C =0.05~0.5rad/s is acceptable when R_V=0.01~0.02Ω (*Attenuation_{I(V)}* > 0.8). Typically, *Attenuation_{I(V)}* > 0.89 when R_V=0.02Ω and ω_C= 0.05~0.5rad/s. So the recommendation settings are ω_C= 0.1~0.5rad/s and R_V=0.01~0.02Ω.

(a)   (b)
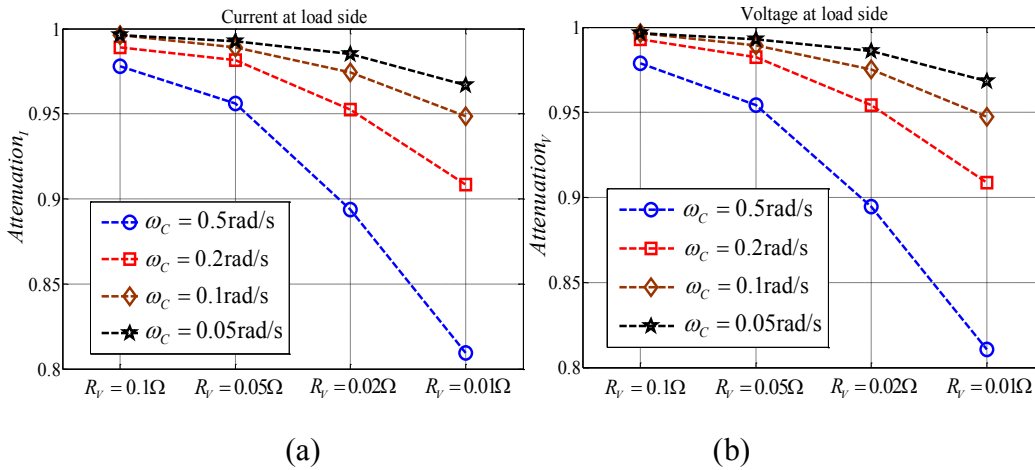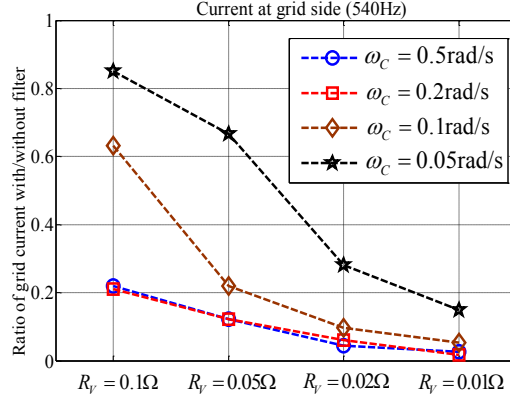
Figure 3.16 Impact of ω_C on system performance under different control gains (virtual impedances). (a) *Attenuation$_I$* (555Hz) at different gains and ω_C. (b) *Attenuation$_V$* (555Hz) at different gains and ω_C. (c) Impact on 540Hz (comparison of with/without Micro-APF).

Figure 3.17 shows the frequency-domain response of $Z_F(s)$ under different ω_C values (540~560Hz). It is obvious that the harmonic impedance of Micro-APF has negative-correlation with ω_C, which is consistent with the previous results, i.e., in order to increase the harmonic impedance, the bandwidth should be decreased accordingly, however, the increase or reduction of harmonic impedance at interharmonics and dominant harmonics are at the same trend. So trade-off exists in terms of ω_C.

Base on the discussion in this section, it can be concluded that trade-off exists in the selection of ω_C values when the impact of notch filter on the equivalent impedances of Micro-APF at both dominant harmonics and interharmonics are concerned about. Due to the fact that when ω_C =0.5rad/s (K_C =1), the notch filters tuned at the dominant frequencies can ensure the harmonic impedances at the selected frequencies to exhibit as desired, the case "ω_C=0.5rad/s and K_C =1" is strongly recommended as for the configurations of notch filters. So "ω_C =0.5rad/s and K_C =1" is used as the base case throughout this thesis. As for

control gains (virtual impedances), the impact of ω_C will be less significant when they are chosen within 0.01~0.02Ω.
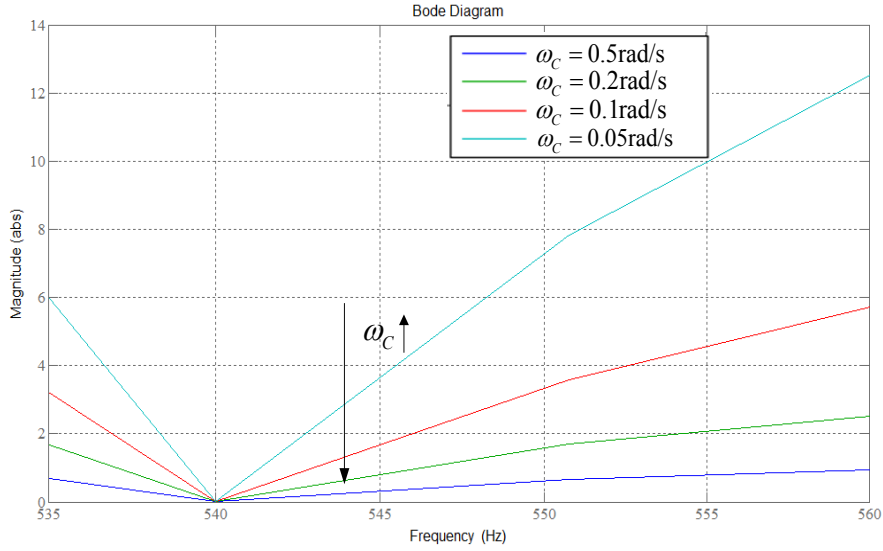
Figure 3.17 Frequency-domain response of $Z_F(s)$ under different ω_C values

(540~560Hz)

Table 3.1 illustrates the simulation results of *Attenuation$_I$* (555Hz) and *Attenuation$_V$* (555Hz) in the base case. It is obvious that the values of *Attenuation$_I$* (555Hz) and *Attenuation$_V$* (555Hz) under the same settings are almost equal. Results of harmonic impedances at 540Hz and 555Hz based on the transfer function of Z_F can be calculated as well. The calculated harmonic impedances are then substituted into equation (3.5) (or equation (3.8)) and equation (3.11), respectively.

Figure 3.18(a) compares the simulation and calculation results of *Attenuation$_I$* (555Hz) by equation (3.5) and (3.11) respectively. Also, the comparison of simulation and calculation results of harmonic content with/without Micro-APF at 540Hz is shown in Figure 3.18(b). According to Figure 3.18, it is clear that the overall trends of calculation and simulation results can match well.

Table 3.1 Simulation results of *Attenuation$_I$* (555Hz) and *Attenuation$_V$* (555Hz) in the base case

	R_V=0.1Ω	R_V=0.05Ω	R_V=0.02Ω	R_V=0.01Ω
Attenuation$_I$	0.9780	0.9560	0.8938	0.8095
Attenuation$_V$	0.9789	0.9544	0.8947	0.8105

(a)　　　　　　　　　(b)
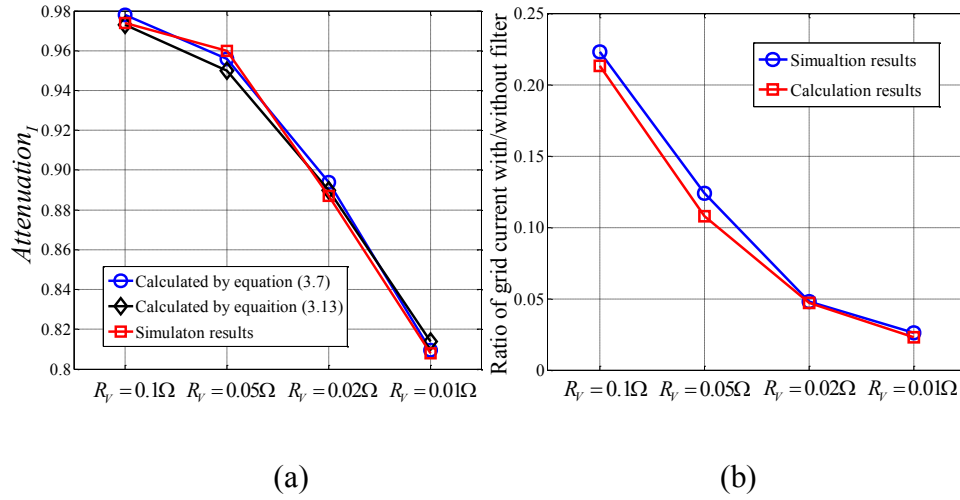
Figure 3.18 Comparison between calculation and simulation results. (a) *Attenuation$_I$* (555Hz) under different control gains (virtual impedances). (b) Harmonic content with/without Micro-APF (540Hz)

3.4　Scheme under Multiple D-Q Frames

As is discussed in Section 3.2 and 3.3, restriction exists in the scheme under stationary frame by notch filters, especially for the AMR scenario. So an intuitive solution is that harmonic extraction block should be improved to overcome the trade-offs as far as the harmonic impedances at both AMR signals and unwanted dominant harmonics are concerned. So this section will discuss the scheme under multiple d-q frames.

Figure 3.19 shows the SHC scheme under rotational d-q frames. Assume that the distorted grid voltage can be expressed by equation (3.16), and after the transform expressed by equation (3.17), d-axis and q-axis components can be obtained:
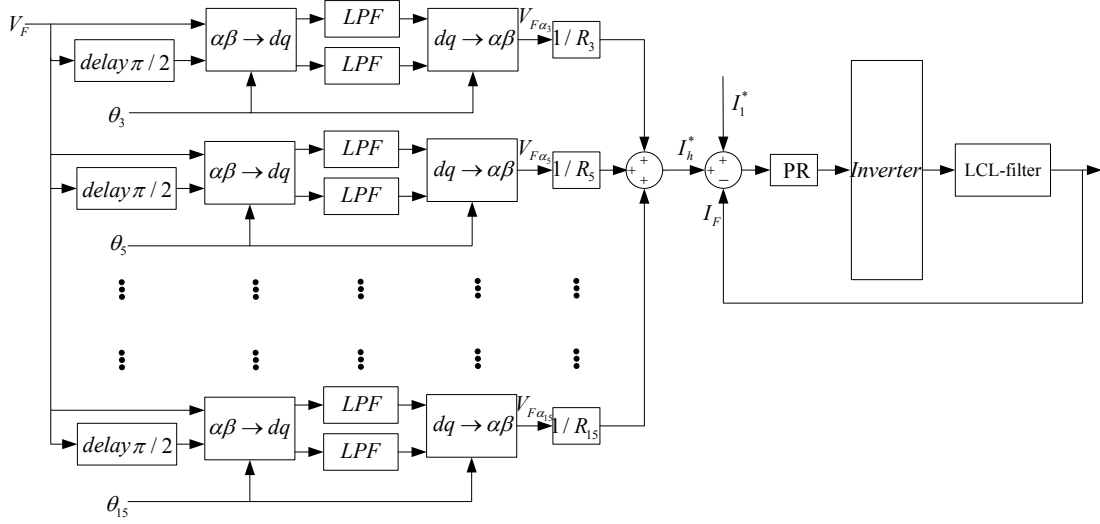
Figure 3.19 Scheme under multiple d-q frames

$$\begin{cases} V_{F\alpha} = \sum_{i=1,3,5...} V_i \cos(i\omega_e t + \theta_i) \\ V_{F\beta} = \sum_{i=1,3,5...} V_i \cos(i\omega_e t + \theta_i - \frac{\pi}{2}) = \sum_{i=1,3,5...} V_i \sin(i\omega_e t + \theta_i) \end{cases} \quad (3.16)$$

$$\begin{bmatrix} V_{Fd} \\ V_{Fq} \end{bmatrix} = \begin{bmatrix} \cos(\omega_r t) & \sin(\omega_r t) \\ -\sin(\omega_r t) & \cos(\omega_r t) \end{bmatrix} \begin{bmatrix} V_{F\alpha} \\ V_{F\beta} \end{bmatrix} \quad (3.17)$$

$$V_{Fd} = \sum_{i=1,3,5...} V_i \cos(i\omega_e t + \theta_i) \cos(\omega_r t) + \sum_{i=1,3,5...} V_i \sin(i\omega_e t + \theta_i) \sin(\omega_r t)$$

$$= \sum_{i=1,3,5...} \frac{V_i}{2} [\cos(i\omega_e t + \theta_i + \omega_r t) + \cos(i\omega_e t + \theta_i - \omega_r t)] - \sum_{i=1,3,5...} \frac{V_i}{2} [\cos(i\omega_e t + \theta_i + \omega_r t)$$

$$-\cos(i\omega_e t + \theta_i - \omega_r t)] = \sum_{i=1,3,5...} V_i \cos(i\omega_e t + \theta_i - \omega_r t) = \sum_{i=1,3,5...} V_i \cos[(i\omega_e - \omega_r)t + \theta_i]$$

54

$$V_{Fq} = -\sum_{i=1,3,5...} V_i \cos(i\omega_e t + \theta_i) \sin(\omega_r t) + \sum_{i=1,3,5...} V_i \sin(i\omega_e t + \theta_i) \cos(\omega_r t)$$

$$= -\sum_{i=1,3,5...} \frac{V_i}{2} [\sin(i\omega_e t + \theta_i + \omega_r t) + \sin(i\omega_e t + \theta_i - \omega_r t)] + \sum_{i=1,3,5...} \frac{V_i}{2} [\sin(i\omega_e t + \theta_i + \omega_r t)$$

$$+ \sin(i\omega_e t + \theta_i - \omega_r t)] = \sum_{i=1,3,5...} V_i \sin(i\omega_e t + \theta_i - \omega_r t) = \sum_{i=1,3,5...} V_i \sin[(i\omega_e - \omega_r)t + \theta_i]$$

Now consider the fact that fundamental current/voltage can be converted into DC quantities under the d-q frame which is rotating at the synchronous speed of $\omega_r = \omega_e$, if the d-q frame is rotating at the speed of $\omega_r = k\omega_e$, the kth harmonic will become DC quantities under this frame. So the DC component corresponding to the kth harmonic under the kth d-q frame can be extracted with a simple first order low-pass filter. Therefore the harmonics can be easily extracted one by one under different d-q frames.

Compared with the notch filters tuned at different selected frequencies in the stationary frame scheme, a first order low-pass filter is enough in this scheme. Also, the factor that may influence the harmonic impedance of Micro-APF and system performance is the cut-off frequency ω_{fc}, while the bandwidth ω_C can make contribution to the performance in the scheme under stationary frame.

Under the kth d-q frame, the frequency range $[kf_e, (k+1)f_e]$ under stationary frame will be converted into $[0, f_e]$. Therefore, under the d-q frame with the synchronous speed of $\omega_r = 9\omega_e$, the frequency range [540Hz, 600Hz] under stationary frame corresponds to [0, 60Hz], i.e., 555Hz and 585Hz will be mapped to 15Hz and 45Hz respectively. So the low-pass filters under different d-q frames can have identical cut-off frequency.

Case study is also carried out by time-domain simulation to verify the system performance under multiple d-q frames. Figure 3.20 compares the steady state performance under different grid impedances and control gains (virtual impedances) by stationary frame scheme and multiple d-q frames scheme. As for the multiple d-q frames scheme, 1st order low-pass filter with cut-off frequency

0.2π rad/s (0.1Hz) is involved while $\omega_C = 0.5$ rad/s and $K_C = 1$ for stationary frame scheme. It is obvious that under multiple d-q frames scheme, the performance at AMR signals is better than that by stationary frame scheme. However, as for the unwanted dominant harmonics (540Hz), the results by stationary frame scheme is slightly better. Overall, the same trends can be obtained by multiple d-q frames scheme compared with stationary-frame in terms of grid impedances and control gains (virtual impedances).
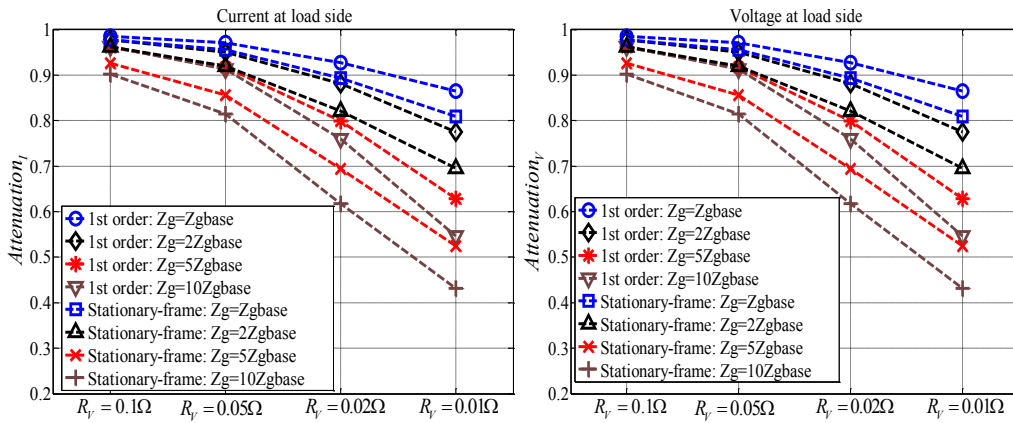
(a)

(b)
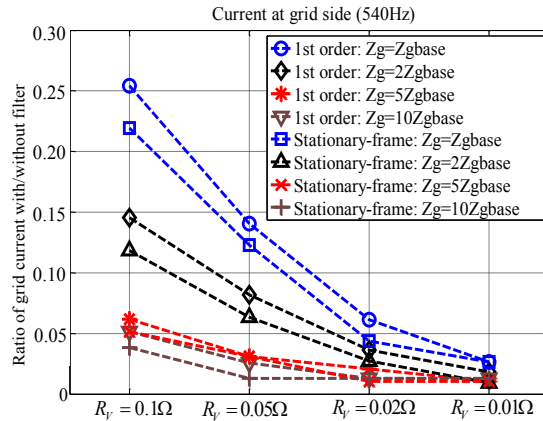
(c)

Figure 3.20 Comparison of results by stationary frame scheme and multiple d-q frames scheme. (a) *Attenuation*$_I$ (555Hz) under two schemes. (b) *Attenuation*$_V$ (555Hz) under two schemes. (c) Impact on 540Hz (comparison of with/without Micro-APF)

According to the frequency-domain response of first-order low-pass filter under different cut-off frequencies, it is easy to conclude that lower cut-off frequency can enable fewer interharmonics to pass through the low-pass filter, and the impact of Micro-APF on AMR signals is accordingly less significant. In this sense, the cut-off frequency should be as low as possible.

Time-domain simulation is also done to study the influence of cut-off frequency under multiple d-q frames scheme. Figure 3.21 shows the impact of cut-off frequency ω_{f_c} on system performance under different control gains (virtual impedances). In this sensitivity study, only cut-off frequency ω_{f_c} in the 9th d-q frame is changed while those in the rest are maintained at 0.2π rad/s (0.1Hz).

It is obvious that the cut-off frequency ω_{f_c} has positive-correlation with its impact on interharmonics, which is consistent with the analysis. According to Figure 3.21 (a) and (b), the impact of ω_{f_c} on the interharmonics is even much more significant when $\omega_{f_c} \geq 0.02\pi$ rad/s ($f_c \geq 0.01$ Hz). Unlike the interharmonics, cut-off frequency ω_{f_c} almost has no impact on the dominant harmonic (540Hz) since the low-pass filters enable the selected frequencies pass through with no attenuation. So in Figure 3.21 (c), the curves will fluctuate around 0.26, 0.14, 0.06 and 0.03 for $R_V = 0.1\Omega$, $R_V = 0.05\Omega$, $R_V = 0.02\Omega$ and $R_V = 0.01\Omega$, respectively. Also, the value can be approximately calculated by equation (3.16).

(a)   (b)

57
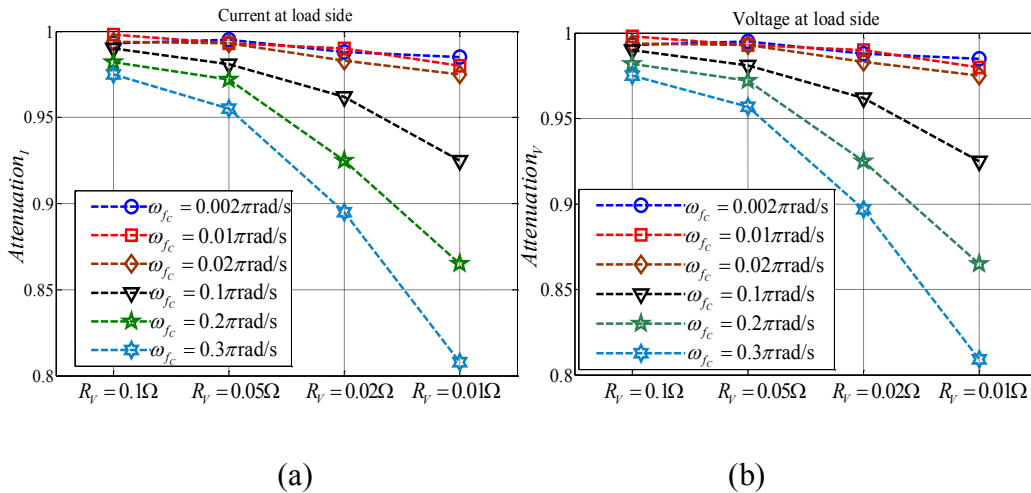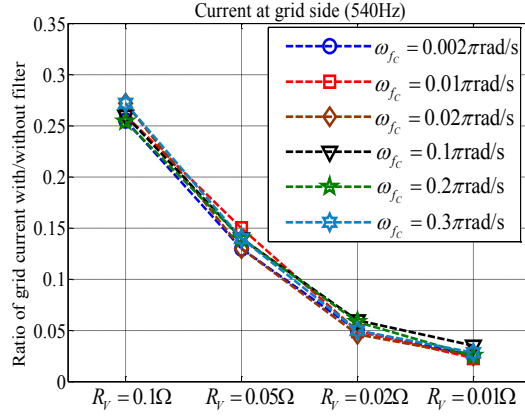
Figure 3.21 Impact of cut-off frequency ω_{f_C} under different control gains (virtual impedances) on system performance (base case). (a) *Attenuation$_I$* (555Hz) under different virtual impedances and ω_{f_C}. (b) *Attenuation$_V$* (555Hz) under different virtual impedances and ω_{f_C}. (c) Impact on 540Hz (comparison of with/without Micro-APF).

According to the results in Figure 3.16 and Figure 3.21, *Attenuation$_{I(V)}$* (555Hz) values for ω_C =0.5rad/s and ω_{f_C} =0.3π rad/s are equal when $R_V = 0.01\Omega$ and $R_V = 0.02\Omega$, respectively. So low-pass filters with cut-off frequency ω_{f_C} can conduct less attenuation for interharmonics compared with notch filters tuned at $\omega_C = \omega_{f_C}$. Also, the advantage of low-pass filters is even more significant for dominant harmonics (540Hz).

Additional case study is carried out when the 1st order low-pass filters are replaced with 2nd order low-pass filters. Figure 3.22 compares the steady state performance under different control gains (virtual impedances) and grid impedances of these two cases. The cut-off frequencies of 2nd order low-pass filters are the same with those of 1st order low-pass filters, i.e., 0.2π rad/s (0.1Hz). It is clear that the results by using 2nd order low-pass filters is better than 1st order

low-pass filters in terms of the steady state performance at both interharmonics and dominant harmonics.

(a)

(b)

(c)
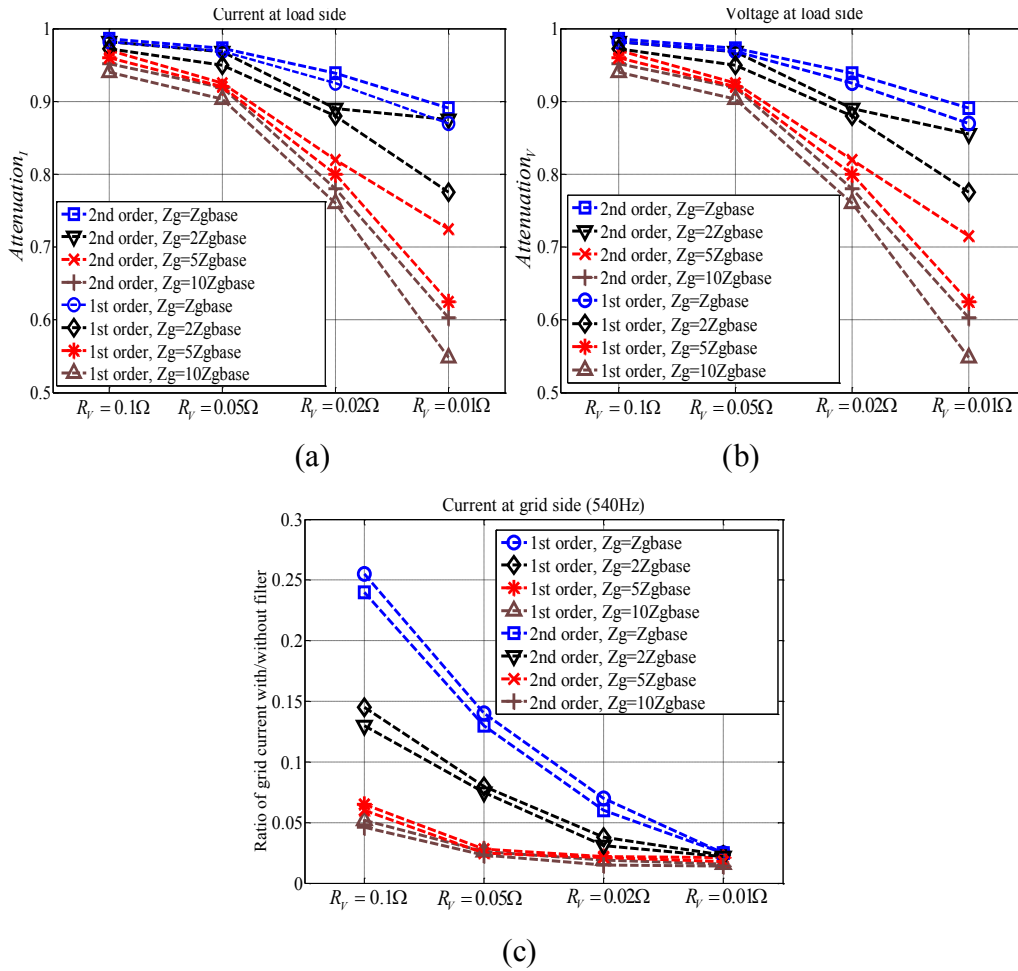
Figure 3.22 Comparison of steady state performance under different control gains (virtual impedances) and grid impedances by 1st order low-pass filters and 2nd order low-pass filters. (a) $Attenuation_I$ (555Hz). (b) $Attenuation_V$ (555Hz). (c) Impact on 540Hz (comparison of with/without Micro-APF).

The above results can be easily illustrated by the frequency-domain responses of 1st order low-pass filter (ω_{f_C} =0.2π rad/s) and 2nd order low-pass filter (ω_{f_C} =0.2π rad/s). In reality, although the steady state performance by 2nd order low-pass filters is better than that by 1st order low-pass filters when they are tuned at the same cut-off frequency, the fact that the higher order low-pass filters will lead to slower dynamic response should not be neglected.

Overall, no matter what scheme is adopted, the filters (notch filters in stationary frame scheme and low-pass filters in multiple d-q frames scheme) will impact the harmonics (dominant harmonics and interharmonics) together with control gains (virtual impedances). According to the curves of *Attenuation*$_{I(V)}$ in Figure 3.21, the impact of control gains (virtual impedances) on interharmonics becomes more prominent when ω_{fc} rises to a certain level. Moreover, larger control gains (virtual impedances) conduct smaller harmonic impedances at both dominant harmonics and interharmonics. From the aspect of interharmonics, cut-off frequency ω_{fc} should be as low as possible; however, smaller ω_{fc} values will slow down the dynamic response as well. So similar to the stationary frame scheme, trade-off still exists when both steady state performance and dynamic response are taken into consideration. So based on the above analysis, the recommended parameters are as follows: ω_{fc} =0.02π rad/s for 9th d-q frame, and ω_{fc} =0.2π rad/s for other d-q frames; virtual impedances $R_9 = 0.1\Omega$ and $R_{i(i\neq9)} = 0.01\Omega$.

Table 3.3 compares the advantages and disadvantages of the control schemes that have been discussed in this thesis.

Table 3.2 Comparison of schemes discussed in this thesis

Compensation Scheme	Advantages	Disadvantages
UHC scheme	Only one high-pass filter is used and the control is relatively simple.	Control bandwidth cannot meet the requirement and selective compensation cannot be achieved.
SHC scheme (Stationary Frame)	Selective compensation can be achieved and the requirement for control bandwidth is lower compared with UHC scheme.	More notch filters are involved and trade-off exists in terms of bandwidth of notch filter.
SHC scheme (Multiple d-q Frames)	Compared with stationary frame, a simple first-order low-pass filter is enough for each d-q frame, and ω_{fc} has less impact on dominant harmonics	Trade-off still exists in terms of cut-off frequency of low-pass filters and more computation is involved for multiple d-q conversion.

Overall, when steady state performance and dynamic response are both taken into consideration, similar trade-offs exist in stationary frame control and multiple d-q frames control, however, multiple d-q frames scheme is still recommended if the time spent on computation is not substantial since results of dominant harmonics will not be affected.

3.5 Summary

This chapter discusses the harmonic impedance of Micro-APF and its impact on system performance. Firstly, a practical scenario is proposed to emphasize the unique advantage of SHC scheme. From the mathematical and circuitry point of view, qualitative analysis on harmonic impedance of Micro-APF and theoretical explanation of the impact on system performance are carried out based on SHC scheme. Sensitivity studies are implemented to study the factors that can influence harmonic impedance. The schemes under stationary frame and multiple d-q frames are compared in this chapter as well, and the theoretical analysis and time-domain simulation results show that similar trade-offs exist in these two schemes as far as the steady state performance and dynamic response are concerned. Based on the case study in this chapter, $\omega_C = 0.5\text{rad/s}$ ($K_C = 1$) is recommended for 9th notch filter, and the virtual impedances are chosen as $0.01\sim0.02\Omega$ for SHC scheme under stationary frame; $\omega_{f_C} = 0.02\pi$ rad/s is selected for the 1st order low-pass filter under 9th d-q frame while $\omega_{f_C} = 0.2\pi$ rad/s for 1st order low-pass filters under other d-q frames in the control under multiple d-q frames, as for the virtual impedances, the settings of $R_9 = 0.1\Omega$ and $R_{i(i\neq9)} = 0.01\Omega$ are recommended.

Chapter 4

Modeling and Analysis of Multiple Micro-APF System

Micro-APF scheme for residential systems can effectively mitigate the harmonics generated by customers' houses and prevent them from flowing into the grid through service transformers. Chapter 2 and Chapter 3 have discussed the control strategies and harmonic impedance of Micro-APF respectively, and the results of case study have shown that the existence of Micro-APF can lead to notable decrease in terms of THD of grid current. The above case studies are carried out for single Micro-APF case. In real distribution systems, each service transformer can be equipped with a Micro-APF to mitigate the harmonics from all customers. However, trade-off has to be made when costs and mitigation results are both taken into consideration. Therefore, on the practical occasion, not all of the service transformers are necessarily equipped with this mitigation device.

The major differences of multiple Micro-APF case from the single Micro-APF case lie in the possible coupling and interference due to the devices at different nodes. The coupling mainly reflects on the stability range of control gains (virtual-impedance). Also, the harmonic distribution in the feeders may be influenced due to the interference between the filters. In this chapter, stability analysis and interference related studies for multiple Micro-APF case are presented. To simplify the analysis, the feeders are assumed to be balanced and decoupled, so only one-phase distribution line and the service transformers along the line are involved when it comes to circuitry analysis or simulation.

4.1   System Modeling

This section describes the modeling for distribution feeders. As is shown in Figure 4.1, a real distribution system usually consists of several feeders, and there

are usually 10 or even more nodes along the distribution lines in a feeder. At each node, the service transformers connected to the grid will convert three-phase power to single-phase and achieve the voltage step-down for residential loads. The Micro-APFs are installed at the secondary side of service transformers. Norton equivalent model can simplify the circuitry analysis for a multiple Micro-APF system. In Section 4.1.1, Norton equivalent model is built up based on single Micro-APF case. Together with housing models in Section 4.1.2, more details on multiple Micro-APF system modeling are discussed in Section 4.1.3.
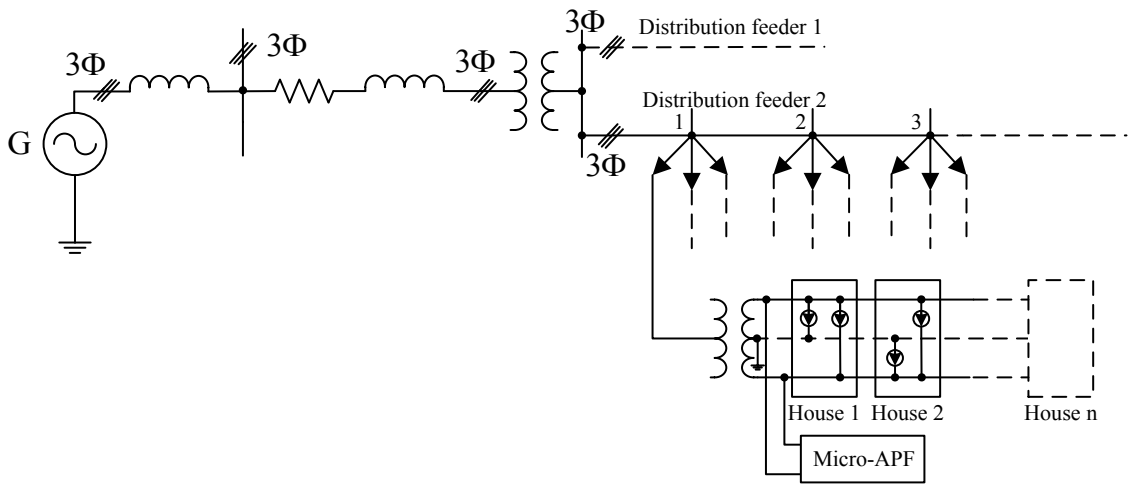
Figure 4.1 The typical topology of residential system

4.1.1 Norton Equivalent Model of Micro-APF

For a Micro-APF equipped at the secondary side of a service transformer, the simplified equivalent circuit is shown as Figure 4.2, where the subscript 'i' represents the unique label of each filter. The filter is connected between two phases of the service transformer, and the load in parallel represents residential loads.
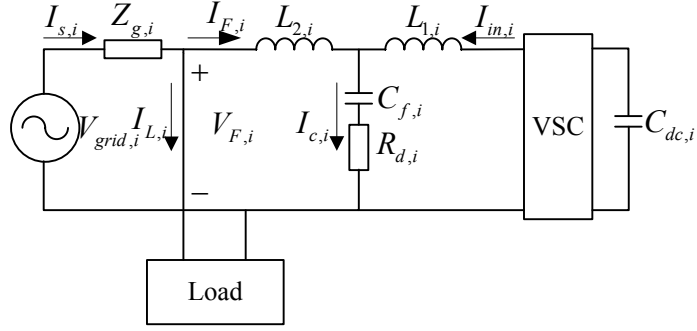
Figure 4.2 Simplified equivalent circuit of the Micro-APF at secondary side of a service transformer

As is mentioned in the previous chapter, equation (4.1) holds for the closed-loop control diagram shown in Figure 4.3, and equation (4.2) can be obtained from (4.1).
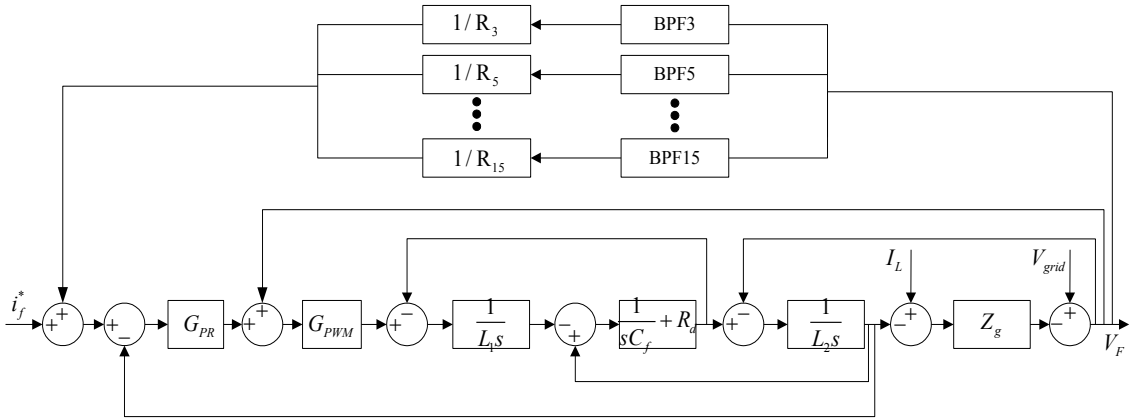
Figure 4.3 Close-loop control diagram

$$
\begin{cases}
I_{F,i} + \dfrac{1}{L_{1,i}s}\left\{\left[\left(I^{*}_{f,i} + V_{F,i}G_{\Sigma,i} - I_{F,i}\right)G_{PR,i} + V_{F,i}\right]G_{PWM} - V_{C,i}\right\} = I_{C,i} \\[4mm]
I_{C,i}\left(\dfrac{1}{sC_{f,i}} + R_{d,i}\right) = V_{C,i} \\[4mm]
\left(V_{F,i} - V_{C,i}\right)\dfrac{1}{L_{2,i}s} = I_{F,i} \\[4mm]
V_{grid,i} - \left(I_{L,i} + I_{F,i}\right)Z_{g,i} = V_{F,i}
\end{cases}
\qquad (4.1)
$$

$$I_{F,i} = Y_{eq,i}V_{F,i} + G_{eq,i}I^*_{f,i} \qquad (4.2)$$

where

$$Y_{eq,i} = \frac{(1+sC_{f,i}R_{d,i})(G_{\Sigma,i}G_{PWM}G_{PR,i}+G_{PWM}-1)-L_{1,i}C_{f,i}s^2}{(G_{PWM}G_{PR,i}-L_{1,i}s-L_{2,i}s)(1+sC_{f,i}R_{d,i})-L_{1,i}L_{2,i}C_{f,i}s^3}$$

$$G_{eq,i} = \frac{G_{PR,i}G_{PWM}(1+sC_{f,i}R_{d,i})}{(G_{PWM}G_{PR,i}-L_{1,i}s-L_{2,i}s)(1+sC_{f,i}R_{d,i})-L_{1,i}L_{2,i}C_{f,i}s^3}$$

$$G_{\Sigma,i} = \sum_{j=3,5,7\ldots} G_{BPFj,i}/R_{j,i}$$

According to equation (4.2), the Norton equivalent circuit model can be expressed as in Figure.4.4. Performance of ($Y_{eq,i}, G_{eq,i}$) and the parameters of Micro-APF are directly related. The control gains (virtual impedance) can influence the performance of equivalent impedance, i.e., the admittance $Y_{eq,i}$ in equation (4.2), as has been discussed in Chapter 3 while $G_{eq,i}$ is only affected by design parameters of Micro-APF.
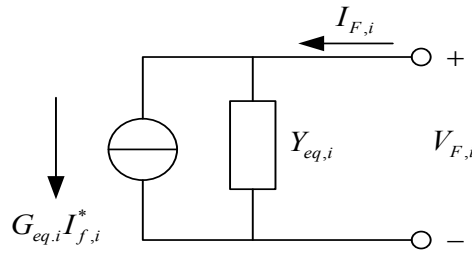
Figure 4.4 Norton equivalent circuit

4.1.2 Housing Model

In North America, three-wire single-phase distribution transformers are most commonly used to supply the residential and commercial customers. As shown in Figure 4.5, the commercial loads or home appliances are supplied with a neutral

and two hot phases and both of the two hot phases are 120V with respect to the neutral, so it is 240V with respect to themselves.
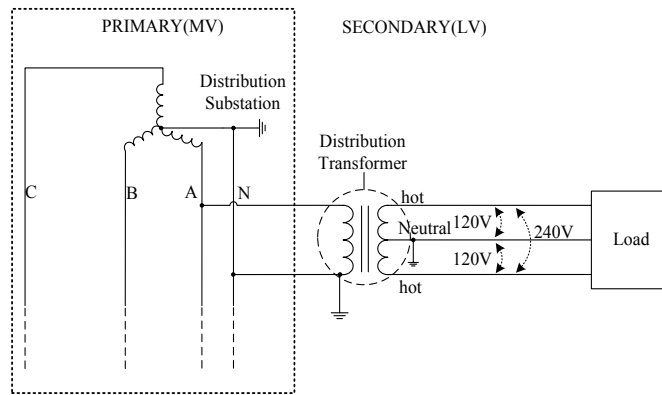
Figure 4.5 Power distribution system for three-wire single-phase feeding systems

Practically speaking, the home appliances in residential systems are randomly connected in the circuits. Most appliances such as PC, microwave, fridge etc. are connected between one hot wire and neutral, and the rest such as dryer are connected between two hot wires. The constructed housing models are shown in Figure 4.6, to simplify the analysis, all the home appliances except dryer are assumed to be connected between hot wire 1 and neutral for housing model 1, whereas the home appliances are connected between hot wire 2 and neutral for housing model 2, and the two-phase appliances are connected between two hot wires for both housing model 1 and housing model 2. A service transformer supplies up to 10 houses in actual case, so the loads connected in secondary side can be represented with lumped impedances in equivalent circuit.
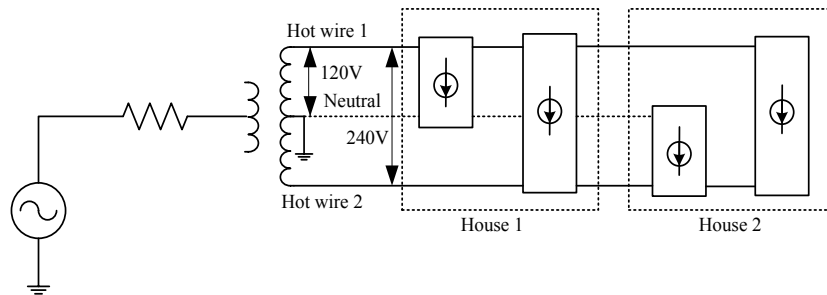
Figure 4.6 Housing models in residential systems

Based on the theoretical analysis in [34], the home appliances of an entire house can be studied by single-phase circuit, as shown in Figure 4.7. All of the linear home appliance impedances are paralleled as Z_{total} and the nonlinear loads current sources add up as a new harmonic source I_{NL}. Actually, both Z_{total} and I_{NL} are time-varying. But in this thesis, they can be assumed to be constant since only the impact of Micro-APF and steady state performance are considered. Similarly, the multiple-house model, as shown in Figure 4.8, is easily obtained based on the above discussion.
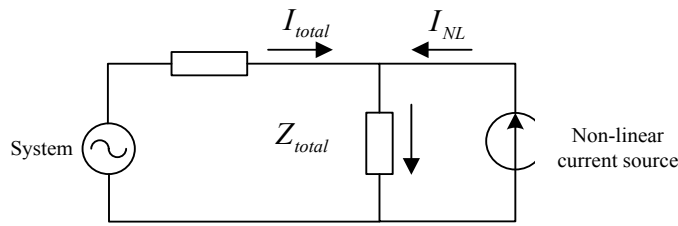
Figure 4.7 quivalent circuit of single house
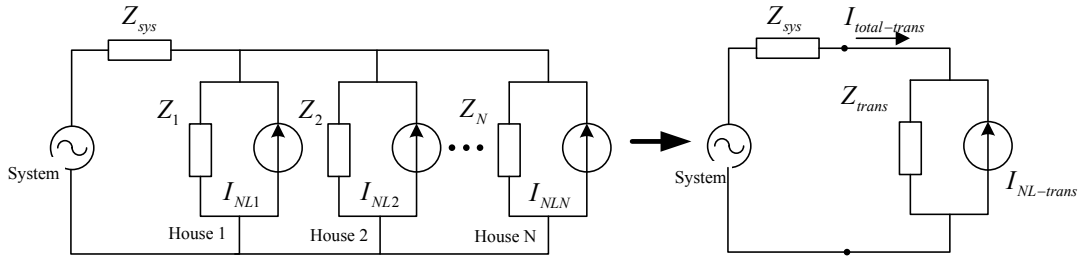
Figure 4.8 Multi-house load model

4.1.3 System Analysis

Since the housing equivalent model has been established, together with the Norton equivalent circuit for Micro-APF, they can simplify the circuit analysis for the distribution systems. Figure 4.9 shows the simplified N-node distribution feeder of the distribution system in Figure 4.1.
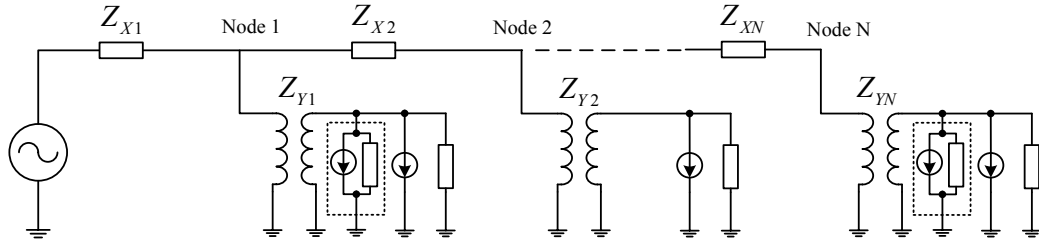
Figure 4.9 N-node feeder model

Apparently, each of the service transformers along the N-node feeder is not necessarily equipped with such Micro-APF. So assume that Micro-APFs are installed at nodes 1, 3…j…n. When referring the system in Figure 4.9 to the primary side of service transformers, the equivalent circuit of such feeder model can be shown as Figure 4.10, where $Z_{X1}, Z_{X2},..., Z_{XN}$ are the line impedances, $Z_{Y1}, Z_{Y2},..., Z_{YN}$ are the equivalent impedances of service transformers referred to primary side, and $(I_{hL,i}, Z_{f,i})_{i=1,...,N}$ are the parameters of housing equivalent models. The N node voltages along the distribution line are expressed by $(V_{grid,i})_{i=1,...,N}$ and $(V_{F,i})_{i=1,...,N}$ represent the voltage of PCC. The compensation currents of Micro-APFs are $(I_{F,i})_{i=1,...,N}$.
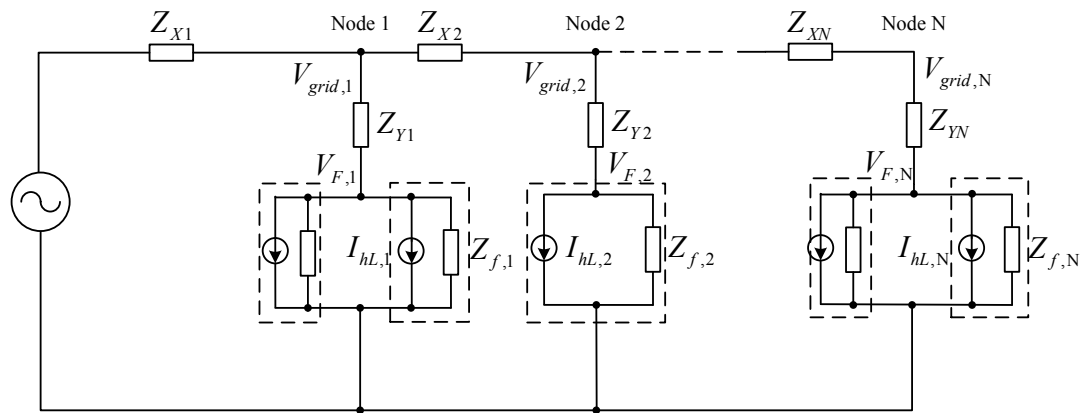
Figure 4.10 Equivalent circuit of N-node feeder model

If the service transformer at the ith node is equipped with Micro-APF, then

$$\begin{cases} V_{grid,i} - (I_{L,i} + I_{F,i})Z_{Yi} = V_{F,i} \\ I_{F,i} = Y_{eq,i}V_{F,i} + G_{eq,i}I_{f,i}^{*} \end{cases} \tag{4.3}$$

Otherwise,

$$\begin{cases} V_{grid,i} - I_{L,i}Z_{Yi} = V_{F,i} \\ I_{F,i} = 0 \end{cases} \tag{4.4}$$

For the ith ($i<N$) node,

$$(\frac{1}{Z_{Xi}} + \frac{1}{Z_{Xi+1}} + \frac{1}{Z_{Yi}})V_{grid,i} - \frac{1}{Z_{Xi}}V_{grid,i-1} - \frac{1}{Z_{Xi+1}}V_{grid,i+1} - \frac{1}{Z_{Yi}}V_{F,i} = 0 \tag{4.5}$$

According to equation (4.3) and (4.4),

$$I_{hL,i} + \frac{V_{F,i}}{Z_{f,i}} + I_{F,i} = \frac{V_{grid,i} - V_{F,i}}{Z_{Yi}} \tag{4.6}$$

Assume there are k service transformers in total equipped with Micro-APFs, and they are located at node number [1], [2]… [k]. Therefore, the compensation currents of Micro-APFs can be calculated from the detected grid voltages and generated harmonic currents by residential loads, as shown in equation (4.7).

$$\begin{pmatrix} I_{F,1} \\ I_{F,2} \\ \dots \\ I_{F,k} \end{pmatrix} = \begin{pmatrix} Y_{g,1} \\ Y_{g,2} \\ \dots \\ Y_{g,k} \end{pmatrix} [V_{grid}] - [I_{hL}] \tag{4.7}$$

where,

$$[V_{grid}] = [V_{grid,[1]-1}, V_{grid,[2]}, \dots, V_{grid,[k]}, V_{grid,[k]+1}]^{T}$$

$$[I_{hL}] = [I_{hL,[1]}, I_{hL,[2]}, \dots, I_{hL,[k]}]^{T}$$

$$Y_{g,i} = [y_1, y_2, ..., y_{k+2}]$$

$$y_j = \begin{cases} \dfrac{1}{Z_{X[i]}} - \dfrac{Z_{Y[i]}}{Z_{f,[i]}Z_{X[i]}}, j = i-1 \\[3mm] \dfrac{Z_{Y[i]}}{Z_{f,[i]}Z_{X[i]}} + \dfrac{Z_{Y[i]}}{Z_{f,[i]}Z_{X[i]+1}} + \dfrac{1}{Z_{f,[i]}} - \dfrac{1}{Z_{X[i]}} - \dfrac{1}{Z_{X[i]+1}}, j = i \\[3mm] \dfrac{1}{Z_{X[i]+1}} - \dfrac{Z_{Y[i]}}{Z_{f,[i]}Z_{X[i]+1}}, j = i+1 \\[3mm] 0, \text{otherwise} \end{cases}$$

4.2 Stability Analysis

System modeling has been presented in Section 4.1, and this section will discuss how to decide the minimum attainable virtual impedances for multiple Micro-APF system. The N-node equivalent circuit model is firstly presented in 4.2.1.

4.2.1 N-node equivalent model

In the N-node/N-transformer system, as shown in Figure 4.11, assume

$$Z_{n(1 \le n \le N)} = \begin{cases} Z_{Ln}, \text{if } Z_{VRn} \text{ is infinite, i.e., no filter} \\ Z_{Ln} \parallel Z_{VRn}, \text{if } Z_{VRn} \text{ is finite, i.e., with filter} \end{cases}$$
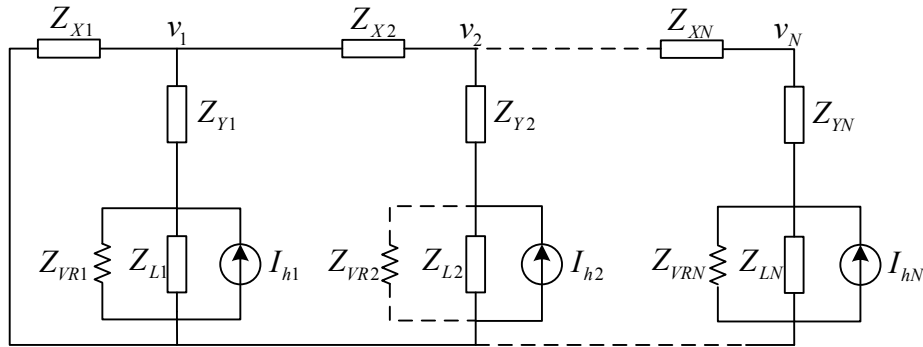
Figure 4.11 N-node system equivalent model under harmonics

So, there are N node-voltage equations.

$$
\begin{cases}
\dfrac{(\dfrac{V_1}{Z_{X1}} - \dfrac{V_2 - V_1}{Z_{X2}})Z_{Y1} + V_1}{Z_1} + \dfrac{V_1}{Z_{X1}} - \dfrac{V_2 - V_1}{Z_{X2}} = I_{h1} \\[4mm]
\dfrac{(\dfrac{V_2 - V_1}{Z_{X2}} - \dfrac{V_3 - V_2}{Z_{X3}})Z_{Y2} + V_2}{Z_2} + \dfrac{V_2 - V_1}{Z_{X2}} - \dfrac{V_3 - V_2}{Z_{X3}} = I_{h2} \\[4mm]
\qquad\qquad \cdots\cdots \\[2mm]
\dfrac{(\dfrac{V_i - V_{i-1}}{Z_{Xi}} - \dfrac{V_{i+1} - V_i}{Z_{Xi+1}})Z_{Yi} + V_i}{Z_i} + \dfrac{V_i - V_{i-1}}{Z_{Xi}} - \dfrac{V_{i+1} - V_i}{Z_{Xi+1}} = I_{hi} \\[4mm]
\qquad\qquad \cdots\cdots \\[2mm]
\dfrac{\dfrac{V_N - V_{N-1}}{Z_{XN}}}{Z_N} + \dfrac{V_N - V_{N-1}}{Z_{XN}} = I_{hN}
\end{cases}
\tag{4.8}
$$

They can be re-written as (4.9)

$$ Jv = I_h \tag{4.9} $$

where

$$ J = [j_1, j_2, ..., j_N]^T $$

$$ j_1 = \left[\frac{(Z_{Y1} + Z_1)(Z_{X2} + Z_{X1}) + Z_{X1}Z_{X2}}{Z_{X1}Z_{X2}Z_1}, -\frac{Z_{Y1} + Z_1}{Z_{X2}Z_1}, \underbrace{0, ..., 0}_{N-2} \right]^T $$

$$ j_{i(1<i<N)} = [\underbrace{0, ..., 0}_{i-2}, -\frac{Z_{Yi} + Z_i}{Z_{Xi}Z_i}, \frac{(Z_{Yi} + Z_i)(Z_{Xi+1} + Z_{Xi}) + Z_{Xi}Z_{Xi+1}}{Z_{Xi}Z_{Xi+1}Z_i}, -\frac{Z_{Yi} + Z_i}{Z_{Xi+1}Z_i}, \underbrace{0, ..., 0}_{N-i-1}]^T $$

$$ j_N = [\underbrace{0, ..., 0}_{N-2}, -\frac{Z_{YN} + Z_N}{Z_{XN}Z_N}, \frac{Z_{YN} + Z_{XN} + Z_N}{Z_{XN}Z_N}]^T $$

Therefore,

$$ v = J^{-1}I_h \tag{4.10} $$

Also,

$$\frac{V_n(s)}{I_{hn}(s)} = J^{-1}(s) \qquad (4.11)$$

4.2.2 Typical Case Analysis

Typically, for a 2-node/2-transformer system, shown as Figure 4.12, equation (4.12) holds according to equation (4.9).
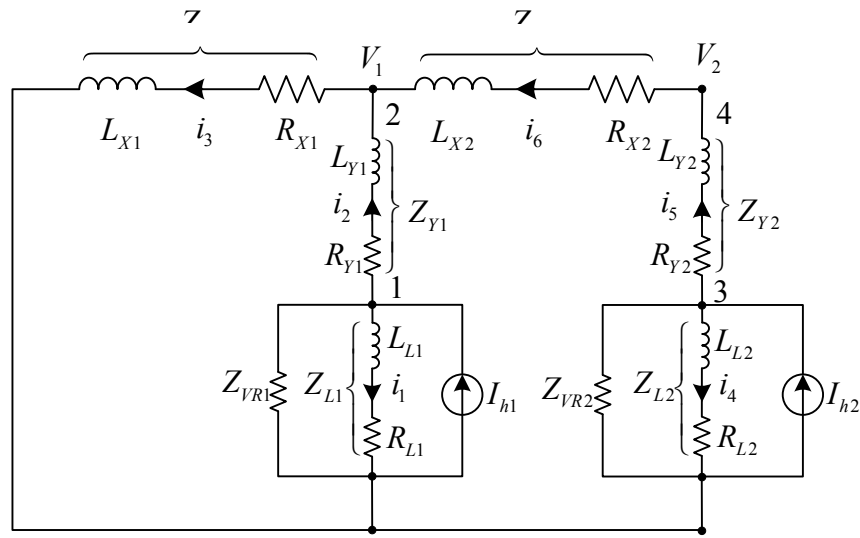
Figure 4.12 Equivalent model of 2-node/2-transformer system under harmonics

$$\begin{bmatrix} \dfrac{(Z_{Y1}+Z_1)(Z_{X2}+Z_{X1})+Z_{X1}Z_{X2}}{Z_{X1}Z_{X2}Z_1} & -\dfrac{Z_{Y1}+Z_1}{Z_{X2}Z_1} \\[3mm] -\dfrac{Z_{Y2}+Z_2}{Z_{X2}Z_2} & \dfrac{Z_{Y2}+Z_{X2}+Z_2}{Z_{X2}Z_2} \end{bmatrix} \begin{bmatrix} V_1 \\ V_2 \end{bmatrix} = \begin{bmatrix} I_{h1} \\ I_{h2} \end{bmatrix} \quad (4.12)$$

So

$$\frac{V_1}{I_{h1}} = \frac{Z_1 Z_{X1}(Z_2 + Z_{X2} + Z_{Y2})}{Z_1 Z_2 + Z_1 Z_{X1} + Z_1 Z_{X2} + Z_2 Z_{X1} + Z_1 Z_{Y2} + Z_2 Z_{Y1} + Z_{X1} Z_{X2} + Z_{X1} Z_{Y1} + Z_{X1} Z_{Y2} + Z_{X2} Z_{Y1} + Z_{Y1} Z_{Y2}}$$

$$\frac{V_1}{I_{h2}} = \frac{Z_2 Z_{X1}(Z_1 + Z_{Y1})}{Z_1 Z_2 + Z_1 Z_{X1} + Z_1 Z_{X2} + Z_2 Z_{X1} + Z_1 Z_{Y2} + Z_2 Z_{Y1} + Z_{X1} Z_{X2} + Z_{X1} Z_{Y1} + Z_{X1} Z_{Y2} + Z_{X2} Z_{Y1} + Z_{Y1} Z_{Y2}}$$

$$\frac{V_2}{I_{h1}} = \frac{Z_1 Z_{X1}(Z_2 + Z_{Y2})}{Z_1 Z_2 + Z_1 Z_{X1} + Z_1 Z_{X2} + Z_2 Z_{X1} + Z_1 Z_{Y2} + Z_2 Z_{Y1} + Z_{X1} Z_{X2} + Z_{X1} Z_{Y1} + Z_{X1} Z_{Y2} + Z_{X2} Z_{Y1} + Z_{Y1} Z_{Y2}}$$

$$\frac{V_2}{I_{h2}} = \frac{Z_2(Z_1 Z_{X1} + Z_1 Z_{X2} + Z_{X1} Z_{X2} + Z_{X1} Z_{Y1} + Z_{X2} Z_{Y1})}{Z_1 Z_2 + Z_1 Z_{X1} + Z_1 Z_{X2} + Z_2 Z_{X1} + Z_1 Z_{Y2} + Z_2 Z_{Y1} + Z_{X1} Z_{X2} + Z_{X1} Z_{Y1} + Z_{X1} Z_{Y2} + Z_{X2} Z_{Y1} + Z_{Y1} Z_{Y2}}$$

To simplify the analysis, some assumptions can be made here, $Z_{X1} = Z_{X2} = Z_X$, $Z_{Y1} = Z_{Y2} = Z_Y$, $Z_{L1} = Z_{L2} = Z_L$ and $I_{h1} = I_{h2} = I_h$, then

$$\begin{bmatrix} \dfrac{Z_X + 2Z_Y + 2Z_1}{Z_1 Z_X} & -\dfrac{Z_Y + Z_1}{Z_1 Z_X} \\[3mm] -\dfrac{Z_Y + Z_2}{Z_2 Z_X} & \dfrac{Z_X + Z_Y + Z_2}{Z_2 Z_X} \end{bmatrix} \begin{bmatrix} \dfrac{V_1}{I_h} \\[3mm] \dfrac{V_2}{I_h} \end{bmatrix} = \begin{bmatrix} 1 \\ 1 \end{bmatrix} \tag{4.13}$$

Accordingly, if the designed parameters of filters are assumed to be identical and the settings are the same as the previous chapters, at the same time $Z_X = R_X + sL_X$ and $Z_Y = R_Y + sL_Y$, then

$$\frac{V_1(s)}{I_h(s)} = \frac{Z_X Z_Y Z_2(s) + 2Z_X Z_1(s) Z_2(s) + Z_X^2 Z_1(s) + Z_X Z_Y Z_1(s)}{Z_Y^2 + 3Z_X Z_Y + Z_X^2 + (2Z_X + Z_Y)Z_1(s) + (Z_X + Z_Y)Z_2(s) + Z_1(s)Z_2(s)} \tag{4.14}$$

$$\frac{V_2(s)}{I_h(s)} = \frac{Z_X Z_Y Z_1(s) + (Z_X^2 + 2Z_X Z_Y)Z_2(s) + 3Z_X Z_1(s) Z_2(s)}{Z_Y^2 + 3Z_X Z_Y + Z_X^2 + (2Z_X + Z_Y)Z_1(s) + (Z_X + Z_Y)Z_2(s) + Z_1(s)Z_2(s)} \tag{4.15}$$

where

$$Z_{1(2)}(s) = \begin{cases} R_L + sL_L, \text{without filter} \\[2mm] \dfrac{(R_L + sL_L)Z_{VR1(2)}(s)}{R_L + sL_L + Z_{VR1(2)}(s)}, \text{with filter} \end{cases} \tag{4.16}$$

$$Z_{VR1(2)}(s) = \frac{(G_{PWM} G_{PR} - L_1 s - L_2 s)(1 + sC_f R_d) - L_1 L_2 C_f s^3}{(1 + sC_f R_d)(G_\Sigma G_{PWM} G_{PR} + G_{PWM} - 1) - L_1 C_f s^2} \tag{4.17}$$

73

Apparently, as for the installation of Micro-APFs, two cases should be considered here, i.e., transformer at node 1 (node 2) is equipped with filter ($Z_1(s) \neq Z_2(s)$) and transformers at node 1&2 are equipped with filters ($Z_1(s) = Z_2(s) = Z(s)$).

When the service transformers at node 1 and node 2 are both equipped with Micro-APFs, then

$$
\begin{bmatrix}
\dfrac{Z_X + 2Z_Y + 2Z}{ZZ_X} & -\dfrac{Z_Y + Z}{ZZ_X} \\[4mm]
-\dfrac{Z_Y + Z}{ZZ_X} & \dfrac{Z_X + Z_Y + Z}{ZZ_X}
\end{bmatrix}
\begin{bmatrix}
V_1 \\[1mm] I_h \\[1mm] V_2 \\[1mm] I_h
\end{bmatrix}
=
\begin{bmatrix}
1 \\ 1
\end{bmatrix}
\tag{4.18}
$$

$$
\frac{V_1(s)}{I_h(s)} = \frac{(Z_X^2 + 2Z_X Z_Y)Z(s) + 2Z_X Z(s)^2}{Z_Y^2 + 3Z_X Z_Y + Z_X^2 + (3Z_X + 2Z_Y)Z(s) + Z(s)^2}
\tag{4.19}
$$

$$
\frac{V_2(s)}{I_h(s)} = \frac{(Z_X^2 + 3Z_X Z_Y)Z(s) + 3Z_X Z(s)^2}{Z_Y^2 + 3Z_X Z_Y + Z_X^2 + (3Z_X + 2Z_Y)Z(s) + Z(s)^2}
\tag{4.20}
$$

where

$$
Z(s) = \frac{(R_L + sL_L)Z_{VR}(s)}{R_L + sL_L + Z_{VR}(s)}
$$

So the stability analysis can be worked out for these two cases based on these settings: R_L=0.7757Ω, L_L=0.82283mH, R_{Xi}=0.043Ω, L_{Xi}=0.015mH, R_{Yi}=32.9221Ω, L_{Yi}=0.0011H.

Figure 4.13 shows the minimum R_V for each dominant harmonic separately under different compensation strategies. The minimum R_V for each dominant harmonic can be calculated as well when R_V for the rest are assumed to be equal at several typical values, and the results are shown in Figure 4.14.
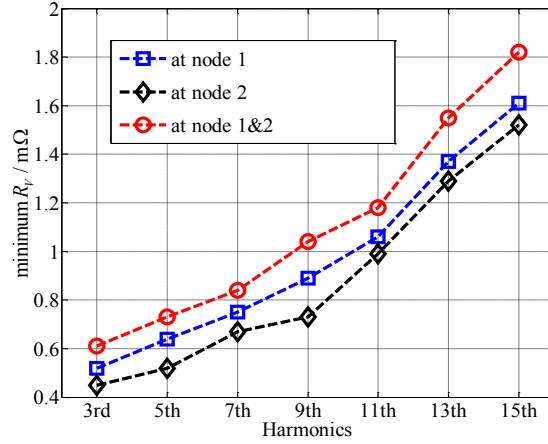
Figure 4.13 Minimum R_V for each dominant harmonic separately under different compensation strategies

(a)

(b)

(c)
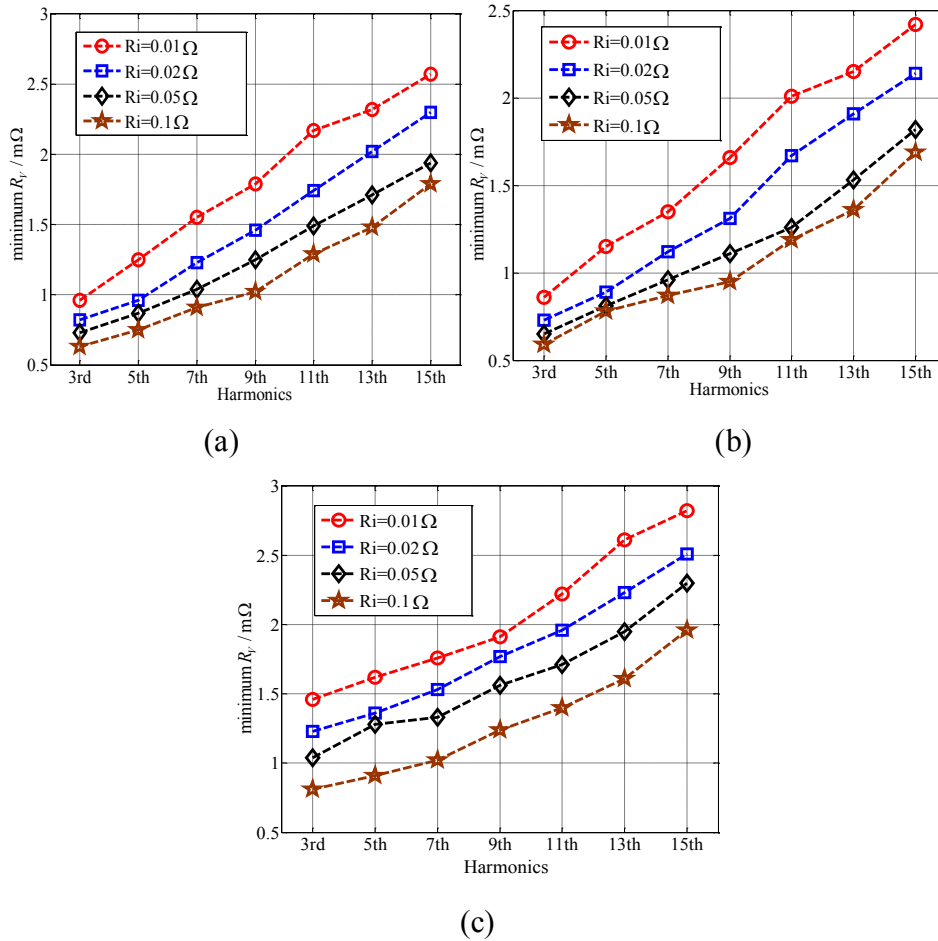
Figure 4.14 Minimum R_V for each dominant harmonic under different compensation strategies when R_V for the rest are assumed to be the same at several typical values. (a) Micro-APF at node 1. (b) Micro-APF at node 2. (c) Micro-APF at node 1&2.

By comparing the above results, it is apparent that the selection of installation site does make a difference for this 2-node/2-transformer system. Overall, Micro-APF installed at node 2 can achieve lower minimum R_i than node 1, i.e., the Micro-APF at node 2 has larger stability margin. For this 2-node/2-transformer system, when the transformers are both equipped with filters, the minimum permissible values for each harmonic is increased, i.e., compared with single Micro-APF case, the stability margin is reduced.

A subjective guess holds that the number of filters can make a difference indeed as far as the stability margin is concerned based on the above results. More specific results will be presented in next section.

4.2.3 General Case Analysis

In an N-node/N-transformer system, assume each of the service transformers along the line is equipped with a filter, which is for conservative concerns in terms of minimum R_V. Also, the analysis in this section can provide an estimation of permissible range of virtual impedance.

Equation (4.10) can be re-written as

$$\frac{1}{I_h}v = J^{-1}I_N = KI_N \tag{4.21}$$

where

$$I_N = [1,1,...,1]^T$$

$$v = [V_1, V_2,...,V_N]^T$$

$$J = [j_1, j_2,..., j_N]^T$$

$$j_1 = \left[\frac{2(Z_Y + Z) + Z_X}{Z_X Z}, -\frac{Z_Y + Z}{Z_X Z}, \underset{N-2}{0,...,0} \right]^T$$

76

$$j_{i(1<i<N)} = [0,\ldots,0,\underbrace{-\frac{Z_Y+Z}{Z_XZ}}_{i-2},\frac{2(Z_Y+Z)+Z_X}{Z_XZ},-\frac{Z_Y+Z}{Z_XZ},\underbrace{0,\ldots,0]^T}_{N-i-1}$$

$$j_N = [0,\ldots,0,\underbrace{-\frac{Z_Y+Z}{Z_XZ}}_{N-2},\frac{Z_Y+Z_X+Z}{Z_XZ}]^T$$

If $K = \{k_{ij}\}$, then

$$\frac{V_n}{I_h} = \sum_{i=1}^{N} k_{ni} \ (n=1,2,\ldots,N) \tag{4.22}$$

According to equation (4.22), the transfer functions from I_h to V_n can be expressed by the sum of elements in the nth row in matrix K. When n=3, the transfer functions are as follows:

$$\frac{V_1}{I_h} = \frac{ZZ_X[6ZZ_Y+4Z_X(Z+Z_Y)+3Z^2+Z_X^2+3Z_Y^2]}{Z(5Z_X^2+12Z_XZ_Y+3Z_Y^2)+6Z_XZ_Y^2+5Z_X^2Z_Y+Z^3+Z_X^3+Z_Y^3+Z^2(6Z_X+3Z_Y)}$$

$$\frac{V_2}{I_h} = \frac{ZZ_X[10ZZ_Y+5Z_X(Z+Z_Y)+5Z^2+Z_X^2+5Z_Y^2]}{Z(5Z_X^2+12Z_XZ_Y+3Z_Y^2)+6Z_XZ_Y^2+5Z_X^2Z_Y+Z^3+Z_X^3+Z_Y^3+Z^2(6Z_X+3Z_Y)}$$

$$\frac{V_3}{I_h} = \frac{ZZ_X[12ZZ_Y+5Z_X(Z+Z_Y)+6Z^2+Z_X^2+6Z_Y^2]}{Z(5Z_X^2+12Z_XZ_Y+3Z_Y^2)+6Z_XZ_Y^2+5Z_X^2Z_Y+Z^3+Z_X^3+Z_Y^3+Z^2(6Z_X+3Z_Y)}$$

The transfer functions of V_n/I_h (n=3,…,N) in a N-node/N-transformer system can be obtained by equation (4.21) and (4.22) as well, then the minimum R_V values can be worked out. The curves in Figure 4.15 shows the minimum R_V for each single harmonic varying with the number of nodes, and Figure 4.16 shows the minimum R_V of each selected harmonic under different numbers of nodes in the multiple-harmonic case, where control gains for the rest of harmonics are all kept at R_i=0.05Ω. From Figure 4.15 and Figure 4.16, it is obvious that the minimum R_V for each harmonic goes up as the number of nodes increases, which means that the stability margin is cut down. The minimum R_V for 3rd harmonic and 15th harmonic are increased from 0.58mΩ and 1.75mΩ (N=1) to 0.89mΩ and 2.02mΩ (N=10) respectively in the single-harmonic case, whereas the curves in multiple-

harmonic case show a more significant upward trend, for example, the values of 3rd and 15th harmonics at N=10 are almost triple and double the values at N=1 respectively. For a 10-node/10-transformer system, if each transformer is equipped with a filter, the attainable R_V value can be approximately as large as 4.2mΩ and it should be pointed out that this is based on the condition "R_i=0.05Ω for the rest of harmonics", which means that there is still enough stability margin if virtual impedances for the dominant harmonics are all set 0.05Ω.
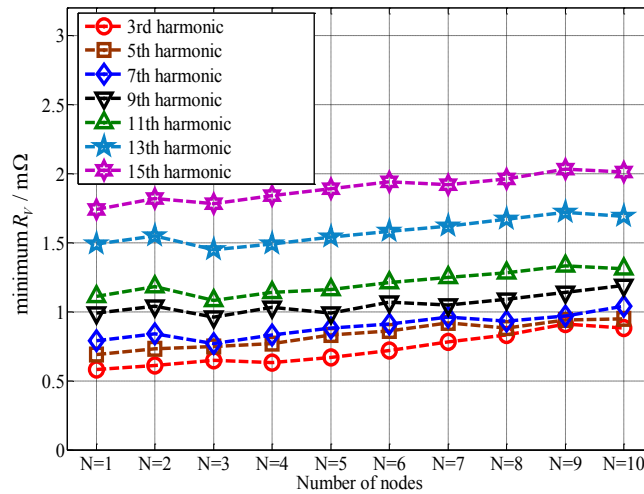
Figure 4.15 Minimum R_V varying with number of nodes for each single harmonic
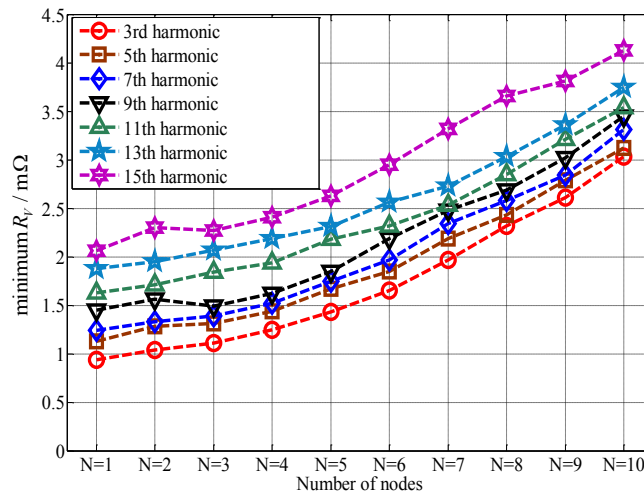
Figure 4.16 Minimum R_V varying with number of nodes for each harmonic when R_i =0.05Ω for the rest of harmonics

78

Similarly, Figure 4.17 shows the results of minimum R_V for each harmonic when $R_i = 0.01\Omega$ for the rest of harmonics. The attainable R_V value can be approximately as large as $5.1m\Omega$ in the extreme case "N=10". So the stability concern is not an issue if the virtual impedances are selected as $0.01\sim0.02\Omega$.
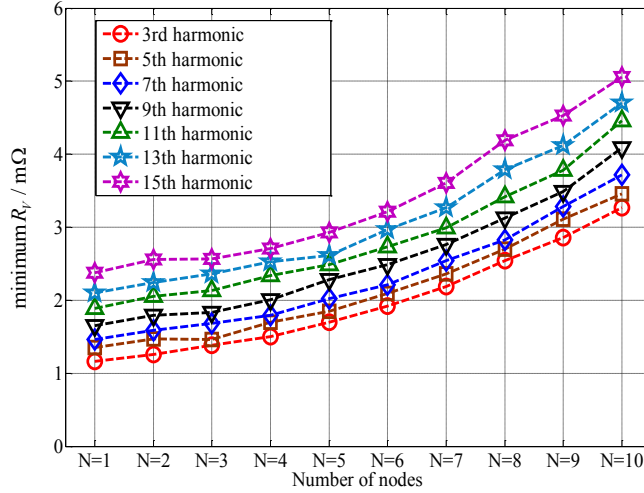
Figure 4.17 Minimum R_V varying with number of nodes for each harmonic when $R_i = 0.01\Omega$ for the rest of harmonics

4.3 Interference on Harmonic Compensation

Section 4.2 has discussed the attainable range of virtual impedances for multiple Micro-APF case. Another concern is interference on harmonic compensation between the filters installed at different sites.

For a 2-node/2-transformer system, equivalent circuits of the three cases, i.e., filter at node 1, filter at node 2 and filters at node 1& 2 are shown in Figure 4.18 [43].

It is clear that the impedances of Z_Y and Z_L are much higher than the impedance of filter at harmonic frequencies, so if the transformers are equipped with a filter, most of the harmonic current generated by residential loads will flow through the filter branches, i.e., Z_{VR1} and Z_{VR2}. For example, in the case "filter at node 1", most of I_{h1} will be absorbed by Z_{VR1}, and I_{h2} will flow through nodes 1 and 2. The

case "filter at node 2" will see the similar results. But for the case "filter at nodes 1&2", most of I_{h1} and I_{h2} will be absorbed by Z_{VR1} and Z_{VR2} respectively, and the harmonic current flowing through nodes 1 and 2 can be significantly reduced. As a result, the harmonic content in V_1 and V_2 are also greatly brought down. Apparently, Z_Y increases as harmonic frequency goes up, at the same time the virtual impedance is unchanged, so the difference between virtual impedance and Z_Y increases. This leads to significant absorption of harmonic by the filter branches. Therefore, the grid voltage/current will be less polluted as well.

(a)   (b)

(c)
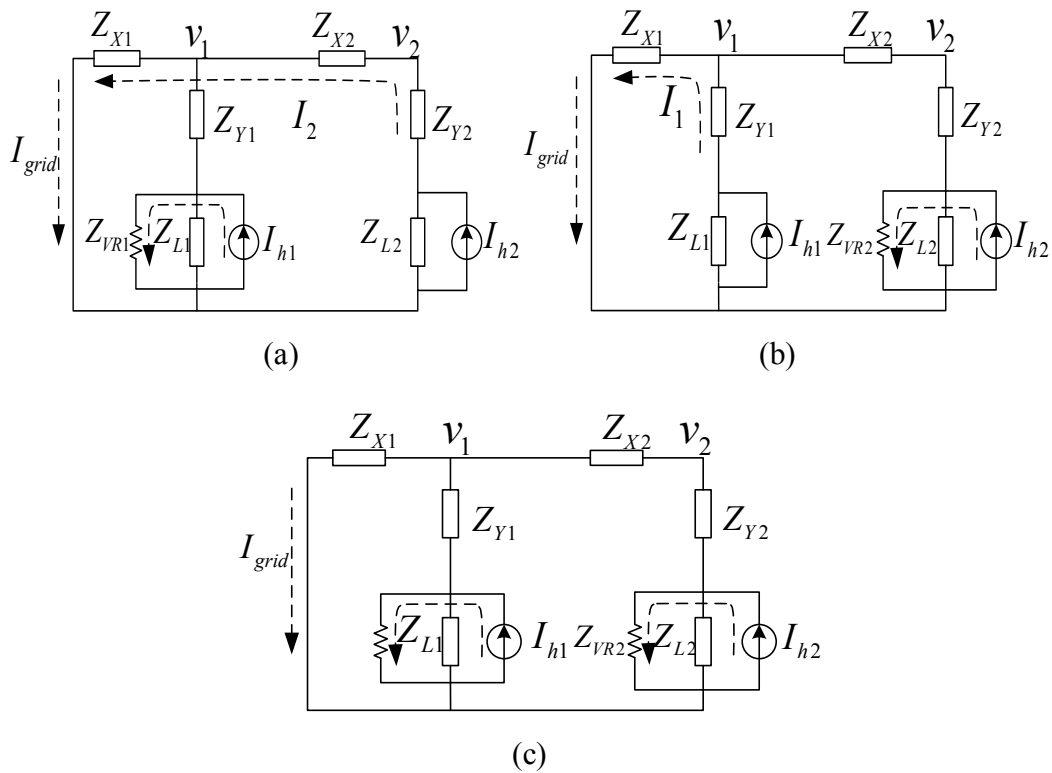
Figure 4.18 Equivalent circuits of (a) filter at node 1, (b) filter at node 2 and (c) filter at nodes 1 and 2

Time domain simulation is done by Matlab/Simulink for this 2-node/2-tranformer system. The line parameters and settings of transformers are the same as previous section. As for the housing models, the equivalent branch of impedance in parallel with current source is involved. Table 4.1 shows the initial line current data at

secondary side of transformers. The three different cases, i.e., filter at node 1, filter at node 2 and filters at node 1& 2, are studied by time-domain simulation.

Table 4.1 Initial line current data at secondary side of transformers

|	fund	3rd	5th	7th	9th	11th	13th	15th
Mag.	143.044	4.258	6.545	3.634	0.686	2.165	0.629	0.289
Ang.	-21.8	135.8	106.7	-173.2	-22.8	176.8	87.6	0.5

The ratio of harmonic content between "transformer with filter" and "transformer without filter" for I_{grid}, I_1 and I_2 can directly demonstrate the above analysis. Figure 4.19 shows the ratios of I_{grid}, I_1 and I_2 with/without filter for the case "filter at node 1". It is obvious that with the existence of filter at node 1, the harmonic content in I_1 is significantly reduced, whereas the harmonic content in I_2 remains unchanged. Overall, harmonic content for each harmonic in I_1 shows a downward trend as the virtual impedance value R_V goes down. Accordingly, the harmonic content in grid current I_{grid} is also continuously decreased until R_V is small enough, for example, when $R_V=0.01\Omega$, the harmonic content in I_1 almost achieves 0 while the harmonic content in grid current I_{grid} is reduced by 50% of the value before filter is equipped at node 1, and in this case, the harmonic current mainly originates from I_2. Exactly the same results (as shown in Figure 4.19) can be obtained for the case "filter at node 2". As for the case "filter at node 1&2", the percentages of harmonic reduction in I_1 and I_2 are almost the same as the single filter case, but the reduction in grid current I_{grid} is doubled due to the reduction in both I_1 and I_2.

According to the curves representing I_2 in Figure 4.19, it is not difficult to conclude that filters at different sites mainly absorb the harmonics generated by the adjacent residential loads. They hardly compensate the harmonics flowing through other nodes, i.e., a filter installed at one site will be responsible for the harmonics generated by all of the houses that the service transformer supplies. The existence of service transformers can decouple the interference on harmonic

compensation due to the extreme contrast between the impedances of transformers and distribution lines.
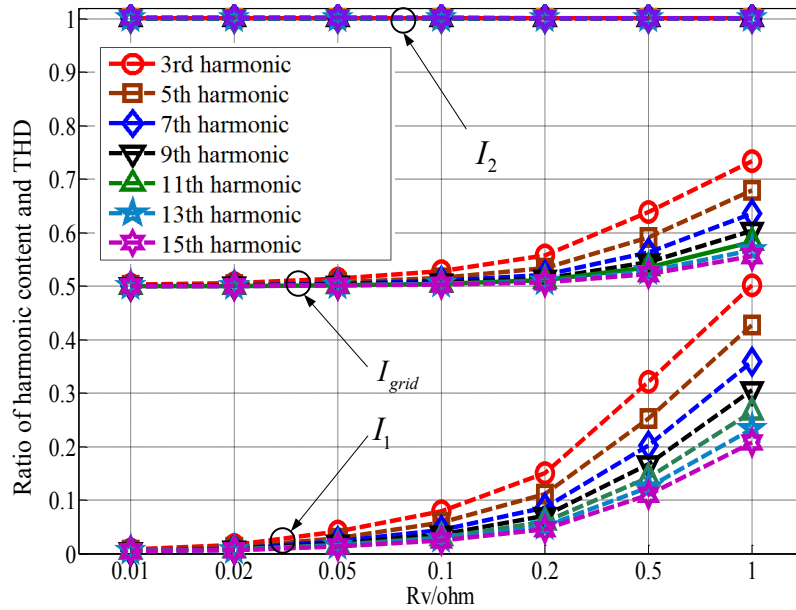
Figure 4.19 Ratios of I_{grid}, I_1 and I_2 after/before compensation for the case "filter at node 1"

Based on the above analysis and simulation results, it is clear that distributed compensation, i.e., the case "filters at node 1&2" for a 2-node/2-transformer system, is a good option in order to achieve ideal mitigation result in terms of the grid current. However, the case for line voltage is more complicated. Figure 4.20 compares the line voltage at node 1 and node 2 under different compensation strategies for $R_V = 0.05\Omega$.

It is obvious that terminal compensation, i.e., Micro-APF at node 2, can achieve better mitigation results in terms of line voltage compared with distributed compensation strategy. The contrast between these two strategies is even more significant for line voltage at the terminal (node 2).
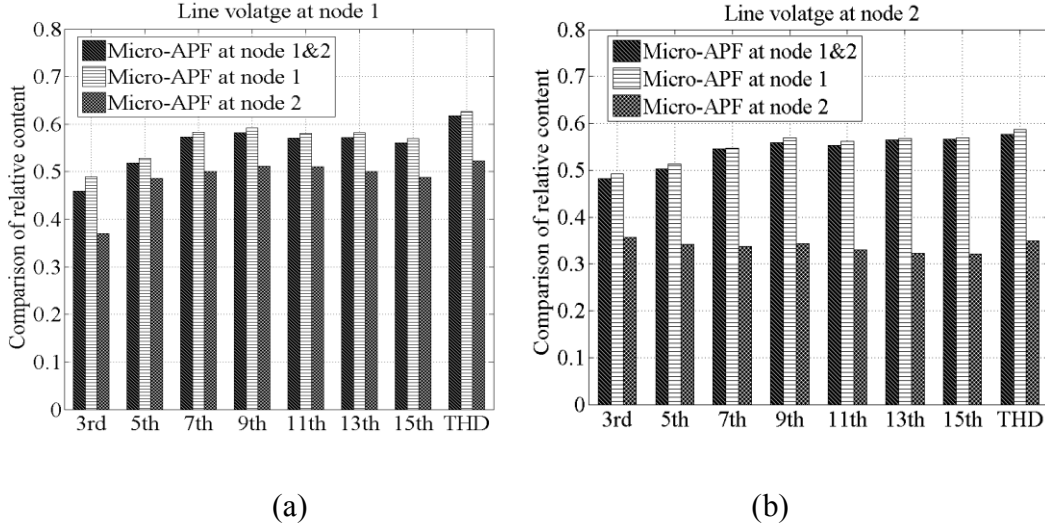
Figure 4.20 Ratios of harmonic content and THD of V_1 and V_2 after/before compensation under different strategies. (a) Line voltage at node 1. (b) Line voltage at node 2.

Figure 4.21 shows the THD ratio of I_{grid} with/without filter varying with number of nodes that are equipped with filters in the 10-node/10-transformer system. The curves under different R_V values are obtained by time-domain simulation with the same settings as the 2-node/2-transformer system. Unlike the previous study, a virtual impedance branch is used to replace the converter link for each filter in this 10-node/10-transformer system. Actually, the harmonic content of I_{grid} is the highest compared with the currents flowing through other nodes. It is obvious that when Rv<0.05Ω, as long as 50% of the transformers (5 out of 10 for this 10-node/10-transformer system) are equipped with filters, THD of the grid current I_{grid} can be reduced by 50% after installation.

In order to achieve a fair comparison, when the total harmonic compensation current (rating of Micro-APF) is maintained equal for different compensation strategies, Figure 4.22 compares the two compensation strategies for the 10-node/10-transformer system, i.e., distributed compensation and end of feeder compensation (Micro-APF at the terminal/node 10 only). It is obvious that end of feeder compensation is better in terms of voltage damping throughout the feeder compared with the distributed compensation in terms of THD$_V$ along the line.

83

For an N-node/N-transformer system (N>=3), assume m (m is a certain value and m<N) nodes/transformers are equipped with filters, the selection of installation sites will not influence the harmonic content of I_{grid} (MV transformer side) under a certain virtual impedance value, but it will affect the harmonic damping for voltage along the feeder line. For low order harmonics, end of feeder compensation is recommended in order to achieve more significant voltage damping results [43].
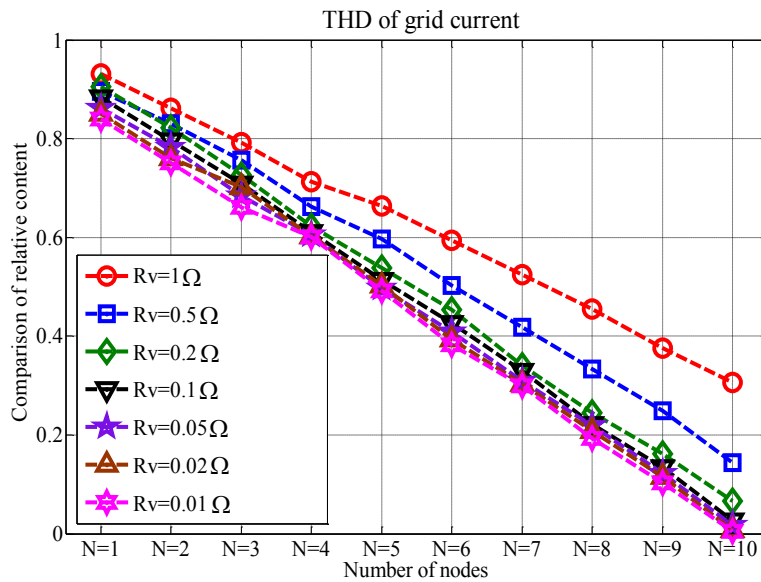
Figure 4.21 THD ratio of I_{grid} with/without filter varying with number of nodes
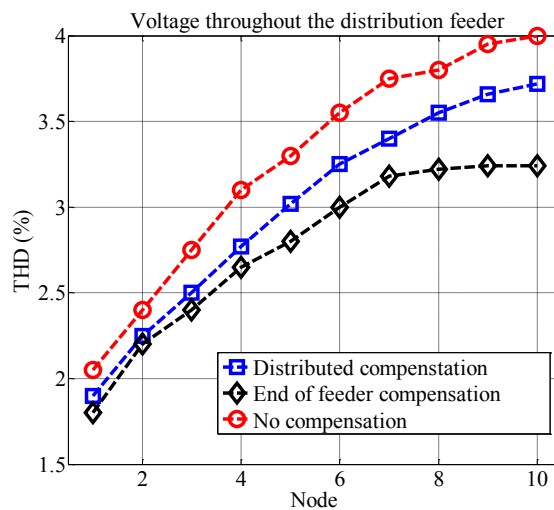
Figure 4.22 THDv throughout the feeder under different compensation strategies

4.4 Summary

In this chapter, the situation of multiple Micro-APF is studied. First of all, the stability of a multiple Micro-APF system is investigated. For simplified purposes, Norton equivalent circuit and housing models are involved for distribution feeder systems. The stability analysis based on an N-node equivalent circuit model is carried out. It is usually not the case that all of service transformers in a feeder are equipped with Micro-APFs with economic consideration. However, an assumption is made in this chapter that 100% of transformers are equipped with filters due to a conservative estimation for the permissible range of virtual impedances. The results show that for a 10-node/10-transformer feeder, the stability can be ensured if virtual impedances are selected as 0.01~0.02Ω, and there is still enough stability margin for this value.

In addition, the interference on harmonic compensation is discussed. The time-domain simulation results show that the service transformers can decouple the interference due to the significant contrast between the impedances of transformer and distribution line. So each Micro-APF will do local compensation, however to improve the damping of harmonic voltage along the distribution line, Micro-APF toward the end of feeder is recommended. Actually, the existence of capacitors in real distribution feeders may lead to possible resonance. This resonance will further affect the distribution of harmonic voltages along the feeder.

Chapter 5

Conclusion and Future Work

5.1 Conclusion

This thesis proposes a Micro-APF-based harmonic mitigation scheme for residential systems. Unlike the traditional MV active power filters, the proposed Micro-APF is specifically designed for the distribution system in North America. It can be connected between the two hot wires of the secondary side of service transformers. As the two hot phases are 120V with respect to the neutral, this Micro-APF is a type of LV active power filter (240V). The virtual-impedance based Micro-APF can exhibit low impedances under harmonic frequencies to sink harmonics from other branches while behaving as open circuit under fundamental frequency. As far as the control scheme is concerned, the Micro-APF in this thesis is voltage-detection based. According to the harmonic voltage extraction approaches, two compensation schemes, i.e., universal compensation and selective compensation are both discussed in Chapter 2. Stability analysis is involved for the decision on permissible range of virtual impedances.

Aimed at the specific industrial concern that the AMR signals (interharmonics) should be not filtered out together with the unwanted harmonics if this Micro-APF is involved, impedance features of Micro-APF branch is discussed in Chapter 3. Case study for factors that may influence the impedance features, i.e., system impedance and notch filters, are carried out under stationary frame. Theoretical analysis shows that trade-off exists in the harmonic impedance of Micro-APF branch as far as mitigation performance is concerned. In addition to stationary frame control scheme, case study under multiple d-q frames control is implemented as well. Similar trade-off can be concluded for multiple d-q frames scheme, i.e., the cut-off frequency of LPFs should be as small as possible for interharmonics, but this is at the expense of dynamic response.

Chapter 4 focuses more about system level study and the equivalent circuit model for feeders is employed to simplify the circuitry analysis. The equivalent circuit model consists of Norton equivalent circuit model for Micro-APF branches and housing model for residential loads. Based on stability analysis, the permissible range of virtual impedances can be conservatively estimated by the assumption that all of the transformers in a specific feeder are equipped with Micro-APFs. The interference on harmonic compensation is analyzed as well. Time-domain simulation is carried out to verify the analysis. The results show that the service transformers can decouple this interference as long as the difference between the impedances of transformer and distribution line is large enough. Although distributed compensation can achieve good performance for the grid current, Micro-APF toward the end of feeder is recommended considering the damping of harmonic voltages along the distribution line. Time-domain simulation results show that the voltage harmonics along the feeder vary with the positons of Micro-APFs.

5.2   Future Work

Based on the research in this thesis, the following future work is suggested:

Firstly, this work assumes that "three-phase feeders are balanced" is involved as the prerequisite in this thesis. So under this condition, the analysis in Chapter 4 is based on single-phase. In realistic distribution systems, the numbers of transformers connected to each phase of distribution lines are usually different, and the VA rating for transformers are not equal in most cases, which depends on the loads they supply. Therefore, the analysis and simulation based on identical parameters can only provide a rough estimation and qualitative study, and a case-by-case model is needed in order to get accurate results for a specific feeder.

Secondly, the inference discussed in Section 4.3 focuses on the impact of Micro-APFs on grid current flowing through the MV transformer side. Although it has been proved that the service transformers can decouple this interference, the

harmonic distribution along the line is not discussed in this work. Also, the resonance may be involved for the voltage along the distribution lines when Micro-APFs are installed at some certain nodes. So extended work can be done for the harmonic distribution of voltages and currents along the distribution lines.

Thirdly, the designed parameters of Micro-APF and case study in the whole thesis are based on theoretical analysis and simulation. So more work should be done in future as for hardware implementation and field tests.

Reference

[1] P. Mattavelli, "A closed-loop selective harmonic compensation for active filters," *IEEE Trans. Industry Applications*, vol. 37, n. 1, pp.81–89, 2001.

[2] A. E. Emanuel, J. Janczak, D. J. Pileggi, E. M. Gulachenski, C. E. Root, M. Breen, and T. J. Gentile, "Voltage distortion in distribution feeders with nonlinear loads," *IEEE Trans. Power Del.*, vol. 9, no. 1, pp. 79–87, Jan. 1994.

[3] N. R. Watson, T. L. Scott, and S. Hirsch, "Implications for distribution networks of high penetration of compact fluorescent lamps," *IEEE Trans. Power Del.*, vol. 24, no. 3, pp. 1521–1528, Jul. 2009.

[4] R. Dwyeret al., "Evaluation of harmonic impacts from compact fluorescent lights on distribution systems," *IEEE Trans. Power Syst.*, vol.10, no. 4, pp. 1772–1779, Nov. 1995.

[5] D. Salles, C. Jiang, W. Xu, W. Freitas and H. Mazin,"Assessing the Collective Harmonic Impact of Modern Residential Loads – Part I: Method," *IEEE Trans. Power Del.*, vol.27, no.4, pp.1937-1946, Oct. 2012.

[6] W.E. Reid, "Power Quality Issues-Standards and Guidelines," *IEEE Trans. Industry Applications*, vol. 32, no. 3, May/June 1996.

[7] D. J. Pileggi, E. M. Gulachenski, C. E. Root, T. J. Gentile, A. E. Emanuel, "The Effect of Modern Compact Fluorescent Lights on Voltage Distortion," *IEEE Trans. Power Del.*, vol. 8, no. 3, July 1993, pp. 1451-1459.

[8] R. Dwyer, A. K. Khan, M. McGranaghan, L. Tang, R. K. McCluskey, R. Sung, T. Houy, "Evaluation of Harmonic Impacts from Compact Fluorescent Lights on Distribution Systems," *IEEE Trans. Power Syst.*, vol. 10, no. 4, Nov. 1995, pp. 1772-1779.

[9] IEEE Recommended Practices and Requirements for Harmonic Control in Electrical Power Systems, IEEE Standard 519-1992.

[10] V. Letschert, Potential Impact of Adopting Maximum Technologies as Minimum Efficiency Performance Standards in the U.S. Residential Sector, eScholarship, 2010.

[11] LCD TV Market Growing Despite Weakness in North America; LED-Backlit Set to Take Lead in 2011, available online at: http://www.displaysearch.com/.

[12] World Development Indicators, World Bank Group, 2010.

[13] The Economist, Pocket World in Figures 2006 and 2010.

[14] Canadian laptop ownership, IPSOS, 2009, available online at http://www.ipsosna.com/news-polls/.

[15] 2008 could be the year laptop sales eclipse desktops in US, January 2008, available online at: http://arstechnica.com/.

[16] H. Wang, "Harmonic Impact of Modern Residential Loads on Distribution Power System and Mitigation Solutions," MSc. thesis, University of Alberta, Canada, 2011.

[17] Gonzalez, A. Damian, McCall, C. John, "Design of Filters to Reduce Harmonic Distortion in Industrial Power Systems," *IEEE Trans. Industry Applications*, vol.IA-23, no.3, pp.504-511, May 1987

[18] T.H. Ortmeyer, T. Hiyama, "Distribution system harmonic filter planning," *IEEE Trans. Power Del.*, vol.11, no.4, pp.2005-2012, Oct 1996.

[19] Chang, G.W., Hung-Lu Wang, Shou-Yung Chu, "Strategic placement and sizing of passive filters in a power system for controlling voltage distortion," *IEEE Trans. Power Del.*, vol.19, no.3, pp. 1204- 1211, July 2004.

[20] Mau Teng Au, Jovica V. Milanovic, "Planning Approaches for the Strategic Placement of Passive Harmonic Filters in Radial Distribution Networks," *IEEE Trans. Power Del.*, vol.22, no.1, pp.347-353, Jan. 2007.

[21] Chang, G.W., Shou-Yung Chu, Hung-Lu Wang, "Sensitivity-based approach for passive harmonic filter planning in a power system," *Power Engineering Society Winter Meeting, 2002. IEEE*, vol.2, no., pp. 937- 940 vol.2, 2002.

[22] Chi-Jui Wu, Jung-Chen Chiang, Shih-Song Yen, Ching-Jung Liao, Jin-ShyrYang, Tzong-Yih Guo, "Investigation and mitigation of harmonic amplification problems caused by single-tuned filters," *IEEE Trans. Power Del.*, vol.13, no.3, pp.800-806, Jul 1998.

[23] Quinn, C.A., Mohan, N., "Active filtering of harmonic currents in three-phase, four-wire systems with three-phase and single-phase nonlinear loads," *Proc. IEEE Seventh Annual Applied Power Electronics Conf. and Exposition, APEC*. 92, 1992, pp. 829– 836.

[24] Singh, B., Al-Haddad, K., Chandra, A., "A review of active filters for power quality improvement," *IEEE Trans. Ind. Electron.*, 1999, 46, (5), pp. 960–971.

[25] Senini, S.T., Wolfs, P.J., "Systematic identification and review of hybrid active filter topologies," *Proc. IEEE 33rd Annual Power Electronics Specialists Conf., PESC*. 02, 2002, vol. 1, pp. 394– 399.

[26] Po-Tai Cheng, Tzung-Lin Lee, "Distributed Active Filter Systems (DAFSs): A New Approach to Power System Harmonics," *IEEE Trans. Industry Applications*, vol.42, no.5, pp.1301-1309, Sept.-Oct. 2006.

[27] Tzung-Lin Lee; Po-Tai Cheng, Akagi, H., Fujita. H, "A Dynamic Tuning Method for Distributed Active Filter Systems," *IEEE Trans. Industry Applications*, vol.44, no.2, pp.612-623, March-april 2008.

[28] K. Wada, H. Fujita, and H. Akagi, "Considerations of a shunt active filter based on voltage detection for installation on a long distribution feeder," *IEEE Trans. Industry Applications*, vol. 38, no. 4, pp. 1123–1130, Jul./Aug. 2002.

[29] P. T. Cheng and T. L. Lee, "Analysis of harmonic damping effect of the distributed active filter system," *Trans. Inst. Electr. Eng. Jpn*., vol. 126-D, no. 5, pp. 605–614, May 2006.

[30] T. L. Lee and P. T. Cheng, "Design of a new cooperative harmonic filtering strategy for the distributed generation systems," in *Proc. IEEE-IAS 40th Annu. Meeting, 2005*, pp. 549–556.

[31] P. T. Cheng, S. Bhattacharya, and D. Divan, "Experimental verification of dominant harmonic active filter for high power applications," *IEEE Trans. Ind. Appl*., vol. 36, no. 2, pp. 567–577, Mar./Apr. 2000.

[32] Tostes, M.Ed.L., Bezerra. U.H., Silva R.D.S., Valente J.A.L., de Moura, C.C.M., Branco T.M.M., "Impacts over the distribution grid from the adoption of distributed harmonic filters on low-voltage customers," *IEEE Trans. Power Del.,* vol.20, no.1, pp. 384- 389, Jan 2005.

[33] P. Bagheri, "Methods to Mitigate Harmonics in Residential Power Distribution Systems", MSc. thesis, University of Alberta, Canada, 2012.

[34] C. Jiang, "A Probabilistic Bottom-up Technique for Modeling and Simulation of Residential Distributed Harmonic Sources", MSc. thesis, University of Alberta, Canada, 2012.

[35] F. Chen, H. Cheung, L. Wang, T. Mander, W. Liu, R. Cheung, "Adaptive D-based Active Power Line Filter for Industrial and Commercial Power Distribution," in *Proc.2007 IEEE PES general meeting Conf*.,pp.1-7.

[36] A. Huang, S. Bhattacharya, M. Baran, B. Chen, C. Han, " Active Power Management of Electric Power System Using Emerging Power Electronics Technology," in *Proc.2007 IEEE PES general meeting Conf*.,pp.1-7.

[37] R. Inzunza and H. Akagi, "A 6.6-kV Transformerless Shunt Hybrid Active Filter for Installation on a Power Distribution System," *IEEE Trans. Power Electronics*, vol. 20, No. 4, pp. 893-900, July 2005.

[38] D. Rivas, L. Morán, J. Dixon and J. R. Espinoza, "Improving Passive Filter Compensation Performance With Active Techniques," *IEEE Trans. Industrial Electronics,* vol. 50, No. 1, pp. 161-170, Feb. 2003.

[39] P. Jintakosonwit, H. Akagi, H. Fujita, S, Ogasawara, "Implementation and performance of automatic gain adjustment in a shunt active filter for harmonic damping throughout a power distribution system," *IEEE Trans. Power Elect*., vol. 17, no.3, pp. 438-447, May 2002.

[40] H. Akagi, "Control strategy and site selection of a shunt active filter for damping of harmonic propagation in power distribution systems," *IEEE Trans. Power Del.*, vol. 12, pp. 354–363, Feb. 1997.

[41] H. Akagi, H. Fujita, and K. Wada, "A shunt active filter based on voltage detection for harmonic termination of a radial power distribution line," *IEEE Trans. Ind. Applicat*., vol. 35, pp. 638–645, May/June 1999.

[42] Wakileh, G. J., Power Systems Harmonics, Fundamentals, Analysis and Filter Design, 2001, Springer.

[43] Munir S., Yun Wei Li, "Residential Distribution System Harmonic Compensation Using PV Interfacing Inverter," *IEEE Trans. Smart Grid*, vol. 4, pp. 816–827, Mar. 2013.